Development of a UV Nanosecond Laser Process for Polyamide Coating Removal from Micro-Scale Platinum Wires

Danial Rahnama

A Thesis

In

The Department of

Mechanical, Industrial and Aerospace Engineering (MIAE)

Presented in Partial Fulfillment of the Requirements
for the Degree of Master of Applied Science at
Concordia University
Montréal, Québec, Canada

April 2025

CONCORDIA UNIVERSITY

SCHOOL OF GRADUATE STUDIES

This is to certify that the thesis prepared

By: Danial Rahnama

Entitled: Development of a UV Nanosecond Laser Process for Polyamide Coating Removal from Micro-Scale Platinum Wires

and submitted in partial fulfillment of the requirements for the degree of

Master of Applied Science (Mechanical Engineering)

Complies with the regulations of this University and meets the accepted standards with respect to originality and quality.

Signed by the final examining committee:

_____Chair

Dr. Mehdi Hojjati

_____Examiner

Dr. Anjan Bhowmick

_____Thesis Supervisor

Dr. Sivakumar Narayanswamy

Approved by _____

Dr. Muthukumaran Packirisamy, Chair of Department of Mechanical, Industrial and Aerospace Engineering

_____2025 _____

Dr. Mourad Debbabi, Dean Faculty of Engineering and Computer Science

ABSTRACT

Development of a UV Nanosecond Laser Process for Polyamide Coating Removal from Micro-Scale Platinum Wires

Danial Rahnama

Precise coating removal from ultra-thin wires is critical in industries such as aerospace, automotive, and biomedical, where maintaining substrate integrity and meeting high-performance standards are essential. Common insulating materials like polyimides and enamels must be removed without damaging the underlying conductor, often requiring advanced methods such as laser ablation, chemical etching, or ultrasonic stripping. Among these, laser ablation offers significant advantages in precision, repeatability, and compatibility with automation, while also minimizing environmental and safety concerns.

This work investigates the use of UV laser ablation for stripping polyamide insulation from 50 µm platinum wires used in the production of high-sensitivity Resistance Temperature Detector (RTD) sensors. The UV laser system operates at a wavelength of 355 nm with a 20 µm spot size, a repetition rate ranging from 20 to 200 kHz, and an average power of 3 watts. The UV enables removal of the polyamide coating, without affecting the platinum substrate. Initial experiments were conducted in air ambient, where various laser parameters such as Number of loops, Line distance, and scanning speed were systematically varied. However, thermal effects from localized heating posed challenges, risking damage to the substrate and reducing surface quality. To overcome these issues, experiments were conducted in water ambient, which provided effective thermal management through a controlled ablation process. Scanning speed of 1200 mm/s; line spacing of 1 µm; and single loop was identified as optimal parameter settings to produce a clean surface comparable to that achieved by chemical stripping.

Further analysis of these parameters using ANOVA in Python highlighted the key influence and their interactions on output parameters such as the Tensile strength and Surface Roughness. Increasing the line distance to 2 µm and introducing an additional loop significantly improved the tensile strength [104 gr.f], and the surface roughness [0.129 µm], as close to that can be achieved by chemical stripping.

These findings contribute to the development of reliable, repeatable laser de-coating protocols for ultra-thin wires. By identifying optimal processing parameters, this work supports the broader implementation of a laser-based process toward automation particularly in SMEs.

Acknowledgement

I would like to express my deepest appreciation and heartfelt gratitude to my supervisor, Dr. Sivakumar Narayanswamy. His constant support, patience, and invaluable guidance have been the cornerstone of my graduate research work. Dr. Narayanswamy's insightful advice and unwavering commitment to my academic and personal growth have significantly shaped the direction and outcome of this research. I am profoundly thankful for his mentorship, which has inspired me to strive for excellence.

I also wish to extend my sincere thanks to Mr. Graziano Chilla for his invaluable collaboration and support. His assistance in providing the necessary instruments and machines for the tests was instrumental to the success of this project. Beyond the technical contributions, Mr. Chilla's continuous encouragement and willingness to go above and beyond in every phase of the project greatly enhanced the quality of my work. His expertise and dedication were pivotal in overcoming the challenges faced during this research.

I would like to express my sincere gratitude to the Mitacs funding agency for their trust in me and for providing the opportunity and support to work on this project. I am also deeply thankful to Professor Mehdi Hojjati and his student Heng Wang for their guidance and for allowing me to collaborate closely with them in their laboratory for the tensile testing procedures. In addition, I appreciate the valuable assistance of PhD candidate Mahdi Derayatfar, who supported me in using the confocal microscope for depth and surface measurements.

Lastly, I am deeply grateful to my wife and my parents for their unwavering support and encouragement. Their love, understanding, and sacrifices have been my source of strength throughout this journey. Their belief in me has been a constant motivator, and I am truly blessed to have them by my side.

Table of Contents

List of Figures

List of Tables

List of Symbols

df– Degree of Freedom

E_{Pulse} – Energy per Pulse

F – Laser Fluence

L – Number of Loops

P_{avg} - Average output power

PPL – Peak power laser

Ra - Average surface roughness

RR – Repetition Rate

SS – Sum of Square

X μ – Line distance in X

α (λ) - Absorption coefficient

λ – Laser wavelength

τ Pulse – Pulse Duration

List of Abbreviations

Al_2O_3: Aluminum Oxide

ANOVA: Analysis of Variance

DPSS: Diode-Pumped Solid State

ETFE: Ethylene Tetrafluoroethylene (insulation)

Er: Erbium

FWHM: Full Width at Half Maximum

HAZ: Heat Affected Zone

K: Kelvin

MRR: Material Removal Rate

Mohs: Mohs Hardness Scale

Nd: Neodymium

Nd:YAG : Neodymium-doped Yttrium Aluminum Garnet

PCB: Printed Circuit Board

PTFE: Polytetrafluoroethylene

PVC: Polyvinyl Chloride

Ra: Average Roughness

RF: Radio Frequency

RTD: Resistance Temperature Detector

SEM: Scanning Electron Microscope

SiO_2: Silicon Dioxide

UTM: Universal Testing Machine

UV: Ultraviolet

WEDM: Wire Electrical Discharge Machining

XLPE: Cross-Linked Polyethylene

Yb: Ytterbium

22MnB5: Steel Sheet Grade

CHAPTER 1: Introduction

1.1 General Overview

In the field of electronics, the application of protective coatings to wires is an essential practice, primarily aimed at ensuring the safety and optimal performance of electrical systems. Wires, available in various types and specifications, are deployed across numerous industrial sectors, each presenting its own distinct requirements and challenges. These wires are often exposed to harsh environmental conditions, physical wear and tear, and potential chemical hazards, all of which can threaten their functionality and lifespan. To mitigate these risks, coatings are applied to act as a protective barrier, shielding the wires from external factors that could cause damage or failure. The selection of the coating material is crucial and must be tailored to the specific demands of the application and operating environment. For example, in industries like aerospace or automotive, where wires are frequently subjected to high temperatures, heat-resistant coatings are essential to prevent degradation or melting. Conversely, in environments where moisture or corrosive substances are prevalent, coatings resistant to water and chemicals are preferred. These coatings not only protect the wires but also significantly enhance their durability, ensuring they can endure the demanding conditions of their respective environments.

In the context of coil winding, where wires are precisely wound around a core to form inductors, transformers, or other electromagnetic components, the significance of the coating becomes even more pronounced. When wires are coiled, they are arranged in a specific, organized manner to create a functional electrical circuit. This circuit is designed to regulate the flow of electrical current, generating either a magnetic field or storing energy, depending on the application. However, in certain regions of the coil, it becomes necessary to remove the coating to enable proper electrical connections or interactions within the circuit. There are several methods employed in industry for removing wire coatings, including mechanical, ultrasonic, cryogenic, chemical, and laser-based processes. The choice of method depends on various factors, such as the wire material, dimensions, coating composition, and the precision required for the task. Each process has its own set of advantages and limitations, and the selection of the appropriate technique is crucial for achieving optimal results while maintaining the integrity of the wire.

1.2 Common Types of Wires Used in Industry

1.2.1 Copper Wire

Copper is known for its exceptional electrical conductivity, malleability, and cost-effectiveness, making it the most widely utilized material in electrical and electronic applications. Its excellent conductivity ensures efficient power transmission, while its malleability allows it to be easily shaped and installed in various configurations. Copper wire is a cornerstone in power generation, transmission, and distribution systems. Additionally, copper wire is integral to electrical equipment and a vast array of electronic devices, from simple household appliances to complex industrial machinery.

1.2.2 Aluminum Wire

Aluminum offers a lightweight and more affordable alternative to copper, though it has lower conductivity. Despite this, aluminum's reduced weight and cost make it ideal for specific applications where these factors are crucial, particularly in large-scale installations. Aluminum wire is frequently used in power transmission and distribution, especially in overhead power lines where its lighter weight reduces the structural load on towers and poles. It is also preferred in aerospace and automotive industries, where weight reduction is critical for fuel efficiency and performance.

1.2.3 Magnet Wire (Enamel-Coated Copper or Aluminum)

Magnet wire, typically made from copper or aluminum, is coated with a thin layer of insulation, usually enamel[1]. This insulation allows for the creation of tightly wound coils without the risk of electrical shorting between adjacent turns, which is essential in electromagnetic applications. Magnet wire is essential in the manufacturing of transformers, inductors, motors, and other electromagnetic devices. It enables the efficient creation of magnetic fields needed for the operation of these devices, playing a critical role in the functioning of countless electrical systems.

1.2.4 Tinned Copper Wire

Tinned copper wire, coated with a thin layer of tin, significantly improves corrosion resistance, making it ideal for environments exposed to moisture and other corrosive elements. It is commonly used in marine,

[1] Enamel is a resin-based coating applied to wires for electrical insulation typically in motors and transformers

outdoor, automotive, and industrial applications where long-term durability and protection against corrosion are crucial.

1.2.5 Nichrome Wire

Nichrome wire, composed of a nickel-chromium alloy, is renowned for its high electrical resistance and its ability to withstand extremely high temperatures without oxidizing or breaking down. Due to its heat resistance, Nichrome wire is widely used in heating elements, such as in toasters, hair dryers, and electric heaters. It is also employed in specific types of resistors and thermocouples, where precise temperature control is required.

1.2.6 Superconducting Wire

Superconducting wire is made from materials that exhibit zero electrical resistance when cooled to temperatures below 77 K for high-temperature superconductors or 4 K for low-temperature superconductors. This unique property allows for the transmission of electrical current with no energy loss, making it extremely efficient for specific high-tech applications.

1.2.7 Silver-Plated Copper Wire

This type of wire combines the excellent conductivity of copper with the superior surface conductivity and corrosion resistance of silver. Silver plating enhances the wire's performance in high-frequency applications and provides additional protection against environmental degradation. Silver-plated copper wire is used in high-frequency applications, such as in RF (radio frequency) transmission lines and microwave systems. It is also found in aerospace and military equipment, where the highest levels of performance and reliability are demanded.

1.2.8 Platinum Wire

Platinum wire is characterized by its exceptional stability, resistance to corrosion, and ability to perform reliably at high temperatures. Its durability and resistance to oxidation make it ideal for use in extreme environments. Platinum wire is often used in thermocouples, where precise temperature measurements are critical. It is also integral in catalytic processes, certain aerospace applications, and medical devices where both performance and reliability under extreme conditions are required.

1.3 Coatings in Industry

Coatings serve a critical role in enhancing the mechanical strength and durability of the wire, protecting it from physical wear, abrasion, and environmental factors such as moisture, chemicals, or UV radiation, which could otherwise degrade its performance over time. In addition, the coating plays a key role in the thermal management of the system. During the operation of the coil, electrical currents generate heat, which, if not properly managed, could lead to overheating and potential damage to the wire or surrounding components. The insulation properties of the coating help dissipate excess heat and reduce thermal buildup, ensuring the wire operates within safe temperature limits. This thermal regulation not only prevents overheating but also prolongs the lifespan of the wire and surrounding components, maintaining system stability and reliability over time.

In tightly wound configurations, where wires are packed closely together and adjacent to the core, the proximity of the wires presents a significant risk of electrical interference or short circuits. Without proper insulation, the electrical current could inadvertently jump between adjacent turns of the wire or between the wire and the core, leading to circuit malfunctions, reduced efficiency, or even catastrophic failures. Such issues could result in power loss, unintended signal interference, or permanent damage to the system. By providing a robust layer of insulation, the coating ensures that each turn of the wire remains electrically isolated from the others, maintaining the integrity of the circuit and preventing any unintended electrical interactions. Table 1.1 demonstrates coatings in different industries where they are applied for protection or insulation.

1.4 Coating removal Methods

1.4.1 Ultrasonic Stripping

Ultrasonic stripping is a method used for coating removal, this technique utilizes high-frequency ultrasonic waves to create cavitation in a liquid medium, which then acts to remove the coating from the surface of the wire. Ultrasonic stripping involves immersing the coated wire in a liquid bath (often water or a suitable solvent) and applying ultrasonic waves. The ultrasonic energy creates rapid vibrations in the liquid, leading to the formation of microscopic bubbles. When these bubbles collapse (a process known as cavitation), they generate small, intense shock waves that can gently but effectively remove coatings from the wire without damaging the underlying material. The liquid medium used in the ultrasonic bath can be tailored to the specific coating material. For example, water-based solutions might be used for some coatings, while

solvents could be necessary for others. Adjusting the frequency and power of the ultrasonic waves is crucial to ensure effective coating removal without damaging the wire. An oscillator is an electronic circuit that generates a periodic oscillating signal, typically a sine wave or a square wave. In the context of ultrasonic stripping, the oscillator generates the high-frequency electrical signals that are needed to produce ultrasonic waves. The frequency at which the oscillator operates is typically in the ultrasonic range, from 20 kHz to 80 kHz, depending on the application.

Row	Application	Coating	Reason for Removal
1	Medical Device Wires [5]	Silicone, PTFE	In medical devices, wires are often coated with biocompatible materials like silicone, PTFE, or polyurethane to protect them and ensure they are safe for use inside the human body. However, at connection points where the wires interface with other electronic components or sensors within the device, the coating needs to be removed. This is done to allow for the proper transmission of electrical signals, ensuring that
2	Magnet Wires in the Electronics Industry [4]	Enamel	Magnet wires are commonly used in the windings of motors, transformers, and inductors. The enamel coating provides electrical insulation between the wire turns. However, to make electrical connections or solder the wire to terminals or other components, the enamel must be removed from the ends of the wire. This removal is crucial to establish a clean, conductive surface for soldering.
3	Copper Wires in Telecommunications [3]	Polyethylene or PVC	In the telecommunications industry, copper wires are often used for signal transmission in telephone and data cables. These wires are coated with polyethylene or PVC for insulation and protection against environmental factors. To connect these wires to terminals, connectors, or circuit boards, the coating must be stripped away from the ends. This ensures that the exposed copper wire can make proper contact.
4	Wiring in the Automotive Industry [2]	PVC, Polyethylene (XLPE), or Teflon	In automotive applications, wiring harnesses are coated with PVC, XLPE, or Teflon to provide insulation and protect against heat, chemicals, and physical abrasion. However, to connect the wires to various sensors, actuators, or control modules, the coating must be removed at the end. This is necessary to ensure a secure and reliable electrical connection, often through crimping, soldering, or terminal connections. Removing the coating also helps to reduce the risk of poor connections, which could lead to electrical failures or malfunctions in the vehicle's systems.
5	Thermocouple Wires in Aerospace and Industrial Applications [1]	Polyimide, Teflon, or Fiberglass	Thermocouple wires, used for temperature measurement, are often coated with materials like polyimide, Teflon, or fiberglass to provide insulation and protect them from harsh environments. In certain sections, especially at the junction where the two different metals meet to form the thermocouple, the coating must be removed. The reason for this removal is to allow the two dissimilar metals to directly contact each other and create the thermoelectric effect necessary for accurate temperature measurement. Additionally, the coating might need to be stripped at the connection points where the thermocouple is integrated with instrumentation or control systems.

Table 1.1 Different coating types in industry application

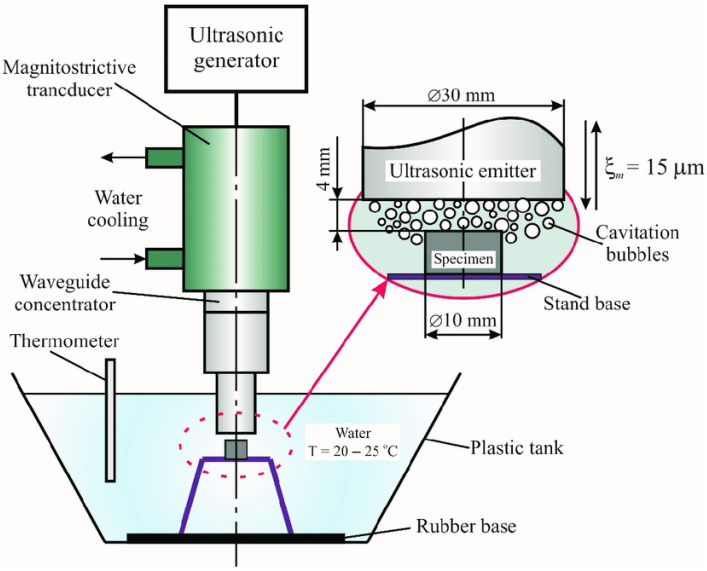

Figure 1.1 ultrasonic schematic in water fluid for coating removal of a 10 mm sample [6].

Long et al [6]investigate the ultrasonic bonding process for removing metal oxide coatings, specifically Al_2O_3, from thin wires, focusing on the mechanisms driving oxide detachment and removal. The process is analyzed in four key phases: pre-deformation, friction, softening, and interdiffusion, where normal force and ultrasonic vibration work together to break the oxide layer at the wire/substrate interface. As vibration is applied, the oxides detach, mill into smaller particles, and are transported to the periphery of the contact area. Transparent SiO_2 substrates are used to visualize the process, and artificially thickened oxide layers are applied to facilitate observation. The results highlight the significant role of ultrasonic vibration in detaching, milling, and removing oxide layers, improving bonding strength by up to three times. This work provides valuable insights into the ultrasonic de-coating process, offering potential improvements for wire bonding technologies in precision applications. However, despite promising results, Ultrasonic stripping faces limitations when applied to ultrathin substrates such as micro-scale wires, where controlling the intensity and precision of the ultrasonic waves becomes challenging

Maeno et al [7] investigate the effectiveness of ultrasonic cleaning for removing thin oxide layers formed during the hot stamping of bare $22MnB_5$ steel sheets, specifically using a diluted hydrochloric acid solution. The oxide scale, which forms during resistance heating by die quenching, can hinder subsequent welding and painting processes, necessitating its removal. The ultrasonic cleaning method demonstrated successful oxide removal, enhancing weldability and paint ability by minimizing spattering during resistance spot welding and ensuring sufficient weld strength. The results highlight the potential of ultrasonic cleaning in

industrial applications, particularly for steel sheets requiring high tensile strength, with a tensile strength of 1800 MPa achieved for the treated parts. it is crucial to note that the risk of unintended damage or deformation to delicate wires, along with the challenge of uniformly applying the cleaning process at the micro-scale, makes ultrasonic de-coating less suitable for industries working with thin wires, especially in high-precision applications that require maintaining wire integrity.

1.4.2 Cryogenic Stripping

Cryogenic removal of coatings from wires is an advanced technique that involves using extremely low temperatures to facilitate the removal of coatings. This method is particularly useful for sensitive applications where other stripping methods might cause damage. Cryogenics involves the use of materials at extremely low temperatures, typically below -150°C (-238°F). Cryogenic removal uses these low temperatures to make the coating brittle and easier to remove. This brittleness can cause the coating to crack or shatter when subjected to mechanical forces. The rapid cooling causes the coating to contract more than the wire, creating stresses at the interface between the coating and the wire. This can lead to the coating separating from the wire. Figure 1.2 shows a typical working diagram of this kind of process.

Weston et al [8] investigate the application of cryogenic blasting, a technique utilizing solid carbon dioxide (CO_2) particles at −78.5°C, as an alternative to conventional methods like sand, steam, and water blasting for surface cleaning and coating removal. The low hardness of CO_2 particles (2–3 Mohs) makes them less abrasive, reducing damage to treated components and allowing for in-situ cleaning or stripping with minimal downtime. Unlike traditional methods, cryogenic blasting generates minimal waste since CO_2 particles sublimate, leaving only the removed material for disposal. The research focuses on the thermo-mechanical effects of cryogenic blasting on a commercially filled polypropylene blend, a polymer widely used in the automotive industry. The study examines the balance between the heat generated by particle impacts and the heat extraction by the cold CO_2 particles and gas, ensuring that the coating is removed without causing excessive damage to the polymer surface. The results highlight operational regimes that preserve surface integrity, enabling defect-free recoating and supporting sustainable recycling practices in industrial applications.

Kapoor et al [9] investigate the effects of deep cryogenic treatment at -184°C on brass wire electrodes used in wire electrical discharge machining (WEDM). The results showed that the cryogenically treated wires exhibited a more refined microstructure and changes in their crystalline phase compared to non-treated

wires, as observed through scanning electron microscopy and X-ray diffraction. Additionally, the electrical conductivity of the treated wires was significantly improved. The performance of the treated brass wires in WEDM was also enhanced, leading to an increased material removal rate (MRR). Using Taguchi experimental design, the study identified optimal machining parameters, with factors such as wire type, pulse width, time between pulses, and wire tension playing significant roles in maximizing MRR. Overall, the deep cryogenic treatment was found to improve the structural, electrical, and machining performance of the brass wire electrodes, demonstrating its potential for enhancing wire properties in advanced applications.

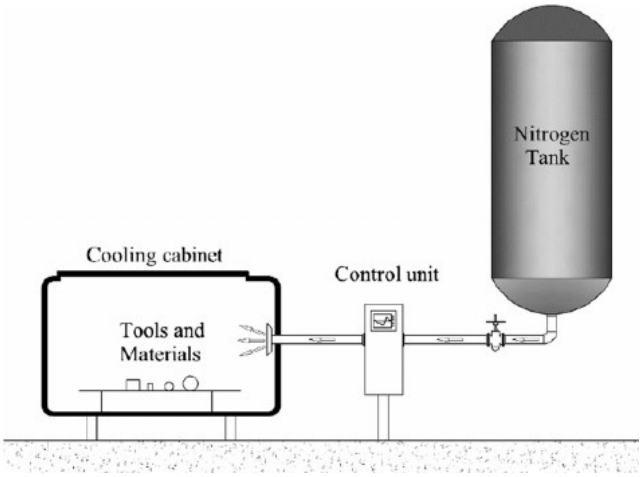

Figure 1.2 Cryogenic diagram process (coating removal) [10].

Cryogenic blasting, typically used to remove hard coatings from larger industrial components, has significant limitations when adapted for de-coating micro-scale wires. The process is less effective on soft polymeric coatings, such as those found on these wires, because the solid CO_2 particles lack the abrasiveness needed to fully strip flexible or thermoplastic layers. Moreover, the lack of precision in cryogenic blasting makes it unsuitable for handling the delicate, fine diameters of micro-scale wires, increasing the risk of deformation or surface damage. Additionally, the intense thermal and mechanical effects caused by the blasting, such as localized temperature changes and impact stresses, can compromise the structural integrity and electrical properties of the wires.

1.4.3 Chemical Stripping

Chemical stripping is a process widely utilized in industries for removing insulation or coatings from wires, especially those with intricate, delicate, or heat-resistant materials. This method employs specialized chemical solutions or solvents formulated to target specific coating materials without adversely affecting the underlying conductor. By dissolving, softening, or chemically breaking down the insulation, the process enables precise and efficient removal with minimal risk of mechanical or thermal damage to the substrate.

Chemical stripping involves a combination of surface chemistry and material science principles. The solvents used are carefully chosen based on their compatibility with the insulation material's chemical composition. For instance, coatings made of polyimide, polytetrafluoroethylene (PTFE), or silicone may require different solvents due to their varied molecular structures and thermal resistances. Acidic or alkaline solutions, organic solvents, or specific formulations like phenol-based compounds are commonly used, depending on the wire's material properties [11].

Chemical coating removal presents several challenges, including the risk of damage due to chemical reactions or physical stress, environmental and safety concerns from hazardous waste and operator exposure, difficulties in achieving uniform and selective stripping, scalability issues for high-throughput applications, high operating costs and economic inefficiency, potential impacts on surface integrity such as residue or roughness, and the need for specialized process control and equipment, making it less favorable compared to alternative methods like laser or ultrasonic stripping.

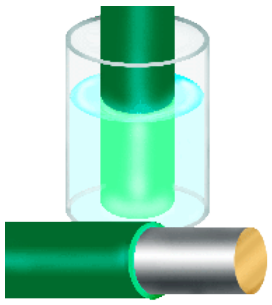

Figure1.3 immersing wires in specific chemical solvent for coating removal [12]

1.4.4 Laser Stripping

Laser stripping is a highly precise and non-contact method of removing insulation or coating using a focused laser beam. This technique is particularly effective for applications requiring extreme accuracy,

such as in the aerospace, medical device, and advanced electronics industries. Unlike mechanical or chemical methods, laser striping does not involve physical contact or the use of potentially hazardous chemicals, making it a clean and efficient option.

The choice of laser for wire stripping depends on the insulation material and the specimen's dimension. Common types include CO_2 lasers, fiber lasers, and UV lasers, each offering different wavelengths and energy levels suited to various coatings. CO_2 lasers are typically used for removing polymer-based or organic coatings, while UV lasers are favored for delicate or thin coatings. UV lasers are more suitable for stripping polyamide coatings because polyamide absorbs shorter wavelengths more effectively. Additionally, for micro-scale samples where preserving wire integrity is critical, UV lasers operating at lower power are preferred, as their shorter wavelengths enable precise material removal with minimal heat generation [13].

The laser beam is focused on a spot, often in the µm range, to target the insulation material without affecting the underlying conductor. Advanced laser stripping machines equipped with precise control systems that allow for the adjustment of laser power, pulse duration, and focus, ensuring that the beam is concentrated on the insulation. The control of these parameters is crucial to avoid damaging the wire itself. Figure 1.4 illustrates the areas of coating removal on a specific wire, performed using laser machine with two different wavelengths. The image shows that the shorter wavelength laser reached the substrate and removed the coating more effectively, although the substrate surface remained rough, a condition that could potentially be improved by adjusting the process parameters. In contrast, the 515 nm laser only caused thermal effects on the coating, without completely removing it. A similar observation was made in the specimens used in this project, which are discussed in detail in the following section.

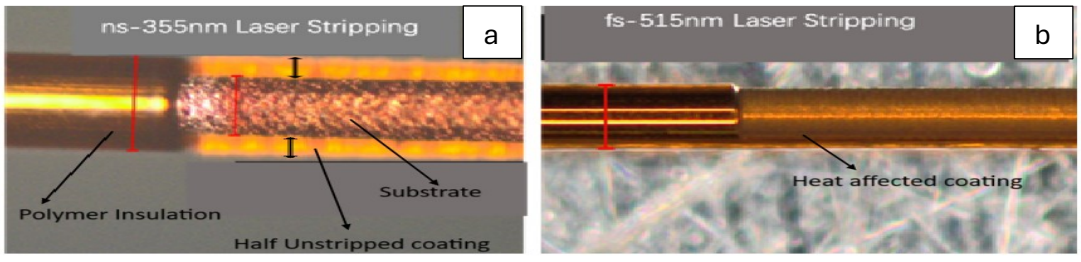

Figure 1.4 coating removal under laser ablation process, (a) 355 nm, (b) 515 nm [14]

As the laser beam interacts with the coating, it causes the material to either vaporize (ablate) or break down into smaller particles that can be easily removed. The ablation process is highly controlled and localized,

meaning only the targeted area is affected, leaving the rest of the wire and its coating intact. This process is non-contact, so there is no risk of physical damage or deformation to the wire. As observed in figure 1.5, UV lasers are particularly well-suited for delicate de-coating processes, where precision and control are paramount. These lasers offer the ability to finely adjust the stripping process, ensuring that the coating is removed without damaging the underlying material. This level of precision is especially important when working with sensitive or intricate components, where even minor errors could lead to significant issues.

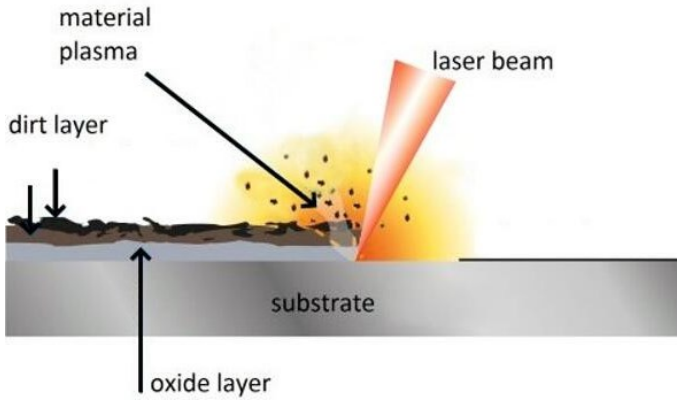

Figure1.5 Laser ablation principal schematic for coating removal without any damage to substrate [15].

Li et al, [13] focus on optimizing the laser wire stripping process for X-ETFE insulated wire, commonly used in aviation. It explores the use of a 405 nm wavelength semiconductor laser for stripping the insulating layer efficiently and with high quality. The research involves developing an energy conversion model, a mobile heat source model, and a finite element simulation model to simulate and analyze the laser stripping process. The study employs a single-factor analysis to evaluate the effects of various process parameters—laser power, scanning speed, and processing time—on key quality indicators such as kerf width, heat-affected zone (HAZ) width, and cutting seam depth. As shown in figure 1.6 The findings reveal that while increasing laser power can improve stripping efficiency, it also results in a broader kerf and larger HAZ. Conversely, increasing scanning speed can reduce the kerf width, suggesting that a balanced combination of power and speed can improve both efficiency and quality. Based on the single-factor analysis, a set of potential parameter levels was chosen for further testing in an orthogonal experiment. The results of the orthogonal test, which aims to identify the optimal combination of laser power and scanning speed, align well with the simulation outcomes, confirming the validity of the simulation approach for determining optimal process parameters. It is also highlighting laser wire stripping as one of the most efficient and high-quality methods for wire stripping, with broad applications in industries such as aerospace and

microelectronics. The essence of the process is described: a focused high-heat flux laser spot is applied to the insulating layer, which, under the effect of heat conduction, decomposes and vaporizes when the material exceeds a certain critical temperature threshold.

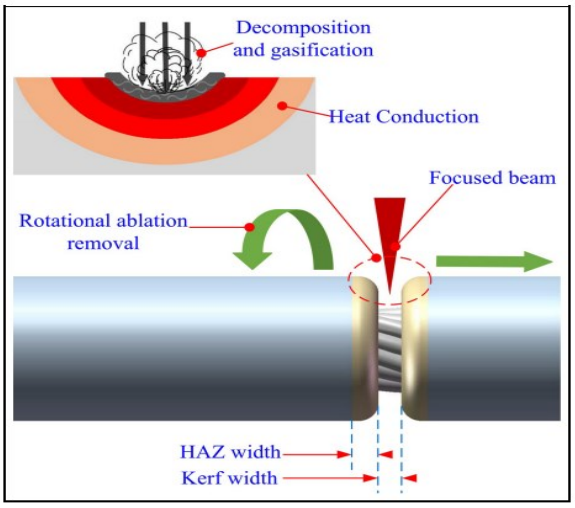

Figure 1.6 Laser wire stripping process [13].

One of the key factors that must be considered before starting the de-coating process is the type of coating material itself. Different materials respond differently to laser ablation, and understanding these interactions is crucial for achieving the desired results. The coating material determines the appropriate laser settings, such as wavelength, pulse duration, and intensity, which are necessary to effectively and safely remove the coating. Laser stripping systems are typically integrated with computer-controlled systems, allowing for precise programming of the stripping pattern, depth, and location. This programmability is especially useful when dealing with complex geometries or when stripping specific sections of multi-layered wires. The system can be programmed to remove insulation in specific patterns or at exact lengths, providing a level of precision unmatched by other stripping methods.

Gordon et al, [16] investigate the application of a frequency-multiplied Nd:YAG laser for drilling via holes and creating larger windows in copper-clad flexible laminates composed of polyimide-based materials. The study focuses on understanding the interaction between the laser beam and various polyimide structures, with the goal of establishing a connection between the material behavior and variations in processing parameters, including beam characteristics and environmental factors. Several methods of examination were used to analyze the samples, including optical, electrical, and reliability tests, to evaluate the material's

response to laser exposure. Figure 1.7 shows some floating copper wires from which the polyimide layer has been ablated. Geometrical analysis was conducted using scanning electron microscopy, surface profiling, and optical microscopy, while surface cleanliness was confirmed through electro- and electroless plating procedures. The results of this research provide new insights into the material processing mechanisms involved in generating vias and windows by laser radiation, offering valuable contributions to the understanding of laser interaction with polyimide-based flexible substrates in the context of electronic and manufacturing application.

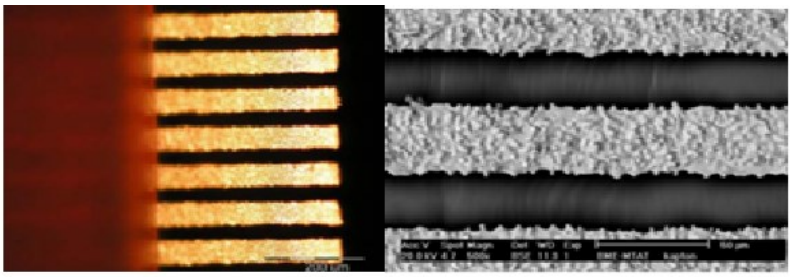

Figure 1.7 Microscopic view of processed polyimide-copper substrate (Left), SEM photo of completely cleaned Cu leads (Right) [16]

To Conclude, it is evident that in comparison to ultrasonic, cryogenic and chemical coating removal methods, laser ablation stands out due to its unparalleled precision and control in the material removal process. This technique is non-contact, which eliminates the risks of mechanical stress, abrasion, or contamination that can occur with ultrasonic or cryogenic methods. Laser ablation enables selective and localized removal of coatings, ensuring that only the coating is targeted without affecting the underlying substrate, which is critical when working with sensitive materials such as thin platinum wires. Furthermore, the process can be easily fine-tuned by adjusting parameters such as laser power, repetition rate, and scanning speed, allowing for high adaptability across different materials and coatings. Unlike chemical methods, which may introduce environmental hazards or leave residues, laser ablation offers a cleaner, more sustainable approach with minimal post-processing. Table 1.2 demonstrate the pros and cons of different stripping methods discussed in this document.

Table 1.2 Pros and Cons of different Coating stripping Methods

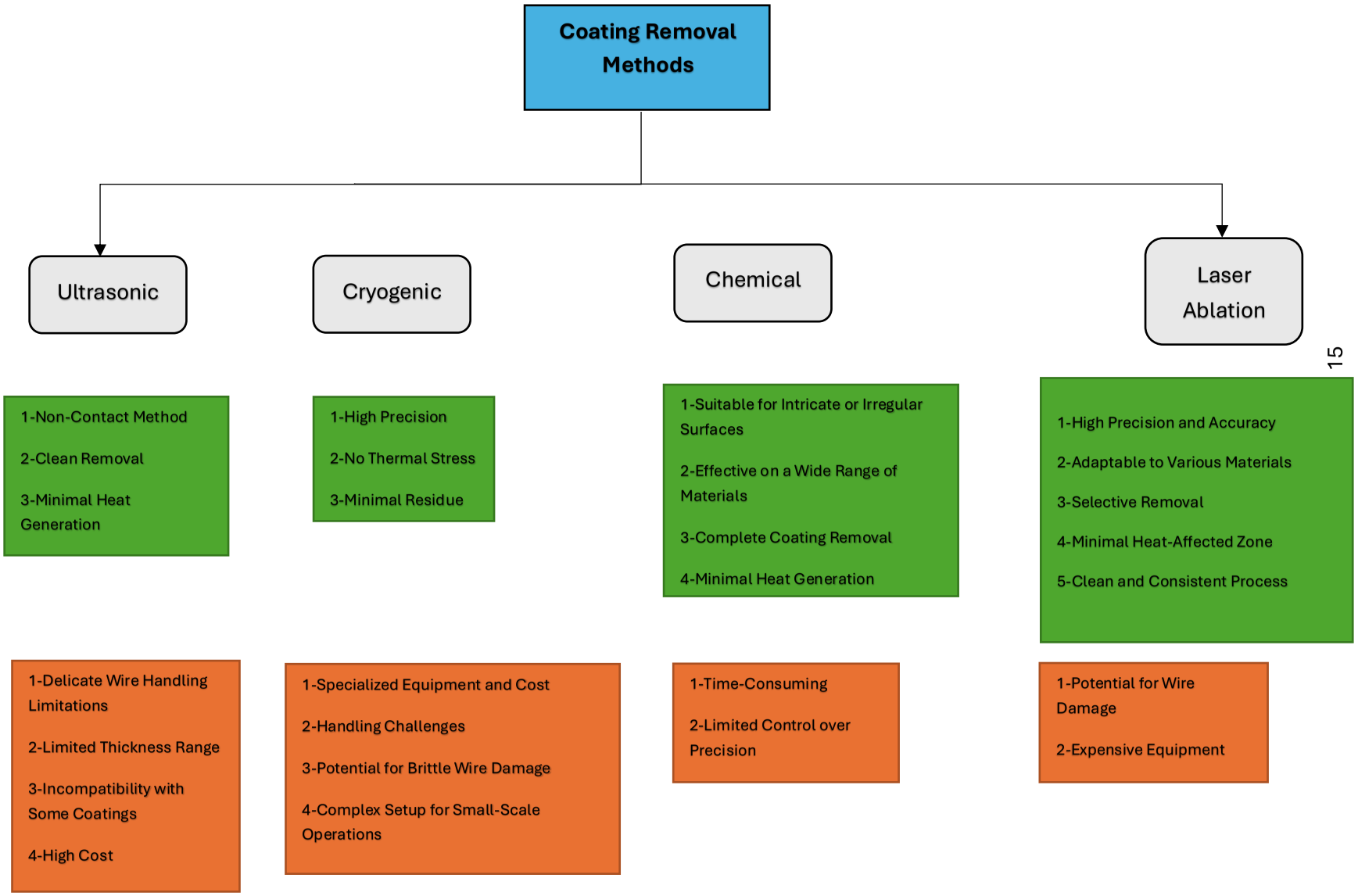

1.4 Types of Lasers in Industry

Lasers, short for "Light Amplification by Stimulated Emission of Radiation," are devices that emit coherent light through a process of optical amplification based on the stimulated emission of electromagnetic radiation. The core principle behind lasers involves stimulating atoms or molecules to emit light photons. When photons pass through an excited medium, they stimulate additional emissions of identical photons, leading to coherent light amplification. For sustained laser operation, a process known as "population inversion" is critical. As depicted in figure 1.8, Population inversion occurs when more atoms or molecules are in an excited state (higher energy level) than in their ground state (lower energy level) [17]. In industrial applications, several types of lasers are used based on material interaction and processing needs. Gas lasers, like CO_2 lasers, are widely used for cutting, welding, and engraving non-metals. Solid-state lasers, including fiber and Nd:YAG lasers, are favored for their high precision in metal processing. Excimer lasers, which use reactive gases, are ideal for delicate micromachining and surface treatments due to their very short ultraviolet wavelengths. Dye lasers, although less common industrially, offer tunable wavelengths for specialized applications. UV lasers, a type of solid-state laser, are particularly suited for fine processing tasks, minimizing heat effects and preserving material integrity. Each laser type is selected based on wavelength, energy, and the specific demands of the application.

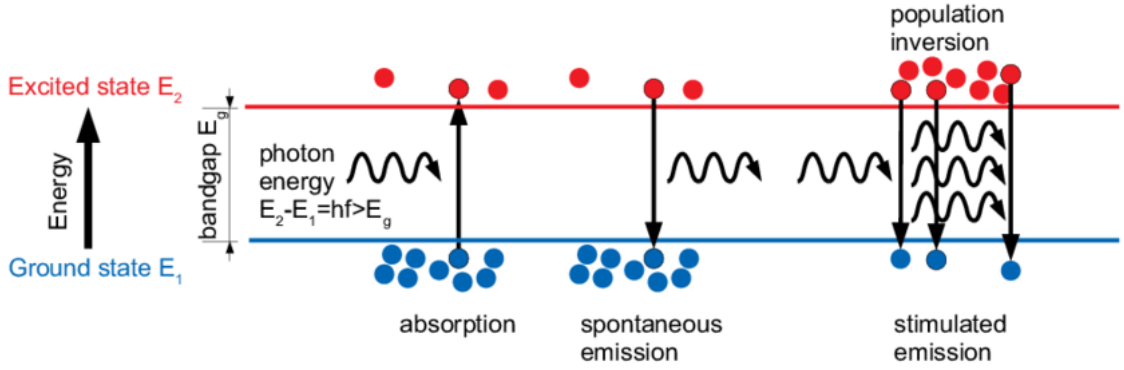

1.8 Fundamental Diagram of Laser Population Inversion [17].

1.4.1 Gas Lasers

These lasers use a gas mixture as the laser medium. Examples include helium-neon (He-Ne) lasers used in scientific and alignment applications, and carbon dioxide (CO_2) lasers used for cutting and welding metals. When an electric current is passed through the gas in the laser tube, the gas atoms or molecules are excited

to higher energy states. Then the excited atoms or molecules return to their lower energy states, they emit photons. These photons stimulate other excited atoms to emit more photons of the same wavelength and phase, leading to the amplification of light through the process known as stimulated emission [18].

1.4.3 Excimer Lasers

Excimer lasers are a type of gas laser that produces ultraviolet (UV) light by using a combination of noble gases and halogen gases. The name "excimer" is derived from "excited dimer," which refers to the temporary, excited-state molecules (or dimers) formed by the gas mixture [19]. These lasers are known for their high-energy UV output, short pulse durations, and ability to ablate materials with precision, making them widely used in various fields such as semiconductor manufacturing, medical procedures, and micromachining. Excimer lasers operate by exciting a mixture of noble gas (such as argon, krypton, or xenon) and halogen gas (such as fluorine or chlorine) to form an excited dimer. These dimers are unstable and quickly dissociate, releasing UV photons in the process. The UV light produced by excimer lasers is of short wavelength, typically in the range of 193 to 351 nanometers (nm) [20].

The UV light produced by the dissociation of the excimers is amplified as it bounces back and forth between the mirrors in the optical resonator. A portion of this amplified light escapes through the partially reflective mirror, forming the coherent UV laser beam. The UV light produced by excimer lasers has a very short wavelength, allowing for precise material processing and fine feature resolution, especially in semiconductor manufacturing and micromachining. Excimer lasers can produce high-energy pulses, which are effective in ablating or modifying materials quickly and efficiently [21].

It is important to note that UV lasers generated by excimer lasers are large, operate at repetition rates below 15 kHz, and are more complex with higher energy consumption.

1.4.4 Dye Lasers

Dye lasers are a type of tunable laser that uses organic dye molecules as the gain medium. These lasers are unique in their ability to emit light over a broad range of wavelengths, making them highly versatile for various applications in spectroscopy, medicine, and scientific research. Dye lasers operate by using a liquid solution containing organic dye molecules as the lasing medium. The dye is dissolved in a solvent, and

when excited by an external light source (usually another laser or a flashlamp), it emits light that can be amplified to produce a laser beam. The key feature of dye lasers is their tunability, meaning they can be adjusted to emit light across a wide range of wavelengths by changing the dye or the optical configuration of the laser [22].

1.4.2 Solid-State Lasers

Solid-state lasers operate by using a solid gain medium, typically crystal or glass doped with rare-earth ions, to amplify light. When pumped by an external energy source, such as a flashlamp or a diode laser, these ions become excited and emit light, which is then amplified to form a coherent laser beam [23]. The gain medium in a solid-state laser is typically a crystalline or glass material doped with ions, such as neodymium (Nd), ytterbium (Yb), or erbium (Er). Common materials include

(Neodymium-doped Yttrium Aluminum Garnet): One of the most widely used solid-state laser materials, emitting light at 1064 nm in the infrared spectrum.

(Titanium-doped Sapphire): Known for tunable wavelengths and ultrafast pulse generation, often used in scientific research.

(Erbium-doped YAG): Emits at 2940 nm and is commonly used in medical applications, particularly in laser surgery.

Solid-state lasers, especially those pumped by diode lasers, as depicted also in figure 1.9, offer high electrical-to-optical conversion efficiency, reducing energy consumption and heat generation. Solid-state lasers can deliver high peak power and pulse energy, making them ideal for cutting, drilling, and other material processing tasks. On the other hand, the high-power densities in the gain medium can lead to thermal effects, such as beam distortion or damage to the gain medium, necessitating efficient cooling systems. Also, while diode-pumped solid-state lasers are more efficient, they can be complex and expensive to manufacture, particularly for high-power or ultrafast applications. The wavelength of the emitted laser light can be tuned by adjusting the diffraction grating or prism within the optical cavity. This allows the user to select specific wavelengths, making dye lasers highly versatile.

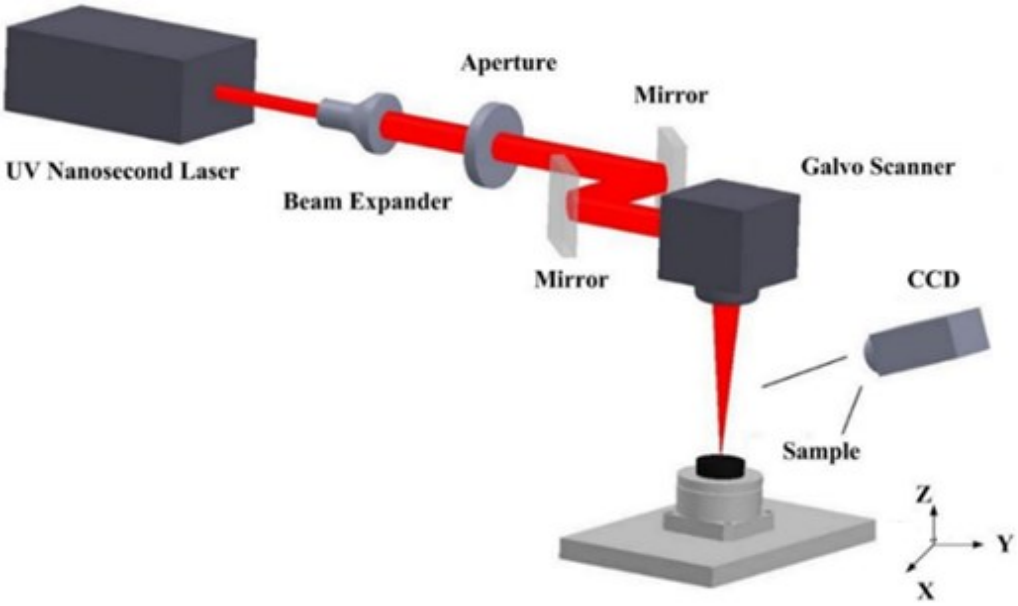

Figure 1.9 UV lasers principal diagram (Diode-pumped solid-state laser) [21]

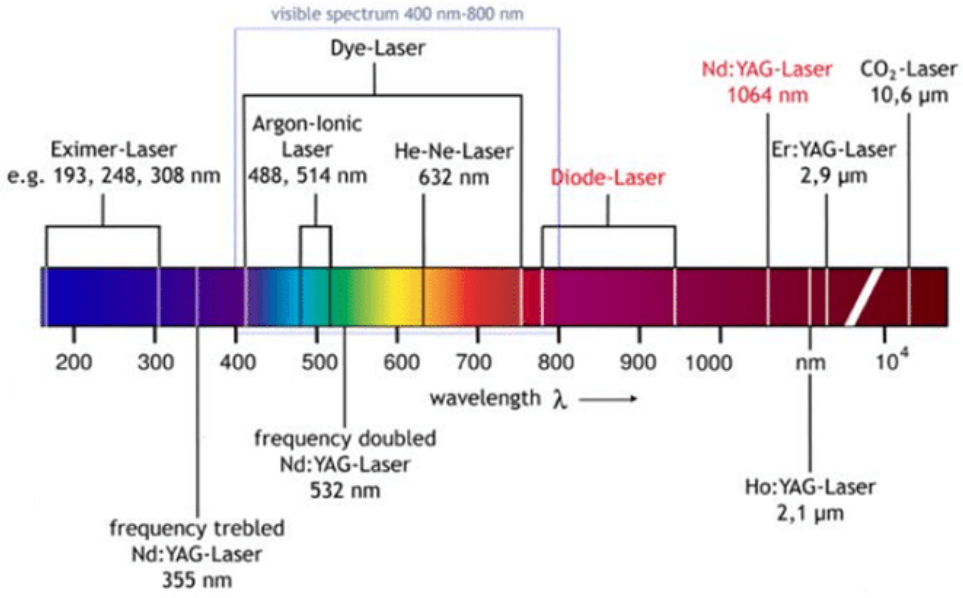

Figure 1.10 Wavelength-based application regions of different laser types. [24]

Table 1.3 Types of Lasers in Industry

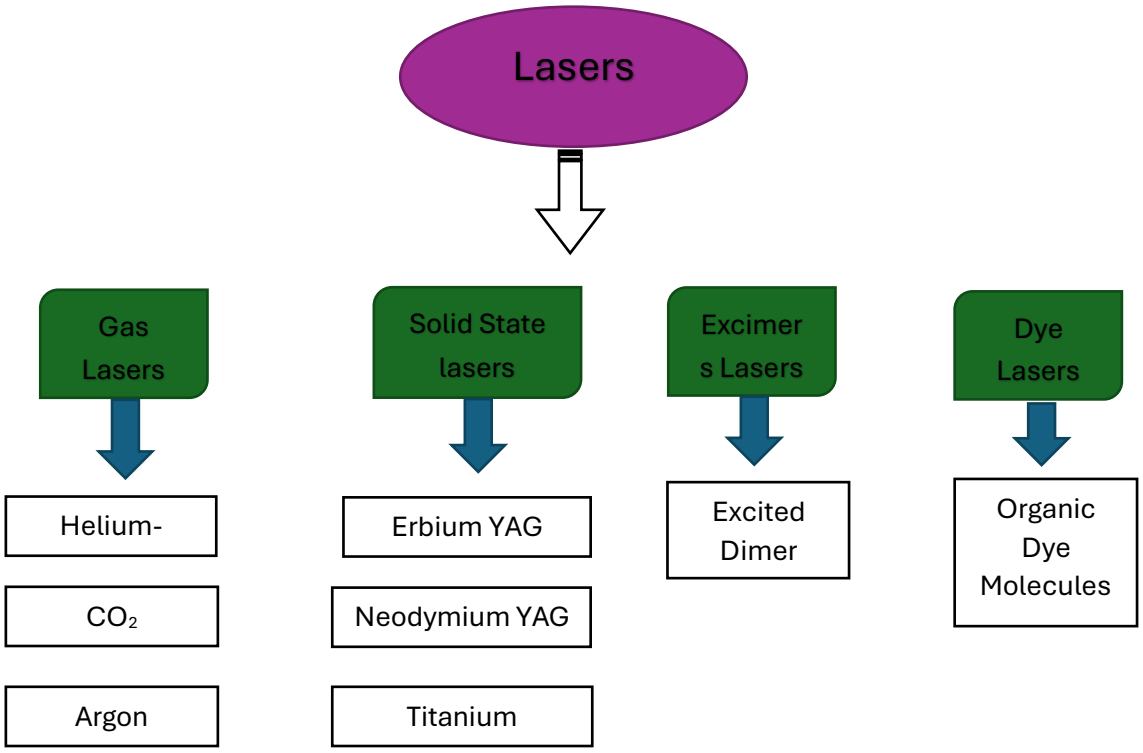

1.5 Laser Ablation

Laser ablation is a highly precise and versatile technique for removing material from a solid surface using a high-energy laser beam. This process begins with the focused laser beam irradiating the material, triggering material removal through sublimation, melting, or vaporization. Initially, the surface absorbs the laser energy as photons interact with the material's atoms or molecules. The energy of these photons exceeds the binding energy of the material, causing excitation of electrons to higher energy states. This absorption stage induces both thermal effects, such as heat generation, and non-thermal effects, including ionization or bond disruption, depending on the laser's wavelength and intensity [25].

In the subsequent energy deposition stage, the absorbed laser energy is transferred to the material, initiating significant physical and chemical changes. This localized energy causes ra[62pid heating of the material, raising its temperature well beyond its melting point in the exposed area. The material may transition from solid to liquid, and with continued energy input, the liquid phase may vaporize. At higher energy densities, the material can bypass the liquid phase and transition directly from a solid to a vapor state, often accompanied by the ejection of vaporized material. For effective material removal, several factors must be

considered based on the type of material. One critical factor is the laser wavelength, which determines how efficiently a material absorbs the laser's energy. Different materials have specific wavelengths at which they absorb energy most effectively. When the laser's wavelength aligns with the material's optimal absorption range, energy transfer is maximized, leading to efficient melting, cutting, or ablation. However, if the wavelength does not match the material’s absorption characteristics, the process efficiency can decrease, resulting in less precise or suboptimal outcomes.

The second critical factor is the laser's intensity and fluence, which determine the energy delivered to the material during processing. Intensity refers to the power per unit area of the laser beam, while fluence represents the total energy delivered per unit area during a laser pulse. Higher intensities and fluences deposit more energy into the material, significantly enhancing the ablation process. Greater fluence enables deeper penetration and more substantial material removal per pulse, making it advantageous for rapid processing or for materials requiring higher energy due to their hardness or thickness [26].

However, excessively high intensities or fluences can lead to undesirable outcomes, such as thermal damage, melting, or plasma formation, potentially compromising the material's quality. Achieving the optimal balance of intensity and fluence is therefore essential for precise, efficient, and high-quality material processing.

Figure 1.11 illustrates the relationship between laser fluence and ablation depth when single pulses of excimer lasers at wavelengths of 193 nm (A) and 248 nm (B) are used. The graphs show that as laser fluence increases, the ablation depth also increases, following a generally linear trend. The point where each fitted line intersects the fluence axis represents the ablation threshold, the minimum fluence required to initiate material removal. Moreover, the slope of the fitted lines can be used to estimate the effective absorption coefficient of the material at each wavelength, reflecting how efficiently the material absorbs laser energy during ablation.

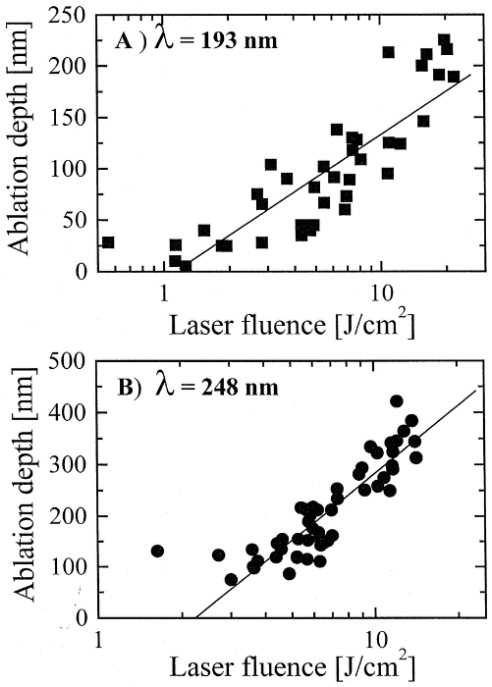

Figure 1.11 ablation depth versus laser fluence for single pulses of (A) 193 nm and (B) 248 nm on excimer laser.

The other critical parameter is pulse duration (or pulse width), which significantly impacts the precision and quality of material processing. Shorter pulse durations, measured in femtoseconds or picoseconds, are highly effective at minimizing thermal diffusion, confining the heat generated by the laser to a small area. This reduces the risk of heat spreading to surrounding regions, enabling precise material removal with minimal thermal damage. Such short pulses are particularly suitable for intricate detailing, delicate materials, and applications requiring high precision. In contrast, longer pulse durations, such as those in the nanosecond range, deliver laser energy over an extended period. This allows more time for heat to diffuse into adjacent areas, creating a broader heat-affected zone. While this can be advantageous for applications requiring deeper penetration or gradual heating, it may compromise precision and increase the likelihood of thermal damage or unintended alterations to nearby regions [27]. As shown in figure 1.12, setting the machine to a lower pulse width reduces debris and penetration depth while significantly enhancing the accuracy of ablation, resulting in minimal damage to the substrate [28].

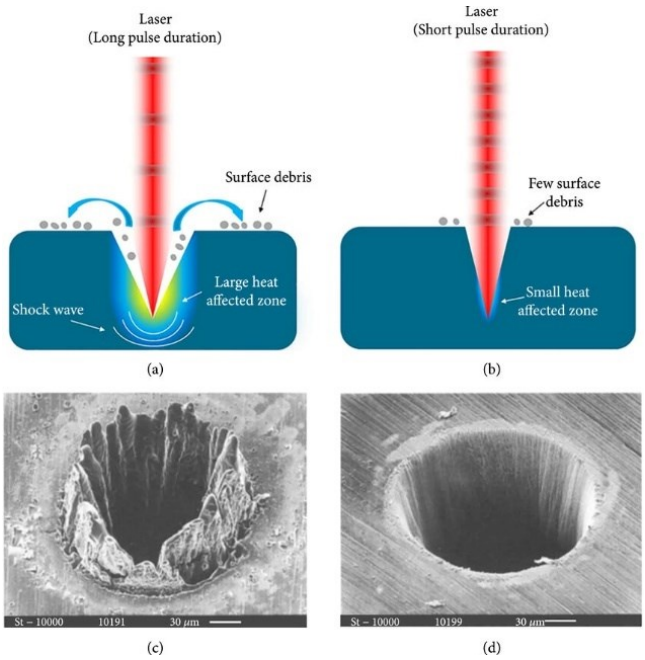

Figure 1.12 Schematic of laser interaction with materials under different pulse durations: (a) long pulse duration (b) short pulse duration. SEM images of laser ablated holes fabricated on a 100 μm steel foil by (c) 780 nm nanosecond laser of 3.3 ns, 0.5 J/cm² and (d) 780 nm femtosecond laser of 200 fs, 0.5 J/cm² [27]

1.7 Motivation of work

This project was driven by the need to develop a precise, reliable, and non-damaging method for removing polyamide coatings from ultra-fine platinum wires. Extensive experimentation in both air and water environments revealed that laser ablation in a water ambient significantly improved surface quality and preserved mechanical strength, outperforming conventional stripping methods. Motivated by these findings, the study focuses on fine-tuning the laser parameters to achieve optimal insulation removal, benchmarking the mechanical and surface properties of untreated, chemically stripped, and laser-stripped wires to validate the process, and laying the groundwork for designing a fixture and optical monitoring system to ensure uniform ablation along the entire wire circumference. These efforts collectively target the development of a more controlled, scalable, and industry-relevant process for precision wire preparation.

1.8 Objective for work

The primary objective of this project is to develop and optimize a laser-based method for removing polyamide insulation from ultra-thin platinum wires used in aerospace thermocouples, ensuring high precision, repeatability, and minimal damage to the substrate. The focus is on utilizing a UV laser system to identify optimal ablation parameters such as laser power, scanning speed, line distance, focal length,

overlap percentage, and number of loops to achieve effective coating removal while preserving the structural and mechanical integrity of the wire. A key aim is to ensure the post-ablation surface is suitable for subsequent soldering without requiring additional processing. To evaluate the thermal and mechanical effects of laser ablation, tensile strength and surface roughness measurements are conducted on untreated, chemically stripped, and laser-stripped wires. These results are benchmarked to determine the relative performance of each method and guide further refinement of the laser settings. Moreover, recognizing the challenge of achieving uniform coating removal around the cylindrical surface of the wire, the project also includes the design and development of a mechanical fixture capable of holding and rotating the wire during ablation. This fixture will feature a secure clamping system with a window for laser access, as well as a high-resolution machine vision setup to aid in precise alignment and inspection. The overall goal is to establish a reliable, high-precision, and operator-friendly system that can be integrated into future manufacturing environments for micro-scale wire processing.

1.9 Organization of the thesis in manuscript-based format

This thesis, structured as a manuscript, consists of five chapters. The current chapter outlines the key reasons behind the need for coating removal in industrial manufacturing and provides an overview of various methods used for this purpose. Laser ablation is highlighted as a cost-effective and precise technique for coating removal in microscale components. Chapter 2 provides a detailed description of the experimental setup, including information on laser adjustments and the controlling software. Chapters 3 and 4 are reproduced from previously published and submitted journal articles. These chapters are presented in a cohesive manner to address the objectives outlined in Section 1.3 and are formatted in accordance with the "Thesis Preparation and Thesis Examination Regulations (version-2013)" of the School of Graduate Studies at Concordia University.

Chapter 3 is based on the following article submitted in journal of Manufacturing and Material Processing, with ID of (JMMP-3611490), Danial Rahnama, Sivakumar Narayanswamy and Graziano Chila "UV Nanosecond Pulsed Laser Parameter Optimization for Removal of Polyamide Coatings from Fine Platinum Wires", Under Review.

In this study we investigated the optimization of a laser ablation process for the precise removal of polyamide coatings from thin platinum wires, with a total diameter of 50 µm, approximately 15 µm of which is coated with polyamide. Initial attempts using air-based ablation were unsuccessful due to

inadequate thermal control and incomplete removal of the coating. To overcome these limitations, a water-assisted ablation technique was explored. A UV laser with a wavelength of 355 nm, a peak power of 3W, and a repetition rate range of 20 to 200 kHz, along with a high-speed marking system, were employed to refine process parameters. Experimental results revealed that a scanning speed of 1200 mm/s, line spacing of 1 μm, and a single pass of ablation effectively removed the coating while preserving the platinum substrate's integrity. The inclusion of a water layer above the ablation region proved essential for efficient heat dissipation, preventing substrate overheating and ensuring uniform removal. Challenges arising from the laser's spot diameter of 20 μm and focal length of 130 mm were addressed through careful calibration to control overlap between successive passes. This work demonstrates the feasibility and reliability of water-assisted laser ablation as a high-precision, non-contact material processing technique for coating removal.

Chapter 4 is Submitted in the journal of Manufacturing and Material Processing with ID of JMMP-3657195, which investigates improvements in surface roughness (Ra), ablation depth, and tensile strength using ANOVA analysis to provide a deeper understanding of the overall process constraints.

This study investigates the optimization of UV nanosecond pulsed laser parameters for the precise removal of polyamide coatings from ultra-thin wires. Through controlled experimentation and statistical analysis using ANOVA, key process parameters including scanning speed, line spacing, number of loops, and overlap percentage were evaluated for their influence on surface roughness (Ra), ablation depth, and tensile strength. The findings highlight critical process constraints and interdependencies that govern the balance between effective coating removal and preservation of wire integrity. Results indicate that specific configurations, particularly those involving moderate scanning speeds with high overlap and multiple passes, yield superior surface quality and minimal thermal damage. The comprehensive analysis provides insight into how laser material interactions can be tailored to meet microengineering application demands, supporting the development of reliable and scalable laser-based wire stripping techniques.

Chapter 5 is the conclusion of the work along with some suggestions for the future work.

1.10 Summary

The progression of wire coating removal techniques plays a pivotal role in enhancing the precision, reliability, and sustainability of contemporary manufacturing processes, particularly in critical sectors such as aerospace, biomedical, automotive, and advanced electronics. This study has undertaken a

comprehensive analysis of various de-coating methodologies, including ultrasonic stripping, chemical stripping, cryogenic treatment, and laser ablation, with a focus on their effectiveness, limitations, and applicability to micro-scale wire systems such as those found in medical devices and ultra-fine platinum conductors.

Among the methods investigated, laser ablation demonstrates significant advantages over traditional approaches. This technique provides exceptional precision, selective removal capabilities, minimal thermal influence on the substrate, and adaptability to a wide range of materials and coating types. The use of ultraviolet nanosecond-pulsed lasers has proven effective in achieving high-quality removal of polyamide coatings without compromising the integrity of the underlying platinum wires. Additionally, the integration of a water-assisted environment further enhances the thermal management of the process, facilitating improved energy dispersion and protection of delicate substrates.

In contrast, ultrasonic and cryogenic methods, although viable in specific industrial contexts, exhibit substantial challenges when adapted to fine wire applications. These include difficulties in maintaining uniform energy distribution and risks associated with mechanical or thermal damage to sensitive wire structures. Similarly, chemical stripping, while commonly employed due to its simplicity, introduces environmental and safety hazards, and often lacks the precision required for micro-scale operations, especially in cleanroom or biomedical settings. The findings of this research underscore the superiority of laser-based stripping processes not only in terms of technical performance but also in alignment with sustainable manufacturing objectives. Laser ablation eliminates the reliance on hazardous solvents, reduces material waste, and enables localized, high-speed processing, thereby supporting eco-efficient production strategies. Furthermore, this work highlights the importance of optimizing key laser parameters, including wavelength, pulse duration, scanning speed, and fluence. These parameters are critical in achieving controlled energy deposition, minimizing the heat-affected zone, and ensuring selective ablation of the coating without impairing the substrate. Statistical modeling and experimental validation, as referenced in this study, contribute to a deeper understanding of laser-material interactions and provide a foundation for further refinement of the process.

CHAPTER 2. Materials and Methods

2.1 Introduction

As outlined in Section 1.8, the aim of this work is to remove coatings from wires using laser ablation. To achieve a cleanly ablated surface free from debris and coating residues, the effects of various laser parameters and ambient conditions were investigated. Additionally, mechanical properties such as surface roughness and tensile strength were analyzed. Different experimental factors, including laser repetition rate, number of loops, pulse overlap, line distances in both X and Y directions, and ambient conditions were varied. During each experimental phase, parameters like the Speed, number of loops or line distance in X direction were adjusted. It is important to highlight that the specimens used in this project have a platinum substrate, which must be preserved without damage during the coating removal process. These wires are specifically intended for RTD (Resistance Temperature Detector) manufacturing for aerospace applications, where they are installed in stators to measure precise temperatures. Given the space limitations within stators, producing highly sensitive sensors is critical. The detailed manufacturing process for these samples will be explained in the following section.

2.2 Sample Description

The samples used in this study are platinum wires coated with a specific polyamide. The platinum substrate has a diameter of 50 µm, while the polyamide coating adds 15 µm, resulting in a total wire diameter of 65 µm, as shown in Figure 2.1. These wires are wound around a specially designed rectangular paper core using a winding machine, as illustrated in Figure 2.2, with the winding pitch varying depending on the product model. The final product is an RTD sensor installed in stators for high-precision temperature measurement.

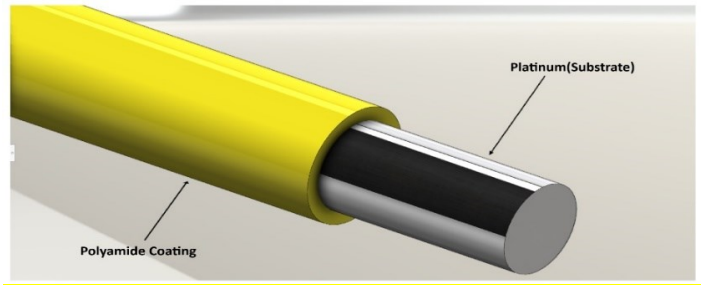

Figure 2.1 shows platinum wire coated with 15 µm of polyamide coating (SolidWorks).

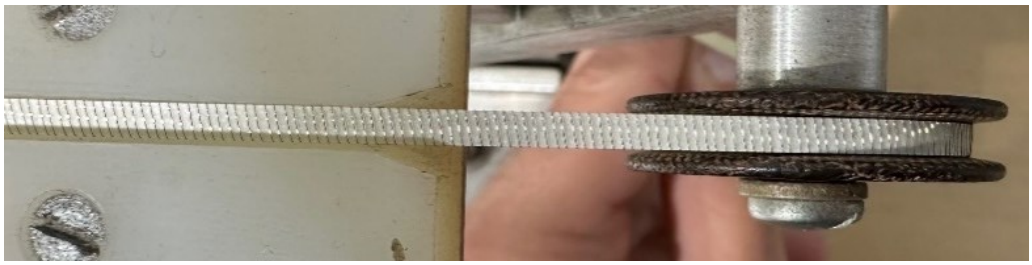

Figure 2.2 shows platinum wires wound around a rectangular paper core

After wires being wound, a special heat-protective wax is applied to one end of the wires and the paper core to secure and protect them during handling. However, the first 5 mm from the wire tips are intentionally left unwaxed. This unwaxed portion allows the operator to easily unwind and straighten the two wires. The wax is then applied over the next 20 mm of the wound section to fix the wires firmly to the core, preventing deformation or breakage. After unwinding the 5 mm tips, the straightened wires are approximately 15 mm long, providing sufficient length for stripping process and subsequent soldering onto a Printed Circuit Board (PCB), an essential step in the manufacturing process. Figure 2.3 illustrates the wound wires after waxing and chemical stripping, prepared for PCB soldering onto the stripped wire ends.

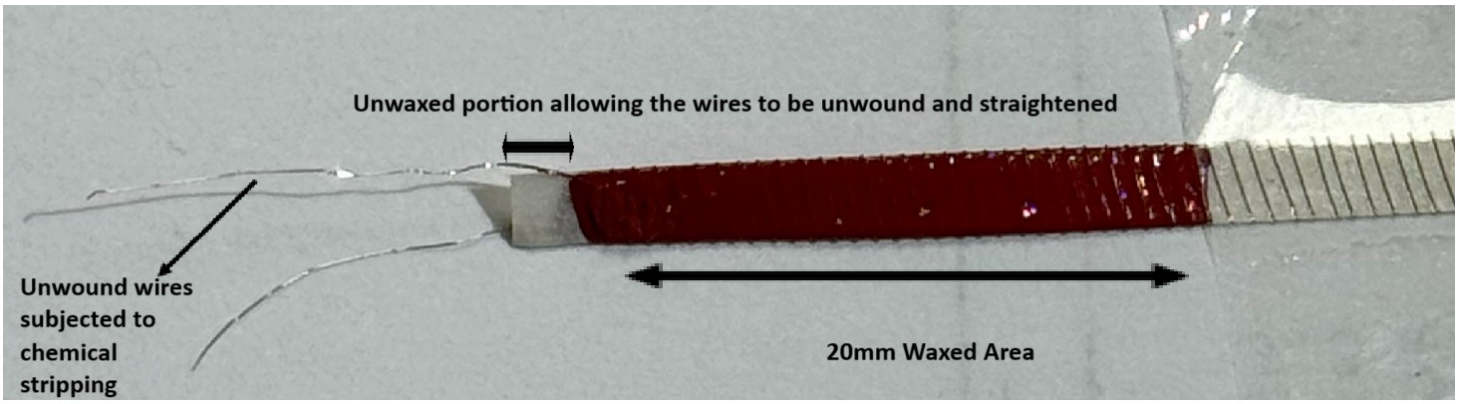

Figure 2.3 Wires stripped at one end, prepared for soldering onto the PCB.

It is important to note that, traditionally, stripping was performed using chemical processes involving corrosive solutions, which were both time-consuming and posed significant hazards to the operator, thereby necessitating the need to find an alternative process.

2.3 Laser Setup

The laser system employed in this study was the UV Series 355-3W from Mactron, operating at a wavelength of 355 nm with a minimum pulse duration of 18 ns and featuring a Gaussian beam profile. It delivers pulsed output with a repetition rate adjustable between 20 and 200 kHz. As illustrated in Figure 2.4, the laser's peak power depends on the repetition rate, reaching its maximum at the lowest setting of 20 kHz. In the figure, τ represents the pulse width which is the duration of each emitted pulse and RR denotes the repetition rate.

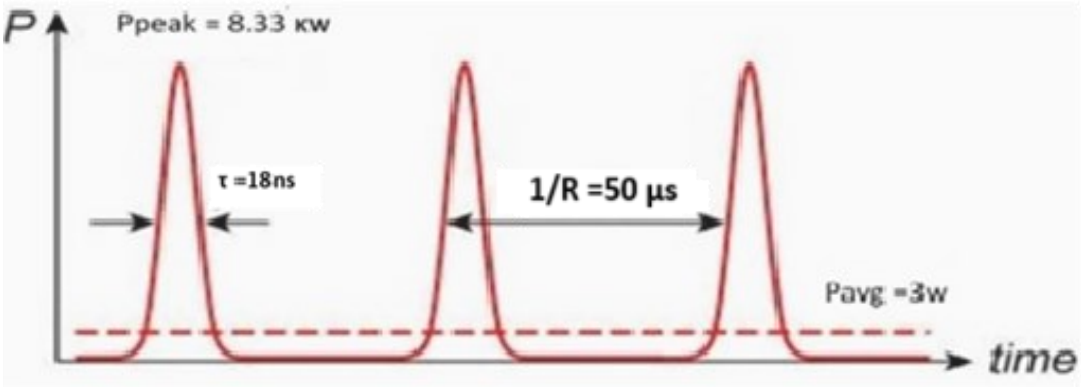

figure 2.4 Temporal profile of the laser power [29]

The optical system was precisely aligned to ensure that the laser beam passed through the central axis of both the galvanometric (galvo) scanner and the F-Theta focusing lens. The galvo head is mounted on a Z-axis adjustable stage, enabling fine control over the focal position. Accurate alignment is aided by two angled continuous laser beams that converge into a single point when the system reaches the correct focal plane, indicating optimal focus.

As illustrated in Figure 2.5, the laser beam is focused through the F-Theta lens to a designated focal point. The focal distance (measured vertically from the lens to the focal plane) represents the point at which the beam achieves its smallest spot size and maximum energy concentration. The focal range denotes the tolerable depth over which the focus remains effective. This configuration is widely used in galvanometric scanning systems for precision laser micromachining, as it ensures consistent focal performance across the working field. In this system, the focal distance is calibrated to 130 mm. The employed machine as of figure 2.6, is a Diode-Pumped Solid-State (DPSS) laser. Although its output power is fixed, the effective power delivered to the sample can be modulated by adjusting the pulse width and repetition rate.

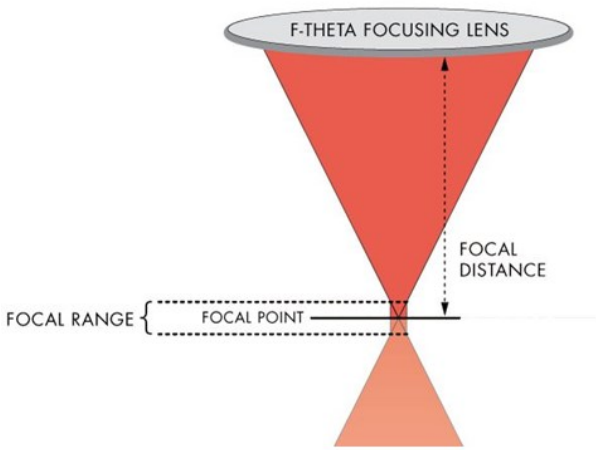

Figure 2.5, Schematic representation of a laser beam focusing through an F-Theta lens

Figure 2.6, Schematic of the laser ablation experiment [30]

2.4 Software for control

The laser system operates using dedicated control software known as EZCad, which is installed on a PC and interfaces with the laser via a specialized communication cable. This software enables the user to define the laser machining area with precision. As shown in Figure 2.7 (inset A), the operator begins by outlining the ablation region, typically a 10 mm × 5 mm rectangular area, where the laser processing will be performed. A critical parameter in this process is the line distance, which determines the spacing between successive laser scan lines. In this study, a range of line distances was explored, from larger intervals down

to finer scales, in order to evaluate the laser's behavior on microscale samples. Figure 2.7B highlights a case where the line distance along the X-axis was set as low as 1 µm, representing the finest spacing used. Additionally, the laser processing conditions can be further optimized by adjusting parameters such as scanning speed, repetition rate, pulse width, and the number of loops (passes), all of which are shown in the software interface depicted in Figure 2.7C.

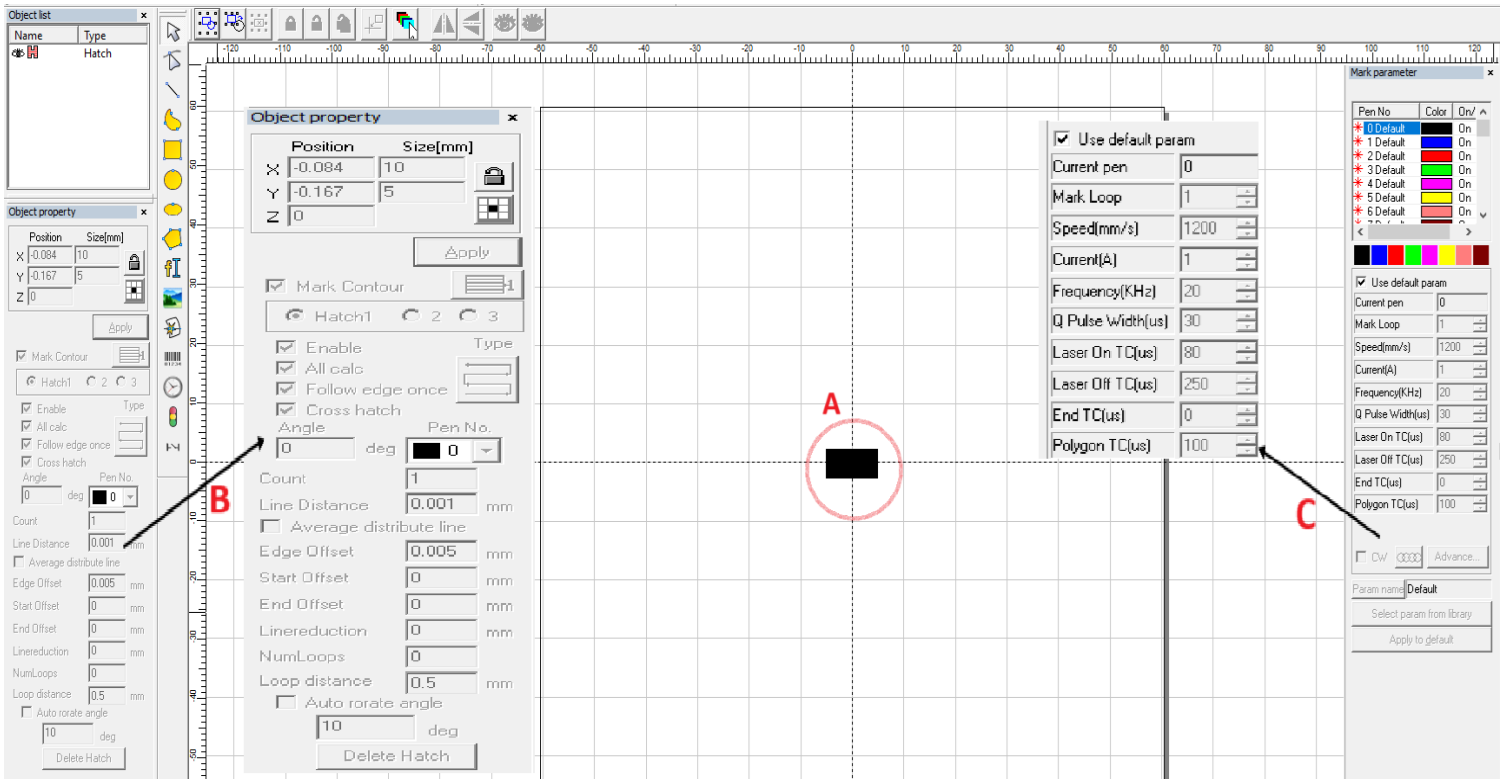

Figure 2.7 Screenshot of the UV2(ezcad) program.

2.5 Design of experiment

In this study, statistical analyses were conducted to investigate the effects of laser fluence, pulse overlap, number of loops, and processing speed on the Average surface roughness (Ra) and tensile strength of polyamide-coated platinum wires. The evaluation process involved the application of Analysis of Variance (ANOVA) and regression analysis to interpret the results effectively. Measurements were performed using a 3D confocal microscope, an optical microscope, and a Universal Testing Machine (UTM).

For this work, the pulse repetition rate was set to 20 kHz and the pulse width to 18 ns. These minimum values were chosen to achieve deeper ablation per pulse, reduce heat diffusion, and ensure precise material

removal without damaging the platinum substrate. These parameters were kept constant throughout all experiments. while the power is fixed at 3 watts, resulting in a peak laser power of 8.33 kW, as calculated using equation 2.1 [31].

$$\text{P peak} = \frac{\text{Average Power}}{\text{Pulse Duration} \times \text{Repetition Rate}} \qquad \text{equation 2.1}$$

Another important factor is overlap, which is controlled by speed and line distance on X. The line distance on the X-axis is managed by the software, while on the Y-axis, it is controlled by the machine's speed, which can be calculated using equation 2.2. For instance, if the line distance is set to 5 µm with a speed of 500 mm/s, the distance between each spot on the X-axis is 5 µm, but on the Y-axis, the distance for the next pass of ablation is 25 µm. These factors influence the overlap during the process.

$$\text{Line Distance (Y)}: \frac{\text{Speed}(\frac{\mu m}{s})}{\text{Repetition rate(Hz)}} \qquad \text{equation 2.2}$$

The overlap on the sample surface during the laser ablation process is determined using Equation 2.3, and in the designed experiments, this value ranged between 75% when the line distance was set at 5 µm and 95% with line distance of 1 µm. Initial trials with lower overlap values, achieved by employing larger line distances like 10 to 15 µm, were also conducted. However, the results were unsatisfactory, as these configurations failed to effectively remove the coating. Consequently, these attempts were excluded from further analysis and the experimental setup was refined.

$$\text{Overlap}: \frac{\text{Spot Diameter} - \text{Line Distnace}}{\text{Spot Diameter}} \qquad \text{equation 2.3}$$

Initial experiments were conducted in both air and water environments using line distances ranging from 10 to 15 µm. Microscopic observations indicated partial thermal alteration of the coating, though complete removal was not achieved, and the platinum substrate remained unaffected, as shown in Figure 2.8 (Right). In contrast, experiments in air with lower overlap settings resulted in wire damage and burning in several samples. For instance, Figure 2.8 (Left) illustrates a case where a 5 µm line distance, a scanning speed of 500 mm/s, and a single loop led to significant wire degradation. This highlighted the inadequacy of lower overlap percentages and larger line distances in achieving the desired outcomes. To overcome these limitations, subsequent experiments were designed with increased overlap percentages and significantly reduced line distances. These refined configurations aimed to optimize coating removal efficiency while ensuring the integrity of the platinum substrate. Specifically, line distances of 1 and 5 µm (representing the

spacing between laser pulses along the X direction) were employed, combined with varying laser speeds. This systematic approach ensured precise ablation, enabling complete coating removal without causing damage to the underlying substrate [32].

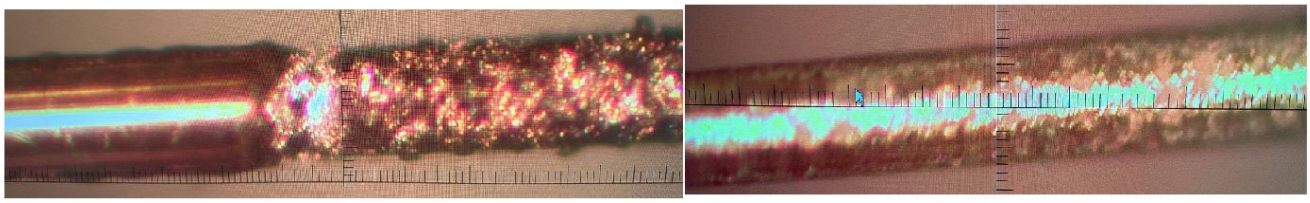

Figure 2.8: Samples ablated in air ambient using 15 µm line distance (right) and 1 µm (left) line distances both with speed of 1000mm/s.

2.5.1 Laser fluence

The laser fluence (F) is a critical parameter that defines the laser energy applied to a specific area, as represented by Equation 2.4. Fluence quantifies the energy delivered by the laser over a given area, making it an essential factor in processes such as material ablation, melting, and surface modification [33]. The energy of a single laser pulse(E) is calculated using Equation 2.5. This energy characterizes the amount of energy delivered to the target material during each laser pulse, directly influencing the effectiveness of material processing techniques [34].

$$F\ (\text{Gaussian}) = \frac{2E\ \text{Pulse}}{\text{Area}} \qquad \text{equation 2.4}$$

$$E_{\text{Pulse}} = P_{\text{peak}} \times \tau_{\text{Pulse}} \qquad \text{equation 2.5}$$

Where, F is the laser fluence, E is energy of a single laser pulse, τ is the pulse width of the laser.

the laser system emits Gaussian-shaped pulses, with the pulse duration measured at Full Width at Half Maximum (FWHM). This formula assumes that the pulse duration at FWHM is already an appropriate measure of the pulse width, and no additional correction factor is needed.

The values for laser fluence used in this work in both ambientes, based on upon calculation is constant and 95.5 J/cm^2.

2.5.2 Overlap

As illustrated in Figure 2.9, another critical parameter examined in this study was the pulse overlap percentage. According to Equation 2.3, the overlap in the X direction is governed by the line distance, which is configured within the software. Meanwhile, the overlap in the Y direction is influenced by the scanning speed, as defined in Equation 2.2 [36]. At higher scanning speeds, the distance between successive spots in the Y direction increases, potentially leading to gaps and zero overlap. Conversely, smaller line distances in the X direction can result in excessive overlap. Therefore, achieving an optimal balance between these two parameters is essential. As previously discussed, results obtained from large line distances, associated with low overlap percentages were not satisfactory. Consequently, for air ambient experiments, overlap values of 75% and 95% were selected based on the calculated parameters.

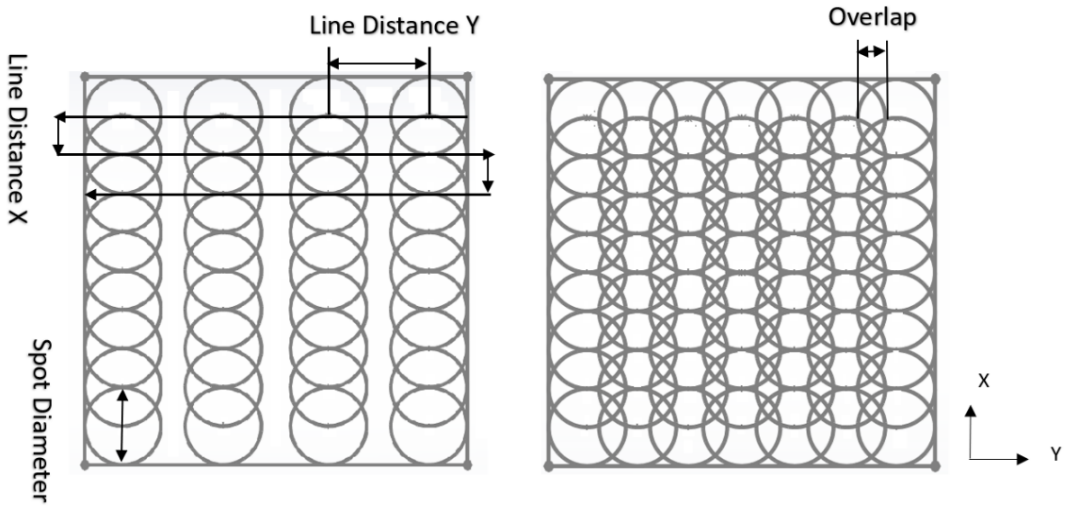

Figure 2.9: Schematic demonstrating the spot overlaps in both axis (Right) and line distance in X and Y which caused gaps in Y (Left).

.

2.5.3 Number of loops

The number of loops represents the count of repeated exposures the wire undergoes under identical laser settings during the ablation process. Each loop reintroduces the laser beam over the same path, ensuring that the energy delivered to the surface accumulates over multiple passes. This repeated exposure is particularly beneficial for thorough processing, as it enhances the likelihood of complete material removal or surface modification, especially in cases where single-pass ablation might be insufficient due to material properties, coating thickness, or processing conditions.

Twelve experimental sets were conducted in air ambient and eight with the wire immersed in water. The detailed laser and scanning parameters for these experiments are presented in Table 2.1 and Table 2.2, respectively. Notably, Table 2.2 shows variations in overlap values, which is influenced by the effective spot diameter that is different in water. This change can result in increased overlap along the Y-axis as well. The underlying reasons for this phenomenon will be discussed in the following chapter.

Sample number	Overlap (%)	Line distance X (μ)	Line distance Y (μ)	Speed (mm/s)	Number of loops
1	95	1	25	500	1
2	75	5		500	1
3	75	5		500	2
4	95	1	50	1000	1
5	75	5		1000	1
6	75	5		1000	2
7	95	1	60	1200	1
8	75	5		1200	1
9	75	5		1200	2
10	95	1	75	1500	1
11	75	5		1500	1
12	75	5		1500	2

Table 2.1 adjustment of laser machine for experiment in air

Sample number	Overlap (%)	Line distance (μ)	Line distance Y (μ)	Speed (mm/s)	Number of loops
1	97.77	1	25	500	1
2	88.88	5		500	2
3	97.77	1	50	1000	1
4	88.88	5		1000	2
5	97.77	1	60	1200	1
6	88.88	5		1200	2
7	97.77	1	75	1500	1
8	88.88	5		1500	2

Table 2.2 adjustment of laser machine for experiment in water.

2.6 Experiments in Air Ambient

As illustrated in Figure 2.10, the samples were securely mounted on a cardboard holder featuring a 5×5 cm window for laser ablation. To achieve confocal focus, the two red laser guide beams were aligned to converge at the same point, ensuring accurate focal height, this alignment was performed on the top surface of the wires. once focus was achieved, the holder was positioned under the defined laser scanning area. The hatch region was set in the software to 10×5 mm with a line distance of 1 µm in the X direction. Based on the parameters listed in Table 2.1, a series of experiments were conducted. However, the results across all samples were unsatisfactory, as all results follows in next chapter.

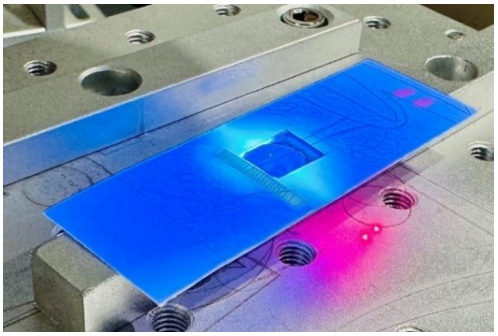

Figure 2.10 sample setup under laser machine for ablation in air ambient.

It became evident that the 20 µm laser spot diameter was insufficient to bridge the spacing in the Y direction, especially at high scanning speeds. Additionally, the energy deposition was excessive, leading to burning and weakening of the wires despite various combinations of speeds, overlaps, and loop counts. This outcome indicates that air-based laser ablation is not suitable under these conditions. For reference and comparison, chemical stripping was also performed. Visual inspection confirmed that none of the air-based laser-treated samples approached the quality achieved through chemical stripping.

2.7 Experiments in Water Ambient

Following the unsuccessful results in air ambient, the experiments were transitioned to a water environment to better manage heat dissipation and control energy deposition on the wire surface. The optical alignment and the sample fixation method using cardboard holders remained unchanged. However, the setup was

modified by placing the weight inside a container and gradually adding water until the wires were fully submerged as of figure 2.11. Through a series of trials, it became evident that the volume of water surrounding the wires played a critical role in the ablation outcome. Initially, the container was filled halfway, but this resulted in insufficient energy delivery to the wire surface. Water was then incrementally added using injectors, and it was determined that maintaining approximately 2–3 mL of water around the wires yielded the most satisfactory results.

To prevent any movement during ablation, the cardboard holders were secured at the bottom of the container using two weights. Despite visually aligning the wires straight in both air and water setups, microscopic observation revealed minor undulations and laminations along the wires. These imperfections likely contributed to uneven energy distribution during laser exposure and underscore the necessity of developing a dedicated fixture for future work.

Nevertheless, before implementing a precise mechanical fixture, it was essential to first validate the feasibility and effectiveness of laser ablation under controlled water conditions.

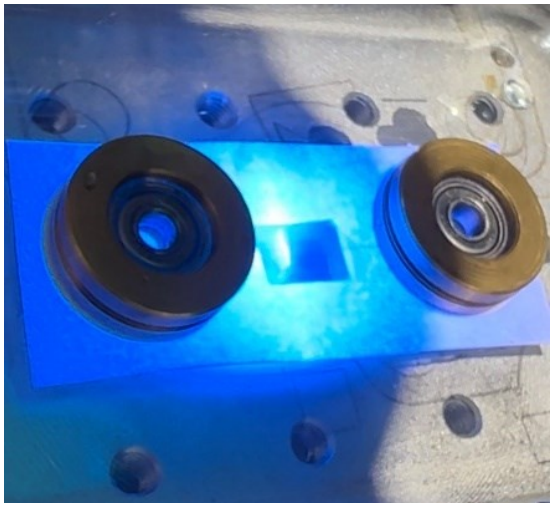

Figure 2.11 sample setup under laser machine for ablation in water

The experiments conducted in air offered valuable insights into the behavior of the samples under specific conditions. At high scanning speeds, samples processed with a 5 µm line distance and a single loop exhibited thermal effects on the coating, but complete removal was not achieved. When the number of loops was increased to two, while keeping the same line distance, partial removal was observed in some areas. These results indicated that a single loop with 75% overlap was insufficient for effective ablation.

As a result, subsequent water-based experiments were modified to eliminate single-loop trials at 88.88% overlap, as they had previously proven ineffective. Instead, all experiments with this overlap percentage were carried out using two loops to improve coating removal consistency. It is important to note that all initial calculations in the water ambient were based on a 20 µm spot diameter. However, as further discussed in Chapter 3, the presence of water and the incident angle, combined with the circular geometry of the wires, led to an effective increase in spot diameter. This change affected both the overlap percentage and the laser fluence. Interestingly, this unintended increase proved beneficial, as it helped compensate for energy gaps and provided more controlled and uniform energy delivery to the wire surface during ablation.

As previously mentioned, the scope of these experiments was not limited to the stated values. Initial tests were conducted at speeds below 500 mm/s and above 1500 mm/s, as well as with larger line distances resulting in low overlap factors. However, these tests yielded unsatisfactory results, failing to achieve the desired outcomes. Consequently, they were deemed ineffective and excluded from further analysis to focus on more promising parameter ranges. Figure 2.12 presents selected samples processed at both low and high scanning speeds in air. The corresponding results from water-based experiments will be discussed in Chapter 3.

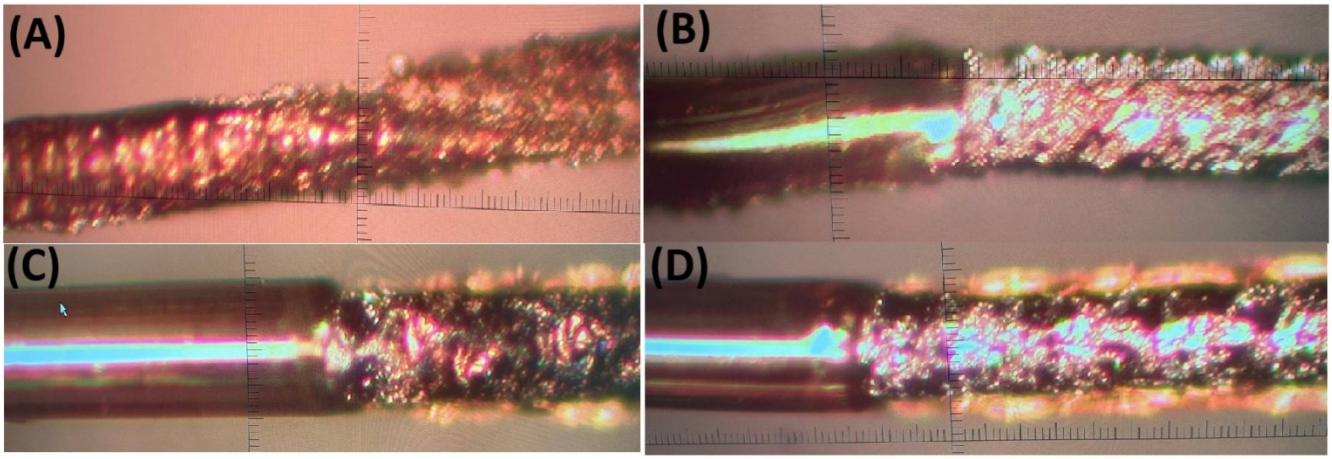

Figure 2.12 (A) speed of 100mm/s-5 µm line distance. (B) speed of 300mm/s- 5 µm line distance (C)speed of 1000mm/s-1 µm (D) speed of 1000mm/s- 2 µm line distance.

2.8 Surface Visual Test

To analyze the surface of the wires and evaluate the degree of removal after each ablation process, a high-magnification microscope equipped with an external camera and integrated measurement software was

utilized. This setup enables detailed examination of the wire's surface at various stages of the de-coating process. The microscope provides a close inspection of surface conditions, while the measurement camera and software offer precise assessments of wire thickness and coating removal. This arrangement ensures effective monitoring of the de-coating process, allowing for accurate evaluation of the results. By thoroughly assessing the post-process condition of the wire, any areas requiring further attention or adjustments can be identified, ensuring consistent quality and achieving the desired outcomes for the project. figure 2.13 shows a sample after ablation under this microscope which the coating removed in some regions but not completely.

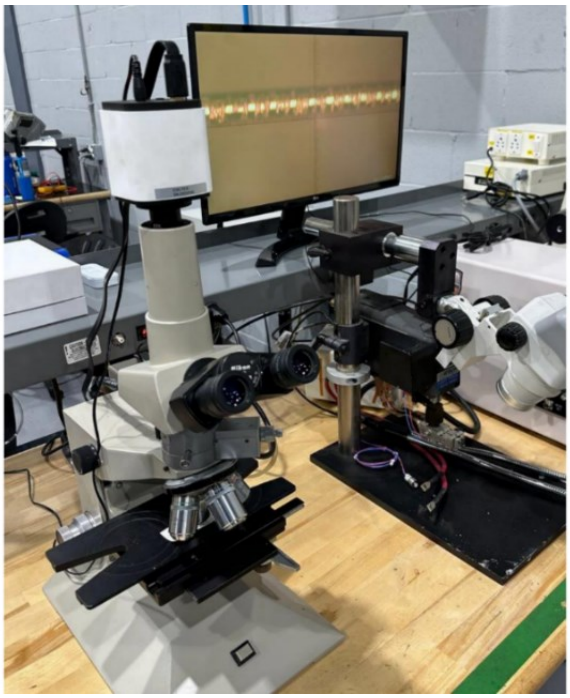

Figure 2.13 Microscope visualization system set up

2.9 Measurement of Ra

Confocal 3D microscopes are widely used in materials science, microelectronics, precision engineering, and micromachining for high-resolution surface characterization. They provide accurate, non-contact measurements of surface roughness, step heights, and complex microstructures. These systems are essential for analyzing wear, coating quality, and microfabrication accuracy, making them valuable tools in both research and industrial quality control [37].

To analyze the surface profile of the RTD wires, the Lext 500 Olympus confocal microscope (Figure 2.14) was utilized. The average surface roughness (Ra) was calculated in compliance with the ISO 25178 standard to ensure consistency and accuracy in surface texture evaluation. Measurements were taken at three distinct points within the ablated regions for three wires under each set of experimental conditions. The average of these values was then determined and assigned as the Ra for each sample, providing a reliable assessment of surface quality.

Additionally, the surface quality results were compared with chemically de-coated wires to establish a benchmark for evaluation. One set of reference wires was also measured under the confocal microscope to serve as a control for this stage of analysis. The primary objective was to achieve an Ra value comparable to, or better than, that of the reference wires.

Figure 2.14 ,3D Confocal measuring machine [35]

2.10 Measurement of Tensile strength

Another critical factor in the manufacturing process is the strength and durability of the wires, as they must remain resilient throughout production to ensure the final product's efficiency and reliability. Tensile strength tests conducted on chemically de-coated wires confirmed their robustness, allowing progression to the next production stage. However, laser ablation introduces unique challenges, necessitating verification of the wires' ability to withstand this method without compromising their integrity or performance. To accurately measure tensile strength post-ablation, as of figure 2.15 Universal Testing Machine (UTM) with a low-range force load cell was employed, ensuring delicate and precise measurements. The machine's grips were carefully selected to secure the wires without slippage, and a testing speed of 5 mm/min was maintained to apply force gradually and methodically.

Tensile analysis was performed on all sets of wires ablated in air and water, with chemically de-coated wires serving as a reference. Notably, some samples ablated in air were excessively fragile, breaking upon minimal handling, rendering tensile measurements impossible. These samples were excluded from further testing due to their lack of structural integrity.

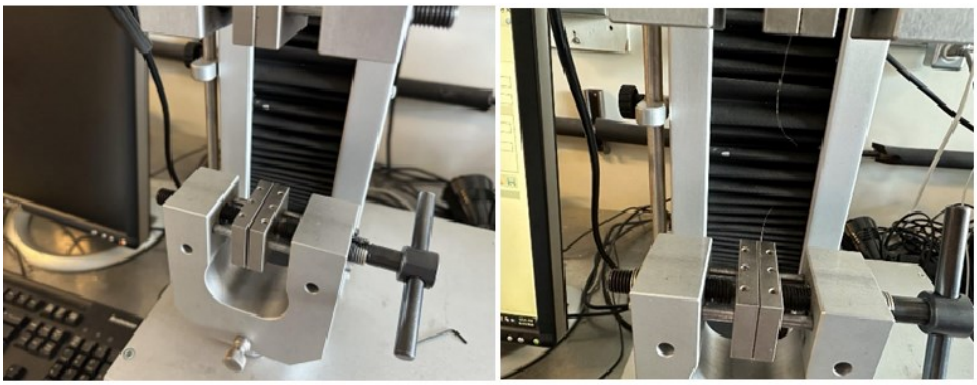

Figure 2.15, Universal Tensile machine at Concordia University (left), sample fractured after determining its tensile strength post-laser ablation(right)

2.11 Summary

This chapter presented a comprehensive overview of the experimental framework developed to investigate the laser ablation process for the selective removal of polyamide coatings from platinum wires. These wires are integral to the production of high-precision RTD (Resistance Temperature Detector) sensors used in aerospace stator systems, where spatial constraints and sensor sensitivity demand exceptional processing accuracy and material integrity.

The study employed a UV nanosecond-pulsed laser system with a fixed repetition rate of 20 kHz and a wavelength of 355 nm. Experimental variables included pulse overlap, line distance in both scanning axes, scanning speed, number of laser loops, and environmental conditions (air vs. water). A key focus was placed on controlling overlap percentages and optimizing line distance to balance coating removal effectiveness with substrate preservation.

Initially, traditional chemical stripping method was evaluated to establish a baseline for comparison. Despite its historical utility, this method posed significant environmental, safety, and process control challenges. The experimental work aimed to establish laser ablation as a cleaner and more controllable alternative.

Samples were subjected to systematic trials in both air and submerged water environments. Results from air-based experiments demonstrated the limitations of lower overlap percentages and larger line distances, which produced incomplete de-coating and substrate inconsistency. This led to the refinement of parameters, including increased overlap (75–95 percent), decreased line spacing (down to 1 μm), and variable scanning speeds. Water-assisted experiments further improved ablation quality by enhancing thermal regulation and preventing substrate degradation. However, the immersion environment influenced the laser beam characteristics, notably increasing spot size and slightly altering effective fluence, necessitating further adjustment of operational parameters.

To assess ablation quality, surface analysis was performed using high-resolution optical and confocal microscopy. The average surface roughness (Ra) values of ablated samples were compared to chemically stripped counterparts. Additionally, tensile strength testing was conducted to ensure structural integrity of the wires post-ablation. Notably, wires ablated in air under suboptimal conditions exhibited fragility and were excluded from tensile analysis due to breakage.

This chapter also outlined the statistical design of experiments (DOE), incorporating parameters such as fluence, speed, loops, and overlap. This approach enabled a structured evaluation of their individual and interactive effects on surface quality and mechanical performance. It was determined that high overlap and multiple loops are critical for achieving complete and consistent coating removal, particularly at higher scanning speeds.

In conclusion, the experimental setup successfully demonstrated the feasibility of replacing chemical de-coating with a precision-controlled laser ablation process. The findings provide a strong foundation for subsequent chapters, which will delve deeper into process optimization, surface quality characterization, and mechanical performance analysis under varying laser-material interaction conditions.

CHAPTER 3: UV Nanosecond Pulsed Laser Parameter Optimization for Removal of Polyamide Coatings from Fine Platinum Wires

This chapter is derived from the manuscript published in the Journal of manufacturing and material processing, which explores the enhancement of surface roughness (Ra), ablation depth, and tensile strength. The study is associated with Tracking Number JMMP-3611490 (Under Review).

Abstract

This study presents the optimization of a laser ablation process designed to achieve precise removal of polyamide coatings from ultra-thin platinum wires. The wires have a total diameter of 65 μm, consisting of a 50 μm platinum core encased in a 15 μm polyamide coating. Utilizing a UV laser with a wavelength of 355 nm and average power of 3W, Repetition rate range of 20 to 200 kHz, along with a high-speed marking system, the process parameters were systematically refined. Initial attempts to perform the ablation in an air medium were unsuccessful due to inadequate thermal control and incomplete removal of the polyamide coating. Hence, a water-assisted ablation technique was explored to address these limitations. Experimental results demonstrated that a scanning speed of 1200 mm/s, coupled with a line spacing of 1 μm and a single ablation pass, resulted in complete coating removal while ensuring the integrity of the platinum substrate. The incorporation of water layer above the ablation region was counted to be crucial for effective heat dissipation, preventing substrate overheating and ensuring uniform ablation. The laser's spot diameter of 20 μm in air and a focal length of 130 mm introduced challenges related to overlap control between successive passes, requiring precise calibration to maintain consistency in coating removal. This research demonstrates the feasibility and reliability of water-assisted laser ablation as a method for high-precision, non-contact coating material.

Key Words: Laser Parameter Optimization, Coating Removal, Liquid Confines, Thermal Effects

3.1 Introduction

In many industries, wire coating plays a vital role in providing protection and meeting specific functional needs. However, there are instances where removing these coatings is necessary based on specific requirements. This paper aims to identify an efficient alternative to existing methods, which are often time-consuming and lack precision, especially for microscale wires. These ultra-fine wires are critical in sectors such as aerospace [36], automotive [37], and biomedical [38], where they are utilized in various high-performance applications.

Ultrasonic stripping is a technique that is commonly used for removing coatings from wires. It employs high-frequency ultrasonic waves to generate cavitation within a liquid medium for material removal [39]. In this process, the coated wire is submerged in a liquid bath, typically water or a compatible solvent, while ultrasonic waves are applied. The ultrasonic energy causes rapid vibrations in the liquid, creating micro bubbles. When these bubbles collapse, they produce small but powerful shock waves that effectively remove the coating without affecting the wire's base material [40]. It is important to note that the extremely fine wires make them particularly vulnerable to mechanical stress. Even though the shock waves produced during cavitation are generally mild, they can still cause physical damage or deformation, resulting in wire breakage, bending, or surface erosion. Additionally, if only a specific section of the wire needs to be stripped, controlling the ultrasonic process becomes even more challenging [41].

Chemical stripping uses specific solvents or chemical solutions to dissolve, soften, or break down the insulation on wires, allowing for easier removal without causing physical or thermal damage to the conductor [42]. This method is especially useful for removing tough, heat-resistant, or delicate coatings that are difficult to strip using mechanical or thermal methods. However, chemical striping can sometimes lead to uneven removal, particularly with very thin wires, leaving residue or partially stripped areas that require further cleaning, which can be a disadvantage [43]. Achieving precision with chemical stripping on ultra-thin wires is also challenging, as the chemicals typically affect the entire submerged area, making it less suitable for stripping specific sections. Additionally, working with these chemicals presents further challenges, particularly in ensuring operator safety and preserving wire integrity [44].

Laser stripping is a highly accurate, non-contact method for removing insulation or coatings from wires using a focused laser beam. This technique is especially effective for applications that demand extreme precision, such as in the aerospace, medical device, and advanced electronics sectors. Unlike mechanical or chemical methods, laser striping avoids physical contact and does not involve potentially hazardous chemicals, making it a clean and efficient solution [45] [15] . Laser ablation enables precise removal of coatings, facilitating targeted processing on specific sections of ultra-thin wires without affecting the surrounding areas, which is crucial for maintaining their structural integrity [15] [46]. Key laser parameters, such as power, pulse duration, and focus, can be adjusted to optimize the process for various coating materials and wire specifications, providing versatility across different applications [47]. Furthermore, this technique can be seamlessly integrated into automated systems, enhancing efficiency and reducing labor costs while ensuring consistent quality in coating removal.

The similarity between shock waves generated by laser ablation and ultrasonic techniques lies in their fundamental mechanism of rapid energy release, leading to the propagation of high-pressure waves. In laser ablation, a high-intensity laser pulse rapidly heats the material, causing localized plasma formation and explosive expansion, which generates a shock wave that propagates through the surrounding medium. Similarly, in ultrasonic techniques, high-frequency mechanical vibrations induce acoustic cavitation, where the collapse of microscopic bubbles releases energy, producing shock waves that impact the material. Although the initiation mechanisms differ, both processes result in high-pressure waves that influence material removal, surface modification, or cleaning in various applications., it is important to note that laser ablation in water offers more precise control over the energy deposition, potentially reducing the risk of physical damage to the wire. The energy of the shock waves can be adjusted through various laser parameters [48].

Notably, various laser parameter configurations have been employed for coating removal on delicate samples across a broad wavelength spectrum, from IR to UV, utilizing technologies such as CO_2, active fiber, active disk, and Nd-YAG (Neodymium-doped Yttrium Aluminum Garnet). The quality of the stripping process is typically evaluated based on surface topography and chemistry. In assessing process performance, samples are subjected to mechanical testing through tensile peeling, with results compared in terms of quality, productivity, and material removal efficiency [49].

This study investigates the effectiveness of a low-power (3W) UV laser with a wavelength of 355 nm, optimized by adjusting the pulse width and repetition rate at lowest range to maximize process accuracy in removing polyamide coatings from fine pure platinum wires. Various ambient conditions were applied to achieve the highest surface quality and precision in targeted areas.

3.2 Materials and Methods

The laser used for the ablation process is a solid-state laser from the MACTRON, with a wavelength of 355 nm, average power of 3W, tunable repetition rate range of 20–200 kHz and a minimum pulse duration of 18 ns. The reason which led to choosing this machine is that the short wavelength of UV lasers is highly absorbed by polyamide coating, this allows for precise energy transfer to the coating while minimizing heat diffusion to the underlying substrate. This machine operates in a pulsed mode with short pulse durations, which reduces thermal accumulation in the surrounding material. This is critical for protecting the integrity

of the platinum substrate during ablation. On the other hand, the interaction of UV light with water enhances the ablation process by creating cavitation bubbles, which assist in cleaning and thermal management [36].

The experimental setup is illustrated in Figure 3.1. The laser beam passes through the galvanometer scanner mirrors along the X and Y axes. Further the beam is focused via a f-θ lens of focal length 130mm, resulting in a final spot diameter of 20μm at the focal point. Given the fineness of the wires, the objective is to remove the coating while avoiding any damage to the substrate and ensuring the highest accuracy. Therefore, the pulse width and repetition rate were set to the lowest values, at 18 ns and 20 kHz, respectively. For the laser system that emits Gaussian-shaped pulses, with the pulse duration measured at Full Width at Half Maximum (FWHM) the peak laser power is calculated as 8.333kw using Equation (3.1) without any correction factor [28-29].

$$P_{peak} = \frac{\text{Average Power}}{\text{Pulse Duration} \times \text{Repetition Rate}} \quad \text{Equation (3.1)}$$

Another crucial parameter is the laser fluence (F), the laser energy applied to a specific area of wire (equation 3.2). Fluence represents the energy delivered by the laser over a given area, which is crucial for processes like material ablation [29].

$$F \text{ (Gaussian Beam)} = \frac{2E_{Pulse}}{\text{Area}} \quad \text{Equation (3.2)}$$

$$E_{Pulse} = P_{peak} \times \tau_{Pulse} \quad \text{Equation (3.3)}$$

Based on the performed calculations, the laser fluence used in the experiments is established as 95.5 J/cm². This value remains consistent across all trials, given the uniform geometry and surface area of the wires, along with the confirmed repeatability of the laser system. However, it is important to note that this fluence was initially calculated assuming a spot diameter of 20 μm. In the subsequent section, it will be demonstrated that this diameter may vary, which directly influences the fluence value.

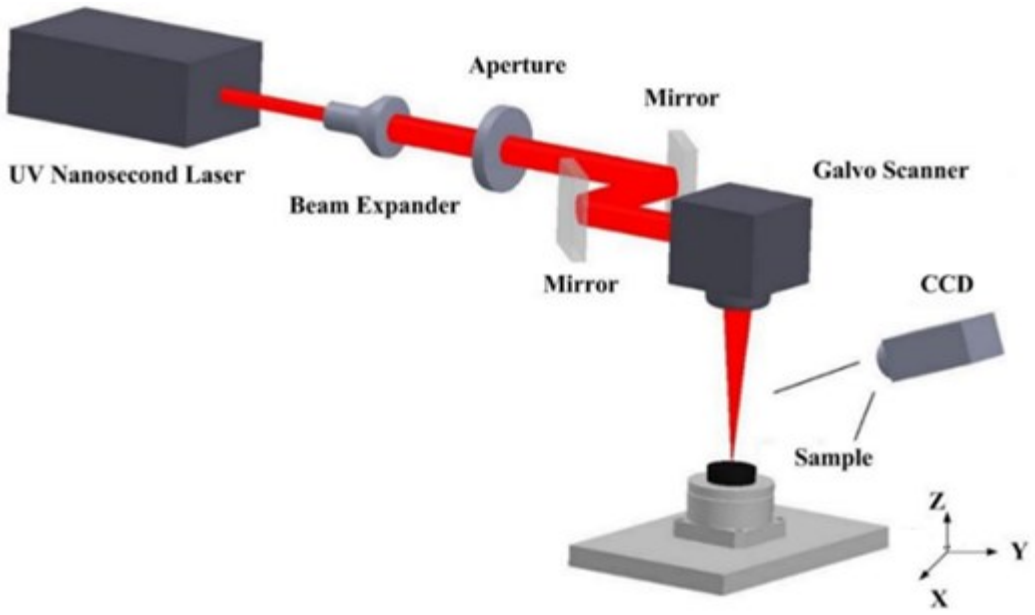

Figure 3.1: Schematic of the experimental setup [15]

The speed of the Galvano mirror on one axis during the raster scan directly influences the percentage overlap between subsequent spots as shown in figure 2 which on this machine on Y axis overlap happens with low speeds. After the first line is complete, the second mirror moves on the orthogonal axis to position the laser spot for the subsequent line scan [50] . This is controlled by the line distance(X)as shown in figure 3.2. The spot overlaps during ablation means that each laser spot deposits energy over a substantial portion of the previously processed area. The degree of overlap between adjacent laser spots is calculated using Equation 4:

$$\text{Overlap (\%)}: \frac{\text{Spot Diameter} - \text{Line Distnace(x)}}{\text{Spot Diameter}} \qquad \text{Equation (3.4)}$$

This increased energy density can improve the efficiency of the ablation, resulting in deeper and more effective material removal. Additionally, this overlap contributes to a smoother surface finish by minimizing irregularities. However, the high level of overlap also results in excessive material removal, which might increase the surface roughness. The localized heating from overlapping passes can increase the temperature of the specimen significantly, creating a larger Heat-Affected Zone (HAZ). Moreover, this excessive heat may lead to issues such as localized melting, warping, or changes in the material properties [51].

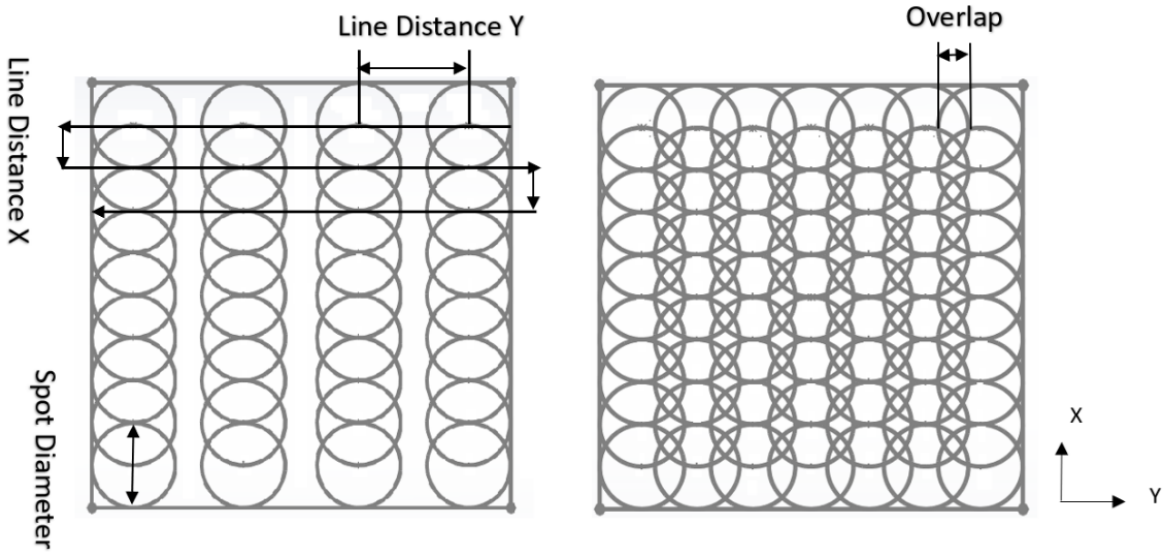

Figure 3.2: Schematic demonstrating the spot overlaps in both axis (Right) and line distance in X and Y which caused gaps in Y (Left).

Initial experiments were conducted using large line distances (10 µm and 20 µm) as well of low value of overlap at different speeds to evaluate their effect on the ablation process. Microscopic analysis of the ablated samples revealed that the coating was primarily affected by heat, with no significant evidence of material removal. Based on these observations, the laser parameters were adjusted, and 12 sets of experiments were conducted. These experiments were initially performed in air which involved four different speeds, two line distances, and varying numbers of loops, as outlined in Table 3.1 The results were analyzed to assess their impact on surface quality, roughness, and tensile strength, and were benchmarked against wires de-coated using a chemical process.

The wire was aligned parallel to the Y-axis, while the laser scanning operation took place along the X-axis. Movement in the X-direction was managed by the galvanometer scanner, enabling precise control of line spacing, which was set to either 1 µm or 5 µm, corresponding to overlap percentages of 95% and 75%, respectively. In contrast, motion along the Y-axis was governed by the scanning speed, which was carefully adjusted and calculated using equation 3.5. This dual-axis control system allowed for precise manipulation of overlap and spacing, ensuring optimal ablation conditions tailored to the experimental requirements.

Line Distance (Y): $\frac{\text{Speed}(\frac{\mu m}{s})}{\text{Repetition rate(Hz)}}$ Equation (3.5)

For instance, at a speed of 500 mm/s (500,000 μm/s) and a repetition rate of 20 kHz (20,000 Hz), the Y-direction spacing was 25 μm, leading to a significantly larger overlap in the X-direction compared to the Y-direction.

Notably, Figure 3.2 illustrates the overlap for the ablation process, highlighting the line distance in the X-direction (controlled by the galvo scanner) and the spot diameter in the Y-direction (determined by the scan speed and repetition rate). The figure represents the actual overlap, where the X and Y-direction spacings differ due to distinct control mechanisms. This variation was carefully considered during the analysis and does not compromise the overall effectiveness of the process.

To ensure precise and uniform line spacing, the galvo scanner positioning was synchronized with the laser pulse repetition rate. This synchronization was critical for maintaining the accuracy of the ablation process, especially at higher speeds, and for achieving consistent overlap as depicted in Figure (3.2).

Speed (mm/s)	500			1000			1200			1500		
Line Spacing (Y, μm)	25			50			60			75		
Line Distance (X, μm)	1	5		1	5		1	5		1	5	
Overlap (%)	95	75		95	75		95	75		95	75	
Number of Loops	1	1	2	1	1	2	1	1	2	1	1	2

Table 3.1 Properties of the laser parameters in Air.

It is notable that the line distance in the Y-direction could be reduced by increasing the repetition rate. However, observations from multiple sets of experiments indicate that this approach compromises the accuracy of the process and can damage the substrate due to the higher number of pulses and increased energy delivered to the wires. Therefore, it was initially decided to set the pulse width and frequency to their lowest possible values to achieve maximum precision.

After completing each experiment, tensile strength was tested using an Instron machine equipped with a 50 N load cell, while surface roughness was evaluated with the Olympus Lext 500 confocal microscope.

3.3 Results and Discussion

3.3.1 surface quality (Air Ambient)

The samples were subjected to ablation in an air medium, and the results were analyzed and compared against those obtained through chemical methods, which served as the benchmark for this study. All images were captured using a confocal microscope equipped with a 20× lens, covering an area of 645 × 648 µm (as shown in Figure 3.4). As depicted in Figure 3.3, the chemical process successfully exposed the platinum surface without causing any damage to the substrate or deformation. To conserve space, images of the samples following the ablation process were cropped for inclusion in this article.

Moreover, experimental observations revealed that wires ablated at lower scanning speeds exhibited significant blackened regions due to excessive heat deposition. This heat accumulation not only resulted in the loss of base material but also caused substantial damage to the wires, rendering them extremely fragile, as shown in Figure 3.4. At a scanning speed of 500 mm/s, combined with both 1-µm and 5-µm line distances, the wires sustained damage, indicating that higher speeds are necessary to achieve satisfactory results.

Figure 3.3: Schematic chemically removed coating without any deformation and damage to platinum.

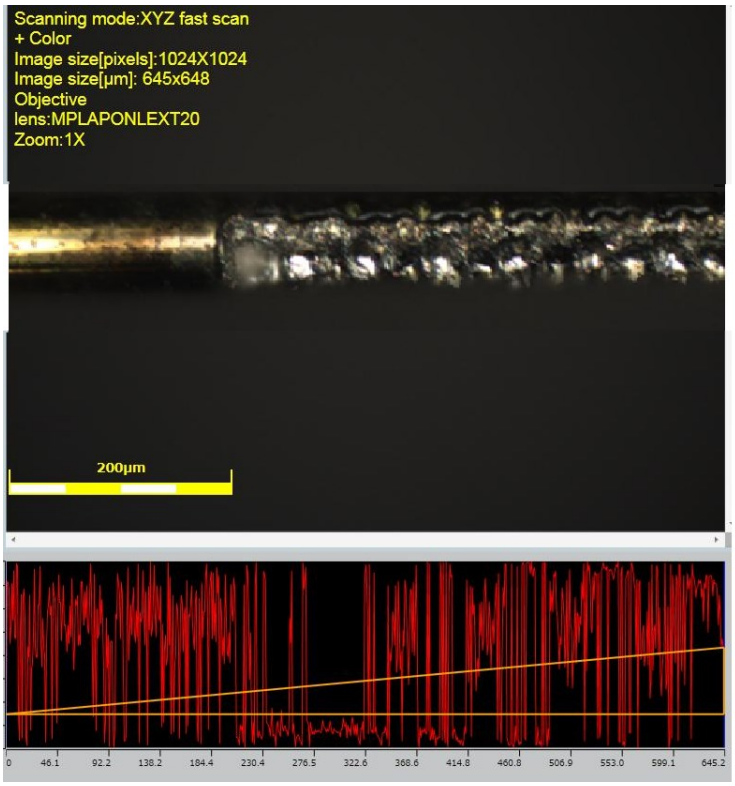

Figure 3.4 laser scan speed 500mm/s, line distance of 1µm.

Further adjustments made in air, as shown in Figure 3.5, demonstrate improved results compared to earlier trials. However, it is evident that in all cases, the coating was not completely removed, and the wire surface remained excessively rough, indicating an insufficient machining process. Figure 3.5-A illustrates the ablation performed at a speed of 1000 mm/s with the smallest line distance and 95% overlap. While the coating was partially removed, the surface quality was significantly inferior to that achieved through chemical processing.

In another setup (Figure3.5-B), the speed was increased to 1200 mm/s, and the overlap was reduced, effectively increasing the line distance. The wires were also subjected to two laser passes (two loops). As depicted, the level of damage to the wire decreased, but the heat affected the coating, causing it to be removed segment by segment. Although this adjustment reduced substrate damage, the outcome was still insufficient to achieve complete coating removal. This demonstrated that increasing the speed and minimizing heat exposure could help preserve the wire's integrity.

Finally, the speed was set to 1500 mm/s with 95% overlap to test whether a smoother surface could be achieved by combining a larger line distance in the Y direction and a lower line distance in the X direction.

As shown in Figure 3.5-C, this adjustment resulted in improved wire integrity and reduced damage. However, the surface quality remained unsatisfactory, with high roughness values, as discussed in the following section. Additionally, several samples from design of experiments showed incomplete coating removal, with the ablation affecting only part of the surface. These samples were deemed unsuitable for further scanning or experimentation due to their compromised condition. In conclusion, due to the sensitivity of the sample, complete coating removal was critical, rendering these adjustments unsuitable. Specific parameters for each wire are detailed in the corresponding figure descriptions.

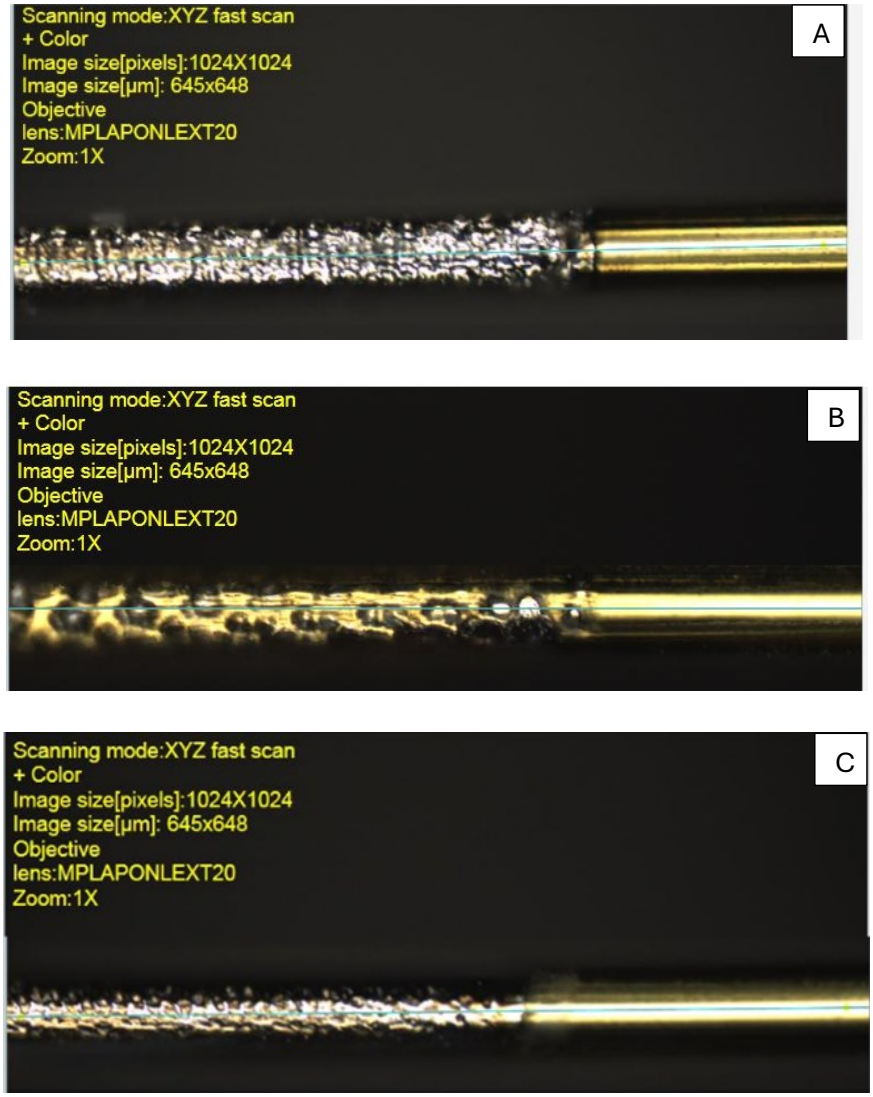

Figure 3.5 (A) laser scan speed 1000mm/s, line distance 1µm. (B) laser scan speed 1200mm/s, line distance 5 µm and 2 loops. (C) laser scan speed 1500mm/s, line distance 1 µm.

3.3.2 Tensile Strength (Air Ambient)

The tensile strength of the samples was analyzed using a Universal Testing Machine (UTM) after the removal of the coating. Figure 3.6 illustrates the tensile strength measurements for various ablation parameters. All samples were cut to identical lengths, and the coatings were removed using standardized procedures. To ensure accuracy and prevent slippage, the samples were firmly secured in the grips of the UTM. The results indicate that chemically de-coated wires exhibited an average tensile strength of 115 gr.f as shown in figure 3.6. In contrast, wires ablated at 500 mm/s in air were excessively fragile and prone to breakage, rendering them unsuitable for mounting and testing on the UTM. Samples processed with a line distance of 5 μm and a single loop demonstrated minimal thermal effects but failed to achieve adequate coating removal. Observations across multiple samples, conducted to ensure process repeatability, revealed that a lower percentage of overlap combined with a single loop, for low speeds was insufficient for effective ablation.

On the other for high speeds and low overlap adjustments, the coating exhibited only minor thermal effects without being removed, rendering tensile strength measurements impractical. Consequently, these samples were deemed unsuitable for further experimental analysis.

The remaining samples demonstrated sufficient stability to be mounted on the UTM grips, and their tensile strengths were successfully measured. Figure 3.6 presents a comparison of tensile strength across different ablation settings in the air environment and chemical serving as reference. However, the results for ablated wires were consistently lower than those of chemically de-coated samples.

It should be noted that at least three samples were tested for each adjustment, and the average tensile strength was recorded and displayed in the figure.

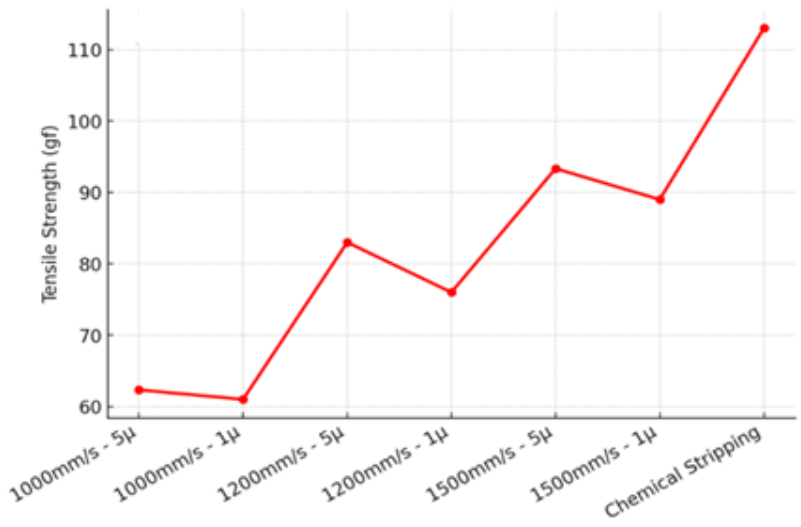

Figure3. 6 tensile strength results in ablation in air in different adjustments compared to chemical ones.

While the tensile strength at higher speeds may seem adequate, it's important to note that the surface quality of all air-ablated samples was unsatisfactory, and the stripping process was incomplete. Ultimately, the process was ineffective due to incomplete coating removal, leaving the surface quality unsatisfactory.

3.3.3 Average Roughness R_a (Air Ambient)

Surface roughness of the samples after material removal was analyzed using the Confocal Olympus Lext 500, in compliance with the ISO 25178 standard to ensure consistent surface texture assessment. The measurement range was between 645 µm and 648 µm, which is within the capacity of the system used. For each wire, roughness measurements were taken at three different segments on three wires of each adjustment. While Ra was primarily determined through 3D profilometry, additional measurements were taken at various orientations to verify consistency. The values obtained were averaged to account for surface variations across the wire.

Figure 3.7 illustrates the roughness measurements obtained from the ablated regions. Conducting roughness measurements for all ablated samples was not feasible, as wires processed at speeds below 500 mm/s exhibited significant burning and cracking, evident through visual inspection. As shown in Figure 3.7, the roughness of the ablated wires was substantially decreased when a line distance of 1 µm was employed, in contrast to 5 µm.

This observation suggests that higher overlap yields smoother surface quality, though it negatively impacts tensile strength. The damage observed in these ablated areas can be attributed to excessive heat exposure during the process. On the other hand, the surface roughness (Ra) can be minimized by employing higher ablation speeds, which mitigate heat concentration. Additionally, conducting laser ablation in multiple loops when overlap was set on 75%, enhances surface smoothness. With each pass, a small layer of material is removed, enabling progressive refinement of the surface and partially compensating for the reduced overlap. This iterative approach provides a balance between smoother surface finishes and minimizing damage caused by heat.

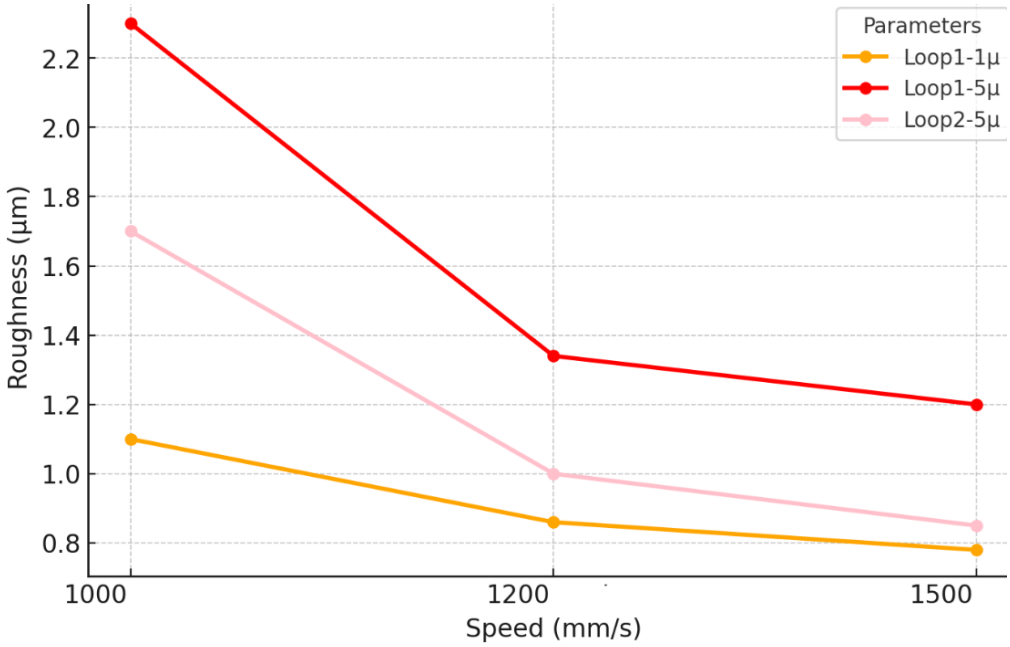

Figure 3.7 Average roughness on air-ambient ablated wires, three wires of each setting.

After measuring the roughness average (Ra) for all samples ablated in air, the results varied between 0.76 to 2.4 µm. In contrast, the chemically stripped wires exhibited an average Ra of 0.1 µm. This significant discrepancy suggests that the surface roughness of the laser-ablated wires should ideally be much lower, approaching that of the chemically treated samples, indicating the potential for achieving a higher quality surface through optimized laser parameters and processing conditions.

3.3.4 Spot Diameter Consideration

Based on these findings, it is essential to emphasize that, according to the experimental design, the X-axis overlap is high. However, initial calculations suggested that increasing the scanning speed in the Y-axis would lead to a greater distance between consecutive laser spots. For instance, at a speed of 1000 mm/s, the center-to-center distance between spots in the Y-axis is 50 µms. Given the spot diameter of 20 µms in the y axis certain section of wire will remain unprocessed (figure3.5-B). To validate whether the laser system behaved as predicted, experiments were conducted on a flat sheet with varying speeds and large value of X line distance. The results confirmed the initial assumption on a flat surface, ablation in the Y-axis occurred in separate sections, with no overlap, leaving unprocessed regions between laser spots as shown in figure 3.8. The sheet images were captured using a confocal machine under the same conditions applied to the wires during roughness measurements.

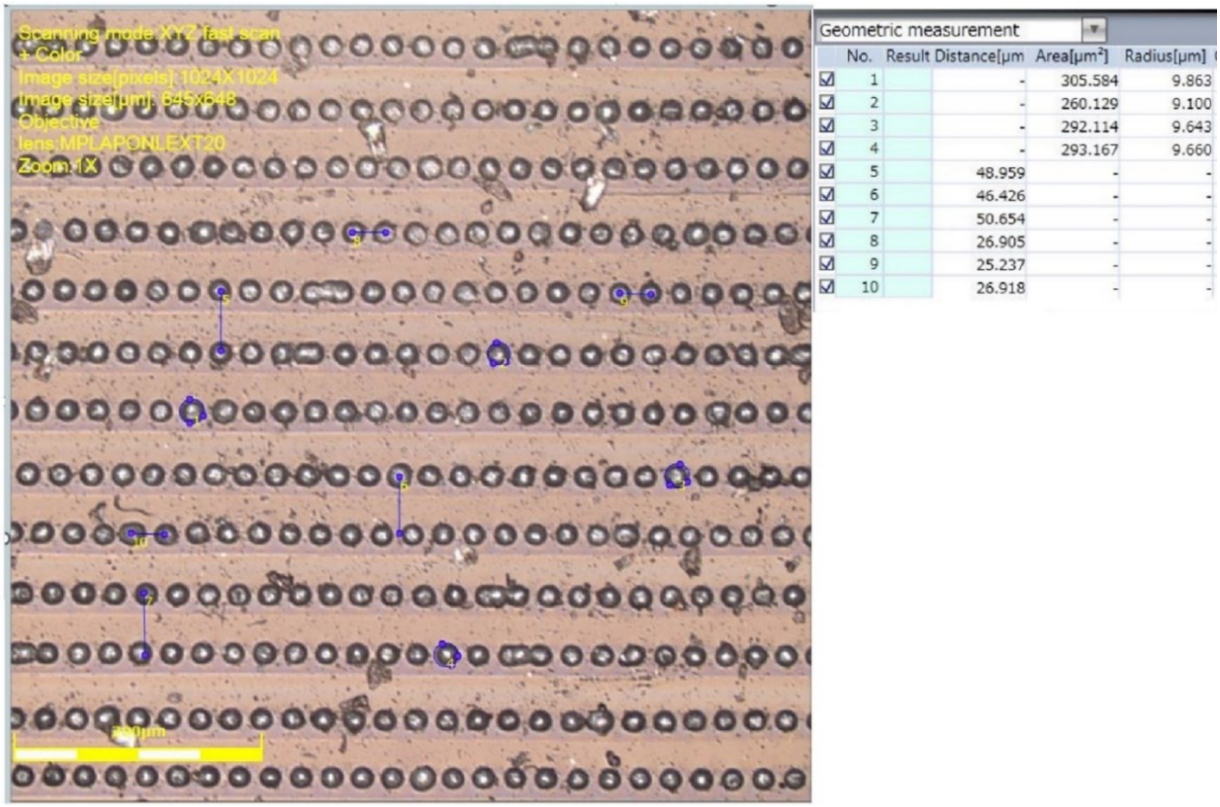

Figure 3.8 Laser processing on flat sheet, Speed of 500mm/s and X line distance of 50 µm.

Figure 3.8 presents a laser-processed sheet analyzed using a confocal microscope, with all measurements obtained through various tools within the machine's software. Notably, a high line distance in the X

direction was deliberately chosen to eliminate overlap, ensuring two key objectives: first, to provide a clearer understanding of the machine's performance through this visualization, and second, to prevent surface damage that could compromise image quality. The laser speed was set to 500 mm/s, resulting in a 25-µm center-to-center spacing between laser spots along the Y-axis. In the X direction, laser passes occurred at 50-µm intervals. As illustrated in the image, noticeable gaps remain in the Y direction between laser spots, confirming that even with a minimal 1-µm line distance in X, overlap occurs only along the X-axis, while gaps persist in the Y-axis.

However, when transitioning from a flat sheet to a cylindrical wire, a notable difference in laser interaction was observed. Since the laser beam only affects a semi-circular section of the wire, variations in the beam's angle of incidence result in different effective focal distances across the curved surface. Given the wire's 65-µm diameter, the focal point naturally shifts by approximately 32.5 µm along the surface, leading to changes in the spot diameter. To investigate this effect, a 2-3-milliliter layer of water was added to a flat sheet (to check the effect of water too) and subjected to laser ablation at a speed of 1000 mm/s with a line distance of 50 µm in the X direction. Microscope measurements revealed an average spot diameter of 30 µm and a center-to-center spacing of 50 µm in the Y direction, aligning with theoretical predictions. This also explains why, at lower speeds such as 500 mm/s—where the Y-axis line distance is 25 µm—excessive overlap occurred. In this case, the expanded spot diameter exceeded the standard value, leading to significant energy concentration, which caused localized burning and increased susceptibility to fracture. It is important to note that while the X-axis overlap was initially calculated based on a 20-µm spot diameter, practical conditions resulted in an actual increase in spot size. Consequently, the effective overlap percentage was higher than expected. As depicted in Figure 3.9, the spot diameter increased to 30 µm at the focal length.

Although the initial spot diameter of 30 µm was calculated based on laser ablation on a flat sheet in the presence of water, the focal length during wire processing was still set to the top surface of the wire. This setup did not account for the effect of the angle of incidence introduced by the wire's circular geometry, which alters the focal position along its curved surface. To address this, it was necessary to position the focus 32.5µm below apex to improve coverage across the wire's surface. However, since the machine's Z-axis scale only permitted adjustments in 1 cm increments, a MITUTOYO height gauge was used to manually elevate the Z-axis by 32 µm. This modification aimed to optimize focus and expand the ablation area.

Subsequent measurements on a flat surface with water confirmed that the average spot diameter had increased to approximately 45 µm. This value corresponds to the largest spot size at the lowest point of the wire's curvature. Conversely, at the highest point where the focus was originally set, the spot size remains closer to 30 µm. As a result, the effective spot diameter varies throughout the process due to both the curvature of the wire and the adjusted focal plane. It is also noteworthy that this ablation process was applied over 180 degrees of the wire's surface, effectively treating half of its circumference.

For subsequent water-ambient ablation trials, this 45-µm spot diameter was considered. The combined effects of the incident angle and the wire's 32.5-µm radius further contributed to increased laser spot size, ultimately affecting overlap in both axes. These combined factors explain why ablation on the wire occurs uniformly without any intact sections, despite the expected gaps in the Y-axis placement.

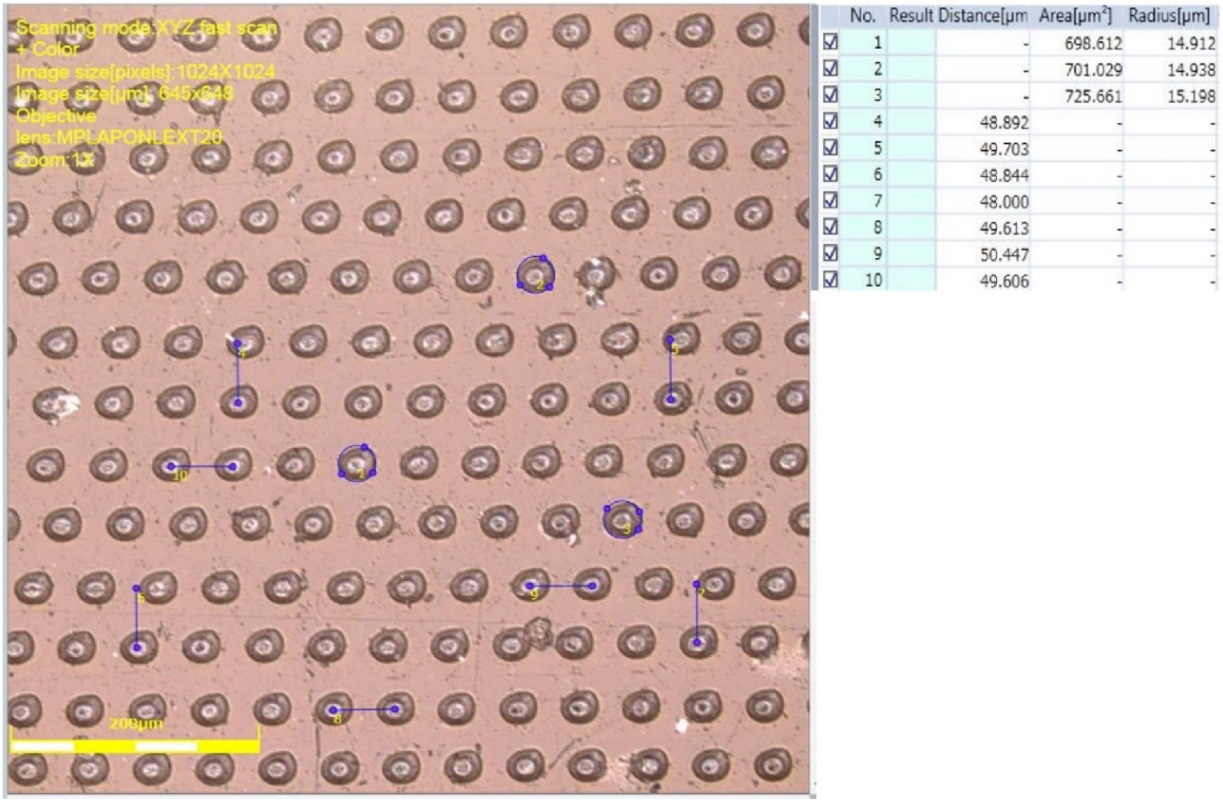

	No.	Result	Distance[µm	Area[µm²]	Radius[µm]
☑	1		-	698.612	14.912
☑	2		-	701.029	14.938
☑	3		-	725.661	15.198
☑	4		48.892	-	-
☑	5		49.703	-	-
☑	6		48.844	-	-
☑	7		48.000	-	-
☑	8		49.613	-	-
☑	9		50.447	-	-
☑	10		49.606	-	-

Figure 3.9 Laser processing on flat sheet with a layer of water at normal focal length, Speed of 1000 mm/s and X line distance of 50 µm (Spot diameter changed to 30 µm)

As the spot diameter increased, the fluence of the laser on the wire surface also changed accordingly, based on the calculated values. While the peak power of the laser remained constant at 8.33 kW, the

fluence decreased to 18.86 J/cm², as determined using Equations (2) and (3). This decrease in fluence resulted from the expanded spot size, which spread the same energy over a larger area. Therefore, under the new configuration, the wires were exposed to a lower fluence.

3.3.5 Surface quality (Water Ambient)

Following the unsuccessful attempts with air-based ablation, experiments were shifted to a water environment to address the excessive heat generated on the wire surfaces during the laser process. In water-based laser ablation, the rapid vaporization of the surrounding liquid produces bubbles that expand and collapse within microseconds. This phenomenon generates shockwaves, microjets, and vibrations, which exert mechanical forces on the wire surface, facilitating the removal of the coating material. The water layer not only dissipates heat effectively, minimizing thermal damage to the wire substrate, but also enhances the de-coating process through mechanical agitation [21]. Observations from the air-ablation trials revealed that a lower overlap of 75% with a single loop was insufficient for effective coating removal, whereas two loops showed improved results. Accordingly, the parameters for the water-based experiments were developed and implemented as detailed in Table 3.2.

Speed (mm/s)	500		1000		1200		1500	
Line Spacing (Y, µm)	25		50		60		75	
Line Distance (X, µm)	1	5	1	5	1	5	1	5
Overlap (%)	97.77	88.88	97.77	88.88	97.77	88.88	97.77	88.88
Number of Loops	1	2	1	2	1	2	1	2

Table 3.2 Properties of the laser parameters in Water.

Immersing the sample in water while maintaining proper support during the laser ablation process posed a significant challenge, as the water level above the wires was found to be a critical parameter. Experiments were carried out using the specified laser parameters within a container of 10 cm in diameter. The samples, each consisting of a 40 mm long wire, were positioned at the bottom of the container, which was half-filled with water to maintain a consistent water layer above the wires. The wires were fixed using double-sided

adhesive tape onto a cardboard support featuring a 5 × 5 cm window at its center, allowing precise exposure to the laser beam, as illustrated in Figure 3.10. As shown in Figure 3.11, the entire setup including the water container, was mounted on a two-axis workbench positioned beneath the laser system's camera for accurate alignment and control during ablation.

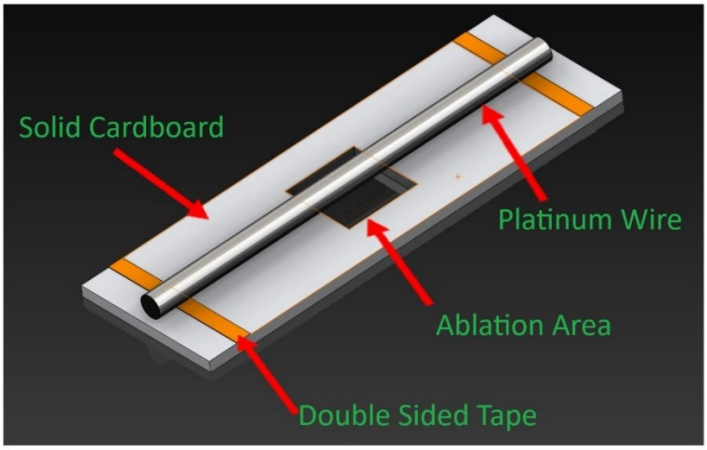

Figure 3.10 Experimental setup for wire support on water-assisted laser ablation.

Microscopic examination of the ablated samples revealed that while the underlying substrate remained intact and partial coating removal was achieved, the results were inconsistent across the wire surface, as illustrated in Figure 3.12. In certain regions, the coating persisted, indicating a degree of stochastic behavior in the ablation process. This inconsistency emphasized the critical role of maintaining a stable and optimal water level above the wire during laser exposure.

Furthermore, each ablation cycle resulted in contamination of the water with debris and detached coating fragments, which negatively influenced subsequent experiments. Consequently, the water had to be replaced, and the container thoroughly cleaned after each trial to ensure process reliability and repeatability.

During laser irradiation, the interaction between the beam and the coated wire in water produced gaseous byproducts, leading to the formation of microbubbles. These bubbles contributed to localized fluid agitation and cavitation phenomena, which played a beneficial role in dislodging and removing surface debris [21].

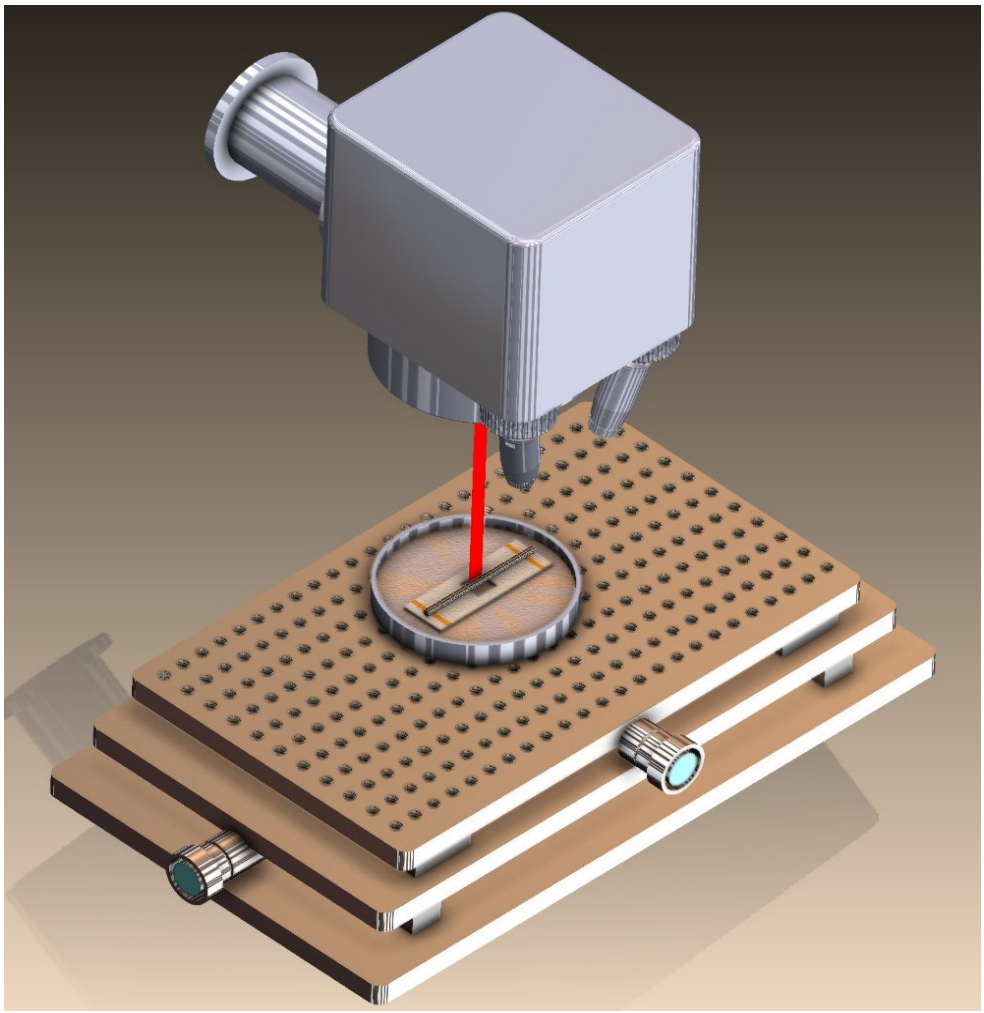

Figure 3.11 Laser ablation of sample immersed in water setup schematic (SolidWorks).

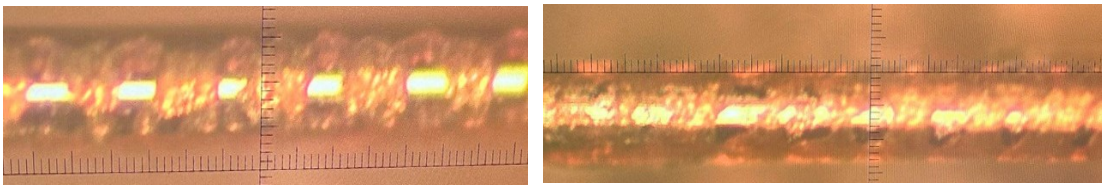

Figure 3.12 Laser ablated wires with excessive amount of water: (left) 1000 mm/s and 5µm line distance, (right) 1200 mm/s with 5µm line distance.

In the subsequent phase, Water was added to the container until it just reached the top level of the wires, ensuring complete submersion without excess coverage. To establish a controlled water layer above the wires for the ablation process, a milliliter-graduated injector was used to incrementally introduce additional

water into the setup. Approximately 2 to 3 milliliters of water were carefully added above the wires, providing the precise conditions required for the experiment.

Figure 3.13 presents confocal images of samples ablated on one side, highlighting the influence of speed on process quality. At a speed of 500 mm/s (Figure 3.13A), localized damage was evident in certain wire segments, Akin to observations made during air-based ablation. This confirmed that such low speeds are unsuitable for fine wires of this nature. At higher speeds—1000 mm/s with 88.88% overlap and two loops, as well as 1200 mm/s with 97.77% overlap and one loop (Figures 3.13B and 3.13C), no damage was observed, and the coating was completely removed. However, further increasing the speed to 1500 mm/s led to incomplete coating removal. As mentioned earlier, the increase in speed resulted in a larger line distance in the Y-axis, creating gaps that neither the water layer nor variations in the beam's incident angle could fully compensate for. Consequently, some regions remained intact. Moreover, the positions of these unablated sections were stochastic, varying from sample to sample due to slight differences in laser interaction with the wire's surface. Regardless of the overlap percentage or number of loops (Figure 3.13D).

To ensure uniform coating removal around the full circumference of the wire, the samples were carefully flipped, and the laser focus was readjusted to target the opposite surface. The ablation process was then repeated under the same conditions. As illustrated in Figure 13E, this dual-sided ablation resulted in complete and consistent coating removal across the wire surface. The image was captured using the on-site optical setup, which consisted of a NIKON Nomarski Differential Interference Contrast (DIC) Microscope with 20× magnification, paired with a CALTEX HD60 Camera equipped with a 0.5X lens.

It is noteworthy that all roughness measurements and profile analyses were conducted under identical conditions using the same confocal microscope specifications to ensure the integrity and consistency of the experimental results.

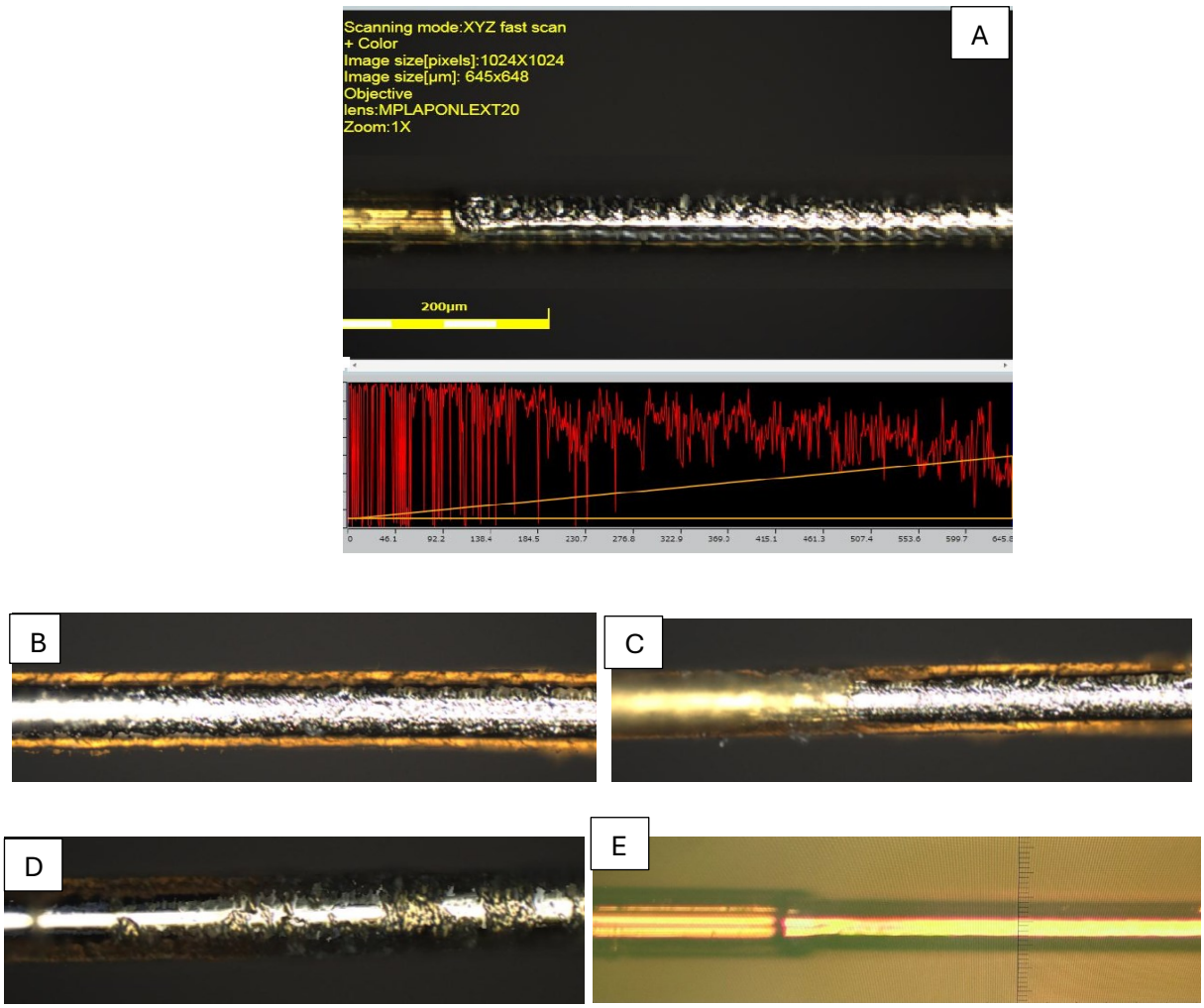

Figure 3.13 Wires ablated in water ambient, (A) 500 mm/s-line distance 1 µ (B) 1000 mm/s-line distance 5µ and 2 loops captured in middle segment (C) 1200mm/s-line distance 1 µ (D) 1500mm/s-line distance 5 µ and 2 loops (E) 1200mm/s and line distance 1µ ablated on both sides

Both speeds, 1000 mm/s and 1200 mm/s, resulted in clean, smooth, and residue-free surfaces, the higher speed of 1200 mm/s would be advantageous in terms of time efficiency as well as lower value of roughness. The effects of Speed, line distance and the number of loops together with the analysis of surface roughness and tensile strength will help with the process parameter optimization.

3.3.6 Tensile Strength (water Ambient)

Following the ablation process, the wires were dried at room temperature and carefully mounted in the grips of a Universal Testing Machine (UTM). Samples ablated at a speed of 500 mm/s exhibited significant damage, like results observed in air ambient tests, rendering them too fragile for tensile testing. Conversely, ablation at 1500 mm/s was insufficient to achieve complete coating removal, making tensile strength evaluation impractical.

As presented in Figure 3.14, chemically stripped wires demonstrated tensile strength average value of 115 g.f, whereas water-ablated samples at 1000 mm/s-1µ showed tensile strength values between 89 and 95 gr.f. Notably, samples ablated at 1200 mm/s-1µ exhibited greater consistency, with tensile strength ranging from 98 to 108 gr.f and a mean value of approximately 101 gr.f, which is approximately 12% lower than the mean tensile strength of chemically stripped wires. This enhanced consistency is attributed to reduced thermal effects on the wire surface.

On the other hand, samples ablated with 88.88% overlap in two loops exhibited higher tensile strength. However, visual inspection revealed inadequate surface quality and incomplete coating removal, rendering these samples unsuitable as a final satisfactory outcome for this research.

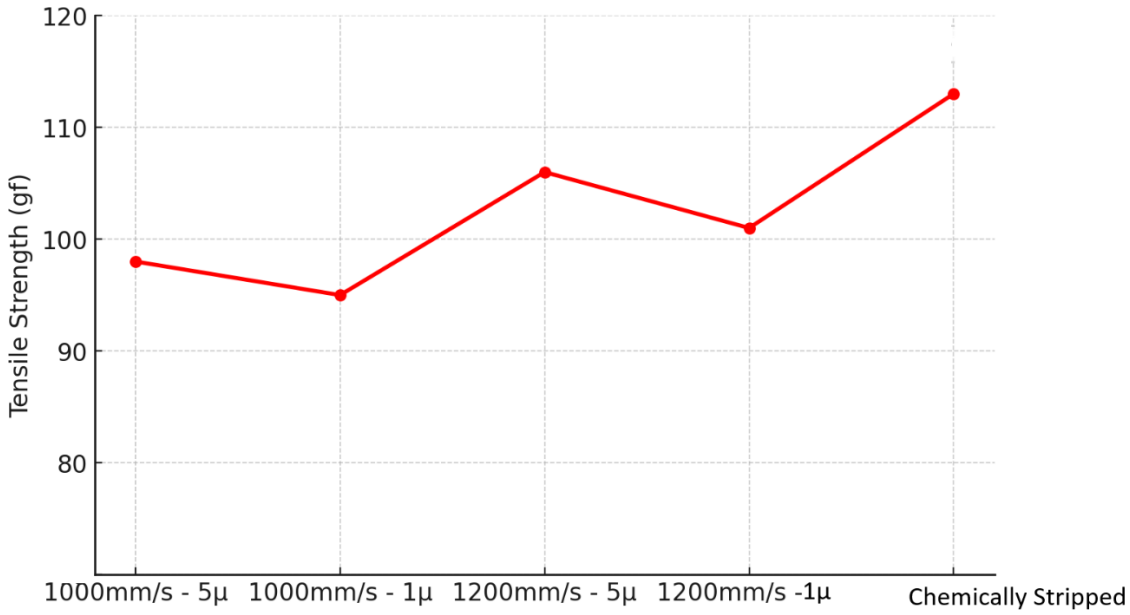

Figure 3.14 distribution of stripped wires chemically and ablated with water film.

3.3.7 Average Roughness Ra (Water Ambient)

To assess the roughness of the samples ablated in water in comparison with those from chemically stripped samples, three samples from each experiment were examined using a confocal microscope. Each wire was analyzed in three distinct segments, with range of 645 μm × 648 μm, and the average roughness values were recorded in Figure 3.15. Although the chemically stripped samples exhibit a smoother surface quality, the laser-ablated wires in water are still considered satisfactory. The inherent nature of laser processing often alters surface quality, significantly impacting the surface texture of materials. This alteration can lead to various surface characteristics, such as roughness and thermal damage, which may not meet the desired specifications for certain applications [22]. The key challenge lies in developing a process to control this effect, thereby achieving the desired outcome.

The samples subjected to ablation at 500 mm/s demonstrated an average surface roughness (Ra) of 0.396 μm, primarily due to extensive thermal damage that weakened the wire's structural integrity. Conversely, ablation at 1500 mm/s resulted in incomplete coating removal, leaving residual material and producing a lower roughness of 0.284 μm. The incomplete removal at higher speeds is likely due to the large line distance in the Y-direction, which was not sufficiently offset by the wire's circular geometry, the expanded spot diameter, or the presence of water. As a result, noticeable gaps formed between consecutive laser spots, leaving some sections intact. Additionally, the results indicated that higher speeds brought tensile strength and surface quality values closer to those achieved through chemical stripping. If an optimized adjustment and procedure can be established to ensure complete coating removal in higher speed, there is potential to enhance both surface roughness and tensile strength beyond the levels attained with chemical stripping. This objective will be the focus of the next study.

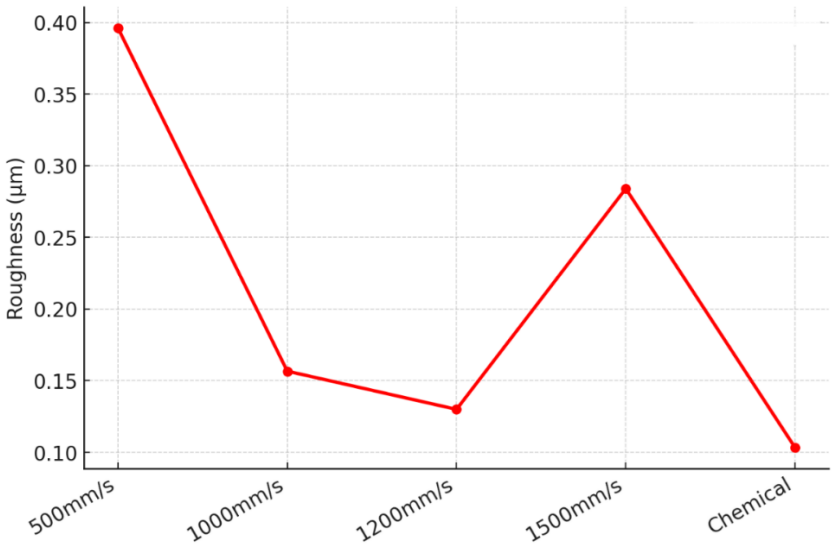

Figure 3.15 illustrates the roughness (Ra) values of water ablated for different speeds with 1 µm line distance in X, and chemical stripped ones.

Ablation at 1000 mm/s with a line distance of 1 µm (97.77% overlap) produced smoother surfaces with an average roughness of 0.155 µm, representing an improvement over similar tests conducted in air. Notably, ablation at 1200 mm/s with a 1 µm line distance in water achieved a mean roughness of 0.129 µm, approaching the chemically stripped wire's roughness of 0.104 µm. This suggests that ablation at 1200 mm/s in water provides superior surface quality, likely due to minimized thermal effects. Visual inspection indicated satisfactory results for both 1000 mm/s and 1200 mm/s speeds; however, roughness measurements confirmed that the 1200 mm/s condition yielded a surface quality more comparable to chemically stripped wires. Additionally, the tensile strength achieved under this condition was higher, and the process was more time-efficient, emphasizing the advantages of water-based ablation with speed of 1200 mm/s.

3.4 Conclusion

This research investigated the efficiency of laser ablation for removing polyamide coatings from ultra-thin wires under both air and water-assisted environments. Key process parameters—including scanning speed, line distances in both X and Y directions, overlap percentage, and the number of loops—were systematically varied and evaluated. The results revealed that water-assisted laser ablation, particularly at scanning speeds of 1000 mm/s and 1200 mm/s with a 97.77% overlap, achieved clean, residue-free surfaces

comparable to those obtained through conventional chemical stripping. The presence of a controlled thin water layer above the wires played a critical role in dissipating heat, mitigating thermal damage, and preserving the structural integrity of the delicate platinum substrate.

An important observation was the variation in laser spot diameter during ablation in water. The curvature of the wire, combined with the angle of laser incidence, led to fluctuations in the spot size. These variations affected the energy distribution across the target and consequently influenced the overall process efficiency. This dynamic underscore the importance of precise calibration when working with curved, ultra-thin targets in fluidic environments. Additionally, laser fluence played a significant role; as the spot diameter increased, the fluence decreased. Interestingly, the results showed that lower energy density was more effective for processing microscale wires, enabling polymer removal to occur even at reduced fluence levels.

The study also showed that speeds above 1200 mm/s led to insufficient coating removal, leaving localized residues, whereas lower speeds—although effective in complete ablation—caused overheating and physical damage to the wires. Through iterative experimentation and systematic elimination of suboptimal parameter combinations, the process was refined to identify the most effective setup for uniform and complete coating removal.

Overall, this study demonstrates the viability of laser ablation in water as a promising alternative to traditional chemical methods for stripping coatings from fine wires. The mechanical and surface integrity of the wires post-ablation were maintained within acceptable limits, making this approach suitable for sensitive applications. Looking forward, future investigations could explore the use of alternative ablation media (e.g., different solvents) to further enhance cleaning efficiency and surface quality. Additionally, increasing scanning speeds and loop counts may offer improvements in surface roughness (Ra) while maintaining consistent coating removal.

In summary, this work serves not only as a successful application of laser micro-processing for fine wire preparation but also as a model for how experimental observations can be validated through rigorous statistical analysis. The findings underscore the importance of optimizing laser parameters to strike a balance between process efficiency, material preservation, and surface quality, paving the way for broader industrial adoption.

CHAPTER 4: ANOVA based Optimization of UV Nanosecond Laser for Coating Removal from Platinum Wires Under Water Confinement

This chapter is based on a manuscript submitted to the Journal of Manufacturing and Materials Processing, which explores laser optimization to enhance surface roughness (Ra), ablation depth, and tensile strength based on ANOVA analysis. The study is currently published with Tracking Number of JMMP-3657195.

Abstract

Platinum wires, known for their excellent electrical conductivity and durability, are widely used in high-precision industries such as aerospace and automotive. These wires are typically coated with polyamide for protection, but specific manufacturing processes require selective removal of this coating. Traditional chemical stripping methods, while effective, are associated with high costs, safety concerns, and long processing times. As a result, laser ablation has emerged as a more efficient, precise, and cleaner alternative, especially at the microscale.

In this study, ultraviolet nanosecond laser ablation is applied to remove polyamide coatings from ultra-thin platinum wires in a water-assisted environment. The presence of water enhances the process by promoting thermal management and minimizing debris. Key processing parameters including scanning speed, overlap percentage, and line distance were evaluated.

The study primarily focuses on analyzing both the main effects and two-factor interactions of these parameters using Analysis of Variance (ANOVA). Interactions such as Speed × Overlap and Speed × Line Distance were statistically examined to identify how combined factors influence tensile strength and surface roughness. The results showed that a scanning speed of 1200 mm/s, with a line distance of 1 μm and a single loop, provided the most effective coating removal while maintaining the structural integrity of the wire. Higher speeds led to incomplete removal, while lower speeds risked damaging the wire.

A second phase of experimentation further expanded the parameter space by increasing the line distance and the number of loops to reduce overlap in the X direction. This allowed for more comprehensive process evaluation. Again, conditions around 1200 mm/s and 1500 mm/s with 2 μm line distance and two loops offered favorable outcomes, although 1200 mm/s was selected as the optimal speed due to better consistency.

These findings contribute to the development of a robust, high-precision laser processing method for ultra-thin wire applications. The statistical insight gained through ANOVA offers a data-driven framework for optimizing future laser ablation processes.

Key Words: ANOVA, Polyamide Coating Removal, Laser Parameter Optimization, Thermal Management, Tensile Strength, Surface Roughness

4.1 Introduction

Platinum has played a significant role in wiring technology, particularly in the aerospace and automotive industries, due to its remarkable electrical properties and exceptional durability, as evidenced by its substantial presence in the market. Additionally, coatings are essential in the manufacturing process, serving various functional and protective purposes. However, in certain fabrication scenarios, these coatings may need to be removed. Traditionally, chemical processes have been employed to achieve this, as they are generally effective across a wide range of applications [52]. Nevertheless, these methods come with significant drawbacks, including high costs, lengthy processing times, and hazardous working conditions, prompting researchers to explore alternative approaches [53].

In this context, laser ablation has emerged as a highly efficient technique for removing coatings, particularly at the microscale. This method offers several advantages, including rapid processing, precise control over the ablation process, and the ability to target specific regions for removal without causing damage to the underlying substrate [54]. Compared to other methods such as ultrasonic, cryogenic, or mechanical techniques, laser ablation demonstrates superior precision, efficiency, and minimal substrate impact, making it a compelling choice for advanced manufacturing applications (49).

Laser ablation has been widely employed in fabrication processes across various environments, with laser adjustments optimized based on the diverse range of lasers available in the market. Different types of lasers require specific parameter configurations to achieve desired outcomes in industrial applications [55]. The selection of the appropriate laser type and specifications—such as average power, peak power, repetition rate, and pulse duration—is critically dependent on the material properties and the intended purpose. These parameters significantly influence the efficiency and precision of the process [51] .

Cost-effective and energy-efficient UV lasers, along with nanosecond (ns) lasers, have demonstrated sufficient capability for precise laser ablation. Their relatively short pulse durations ensure high processing accuracy while maintaining lower equipment costs compared to other laser types with similar average

power outputs [56]. Additionally, laser ablation in liquid environments has emerged as a promising method for debris-free microfabrication, particularly for optoelectronic devices [57], and for generating nanoparticles in colloidal solutions [58].

In the context of aqueous laser treatment of platinum, molten material is effectively removed by bubble motion, where the debris is carried away through liquid thermal convection or bubble-induced motion [59]. The use of liquids, such as water, in laser processing offers significant advantages, including the fabrication of cleaner, debris-free microstructures. The high cooling rate of water compared to air reduces the extent of the heat-affected zone, leading to improved tolerances and enhanced precision during laser ablation [59]. The aim of this study is to systematically evaluate the influence of key laser processing parameters on the mechanical and surface characteristics of ultra-thin wires using Analysis of Variance (ANOVA). In precision laser-based processes, factors such as scanning speed, overlap percentage, and line distance play a crucial role in determining outcomes like tensile strength and surface roughness. However, their individual effects and interactive influences remain complex and require statistical validation [60].

Through a structured experimental design, this study applies ANOVA to identify statistically significant factors and interactions, distinguishing which parameters have the greatest impact on material performance. By examining both main effects and interactions such as Speed × Overlap and Speed × Line Distance we aim to provide a data-driven framework for optimizing laser ablation conditions. The findings will contribute to enhancing process efficiency, minimizing defects, and improving the precision of laser-based material processing, ensuring optimal parameter selection for future applications [61].

4.2 Materials and Methods

Figure 4.1 presents a schematic depiction of the experimental setup used for nanosecond laser ablation in a water environment. The process was conducted using 18 ns laser pulses at a wavelength of 355 nm and a pulse frequency of 20 kHz. A UV laser system with a Gaussian beam profile, supplied by MACTRON Inc, was utilized. The experiment involved a 50 µm platinum wire coated with polyamide, resulting in a total diameter of 65 µm. The platinum wire, including its polyamide coating, was fully submerged in a 2–3 ml layer of water within a glass container. The ablation process was conducted in two rotations of 180° each, ensuring that only half of the wire's circumference was ablated per pass. The laser focus was set at the top of the wire (65 µm level), meaning that the lowest point reached by the laser beam during ablation was 32.5 µm from the bottom of the wire. This setup allowed for complete circumferential ablation in two passes

while ensuring the water layer provided effective thermal regulation and debris removal. The sample was secured on a three-axis translation stage, with the ablation area set to a 10 mm × 10 mm square. The laser's interaction with the target material was governed by the frequency control of galvo scanner mirrors, as depicted in Figure1. To achieve a beam spot size of 20 μm, a 130 mm focal length lens was positioned from the galvo scanner, ensuring the beam was perpendicular to the surface within the ablation area. Adjustments were made to account for the refractive index difference between water and air, which necessitated parameter modifications compared to dry ablation experiments. A detailed description of this experimental setup and its parameters has been documented in earlier water-based laser ablation studies [54].

The research focuses on achieving optimal coating removal by utilizing higher scanning speeds, multiple ablation loops, and increased line distances in the X direction. This approach aims to enhance surface quality while improving process efficiency and reducing operational time.

The primary modification in this study, compared to previous research [54], is based on prior findings that demonstrated the significant impact of the incident angle on the curved wire surface and the presence of a water layer on spot diameter. These factors facilitated uniform ablation across the wire's surface, eliminating gaps as predicted by theoretical calculations [62]. However, in the current adjustment, the process parameters will be altered to incorporate higher scanning speeds, resulting in an increased line distance in the Y-axis, along with a greater number of loops to compensate for potential ablation gaps. It is important to note that the initial spot diameter of the laser system in air, when focused on a flat sheet, is 20 μm. However, as demonstrated in a previous study, the presence of water and the angle of incidence, due to the circular shape of the wires, cause the spot diameter to increase. The refractive index of water affects the laser's focus, altering the beam's behavior and causing the spot size to expand. Experiments show that when a flat sheet is submerged in 3ml of water, the spot diameter increases to approximately 30 μm. With the added factor of the angle of incidence, which is influenced by the curvature of the wire’s surface, the spot diameter increases further. For a clearer understanding, on a flat sheet in the presence of water, the beam’s divergence causes the focal point to shift slightly, positioning by around 32.5 μm (Half of wire) below apex, as measured by the laser ruler. Consequently, the spot diameter on this sheet was measured at an average of 45 μm, which could be considered the maximum spot diameter for this sample. This increase in spot size is largely due to both the water medium and the angle of incidence on the surface. Therefore, for calculation purposes, the spot diameter is assumed to be an average of 45 μm, representing the largest observed diameter under the experimental conditions.

This adjustment introduces a critical consideration: ensuring that the energy per unit area remains sufficient for effective ablation. While increasing the focal length inherently reduces the energy density, it simultaneously expands the coverage area, which could enhance uniformity. A well-balanced combination of spot size, scanning speed, and loop count is essential to achieving a smoother and more efficient ablation process. If optimized correctly, this new configuration could lead to faster ablation rates while maintaining complete coating removal without compromising the integrity of the platinum wire.

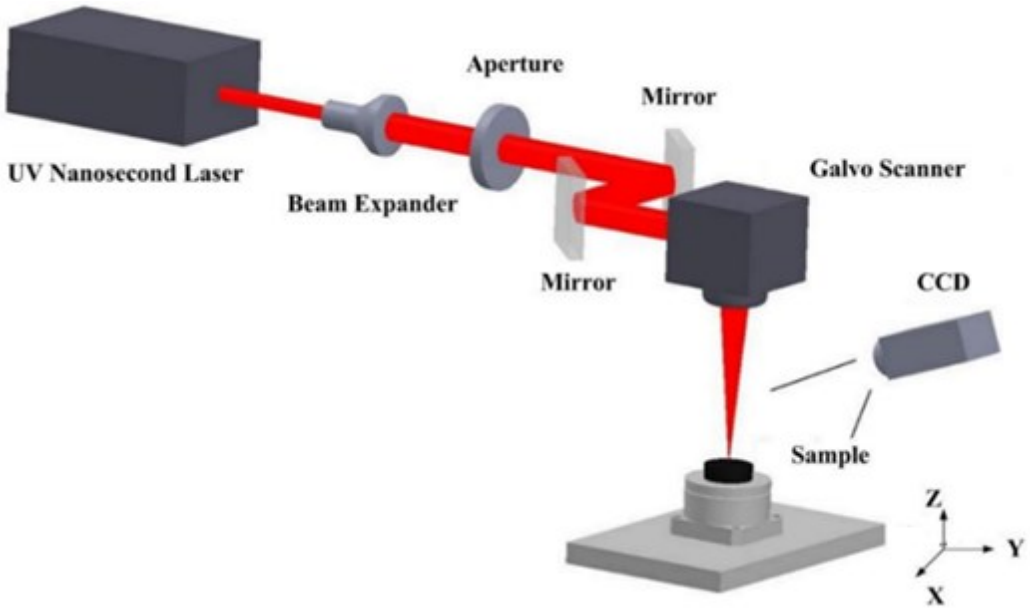

Figure 4.1 UV lasers principal diagram (15).

4.3 Results and discussion

The experiments were conducted using three distinct scanning speeds and multiple ablation loops to assess their influence on the process. The overlap percentage, determined using Equation (4.1), was dependent on the line distance along the X-axis, while the line distance along the Y-axis was influenced by scanning speed, as described by Equation (4.2). However, the impact of the Y-axis line distance remained stable throughout the experiments.

$$\text{Overlap: } \frac{\text{Spot Diameter} - \text{Line Distnace(x)}}{\text{Spot Diameter}} \qquad \text{Equation (4.1)}$$

$$\text{Line Distance Y (µm): } \frac{\text{Speed}(\frac{\mu m}{s})}{\text{Repetition rate(Hz)}} \qquad \text{Equation (4.2)}$$

or a laser system emitting Gaussian-shaped pulses, the pulse duration is typically measured at Full Width at Half Maximum (FWHM). The peak laser power can be estimated using Equation (4.3), assuming no correction factor is applied. Given that the average power of the system is 3 W and using the relationship between peak power and average power in pulsed laser systems, the calculated peak power is 8.33 kW.

$$P_{peak} = \frac{\text{Average Power}}{\text{Pulse Duration} \times \text{Repetition Rate}} \quad \text{Equation (4.3)}$$

Speed (mm/s)	1200		1500		2000	
Line Spacing (Y, μm)	60		75		100	
Line Distance (X, μm)	2	10	2	10	2	10
Overlap (%)	95.55	77.77	95.55	77.77	95.55	77.77
Number of Loops	2	3	2	3	2	3

Table 4.1. adjustment of laser machine for experiment in water.

$$F\ (\text{Gaussian Beam}) = \frac{2E\ \text{Pulse}}{\text{Area}} \quad \text{Equation (4.4)}$$

Before calculating the fluence, it is essential to determine the pulse energy which can be obtained using Equation (4.5). This equation provides a direct relationship between the peak power and the energy delivered per pulse. Once E_{pulse} is determined, it can be used to compute the fluence, which quantifies the energy density delivered to the material during laser ablation. τ_{Pulse} is 18 nanoseconds for this system.

$$E_{Pulse} = P_{peak} \times \tau_{Pulse} \quad \text{Equation (4.5)}$$

Consequently, the fluence, calculated using Equation 4.4, was determined to be 18.86 J/cm², which remained consistent across all experimental configurations. Initially, with the machine's standard spot diameter, the fluence was calculated to be 95.5 J/cm². However, as the spot diameter increased due to factors such as the angle of incidence and the presence of water, the fluence consequently decreased. This reduction in fluence is a direct result of the larger area over which the laser energy is distributed, leading

to less energy being delivered per unit area on the target. Table 1 presents the experimental design for water-based ablation, incorporating higher scanning speeds and multiple loops. These parameters were optimized to achieve superior surface quality compared to previous adjustments and demonstrate improvements over the chemical methods referenced in earlier research [54]. Following the completion of all experiments on the samples, including tensile strength and surface roughness measurements, the collected data was analyzed using ANOVA with the assistance of Python. The results of this analysis are presented in the subsequent sections.

All wire samples underwent tensile strength testing and surface roughness evaluation following the ablation process. To prevent slippage during testing, the wires were securely held by grips, and tensile strength measurements were performed using an Instron Inc. universal testing machine (UTM) equipped with a 50 N load cell. The UTM was set to a crosshead speed of 5 mm/min to ensure precise and controlled measurements, minimizing potential errors. For each experimental condition, tensile strength was measured on three separate wire samples.

Surface roughness analysis was performed using an Olympus Lext 500 confocal microscope. A 3D scan of each sample was captured at 20x magnification, with an image resolution of 645 × 645 μm. Linear roughness measurements were then carried out along multiple lines across three different sections of each wire. This process was repeated for three wires per experimental condition. The average values obtained from these measurements were subsequently used for analysis.

4.3.1 Tensile Strength

As shown in Figure 4.2, the design of experiments revealed that certain parameter adjustments did not result in satisfactory surface quality, even when tensile strength values were comparable to those of successful samples. Among all configurations, only the samples processed at 1500 mm/s and 1200 mm/s, both featuring high overlap in the X direction and two loops, demonstrated acceptable surface characteristics. Notably, the sample at 1200 mm/s exhibited the best surface quality overall, outperforming all other adjustments. Figure 4.2B, as also described below the figure, shows that although the coating was removed, the surface roughness still had room for improvement. Additionally, as speed and line distance increased, the ablation affected the coating, but residual material remained on the surface, indicating that the process was unable to fully reach the substrate. Due to space limitations, the images for the remaining samples were

cropped accordingly. For each adjustment, a minimum of three wires were evaluated, with three segments measured on each wire to ensure reliable and representative results.

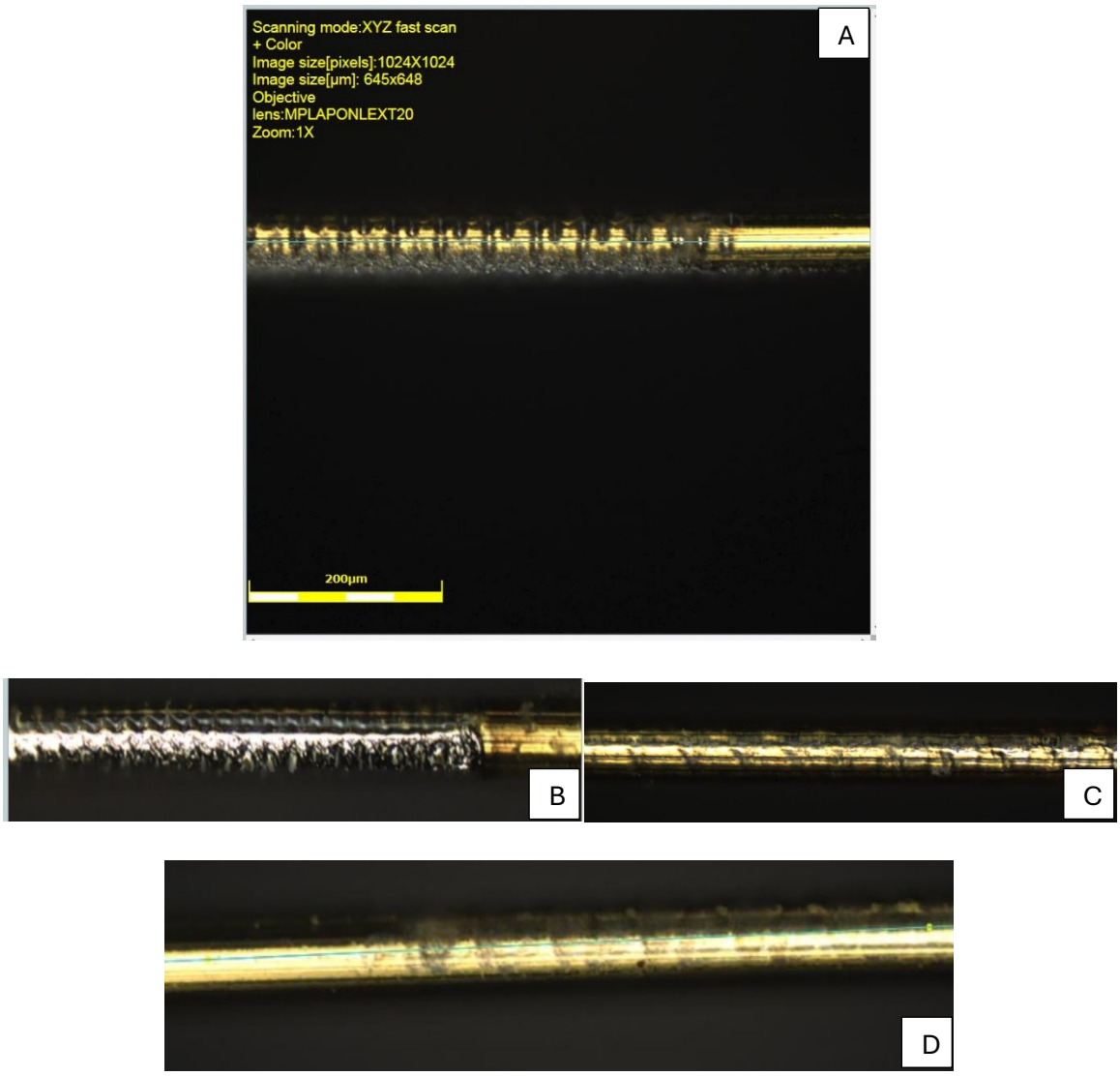

Figure 4.2 (A) laser scan speed 1500mm/s, line distance 10 µm and 3 loops. (B) laser scan speed 1500mm/s, line distance 2µm with 2 loops. (C) laser scan speed 2000mm/s, line distance 2 µm with 2 loops. (D) Laser scan speed 2000mm/s, line distance 10 µm with 3 loops.

Based on the previously discussed experimental conditions, the laser-ablated wire samples were subjected to tensile strength measurements, and the average values for each sample are presented in the figure 4.3. As anticipated, an increase in line distance, which directly reduces the overlap in the x-direction, resulted in higher tensile strength. Additionally, higher processing speeds exhibited a lesser weakening effect on the wires, leading to samples processed at higher speeds demonstrating superior tensile strength. The obtained

results closely align with those achieved through the traditional chemical stripping process from prior studies [54], while also demonstrating greater efficiency in both processing time and outcomes compared to the final water-assisted laser ablation adjustments conducted in the earlier study.

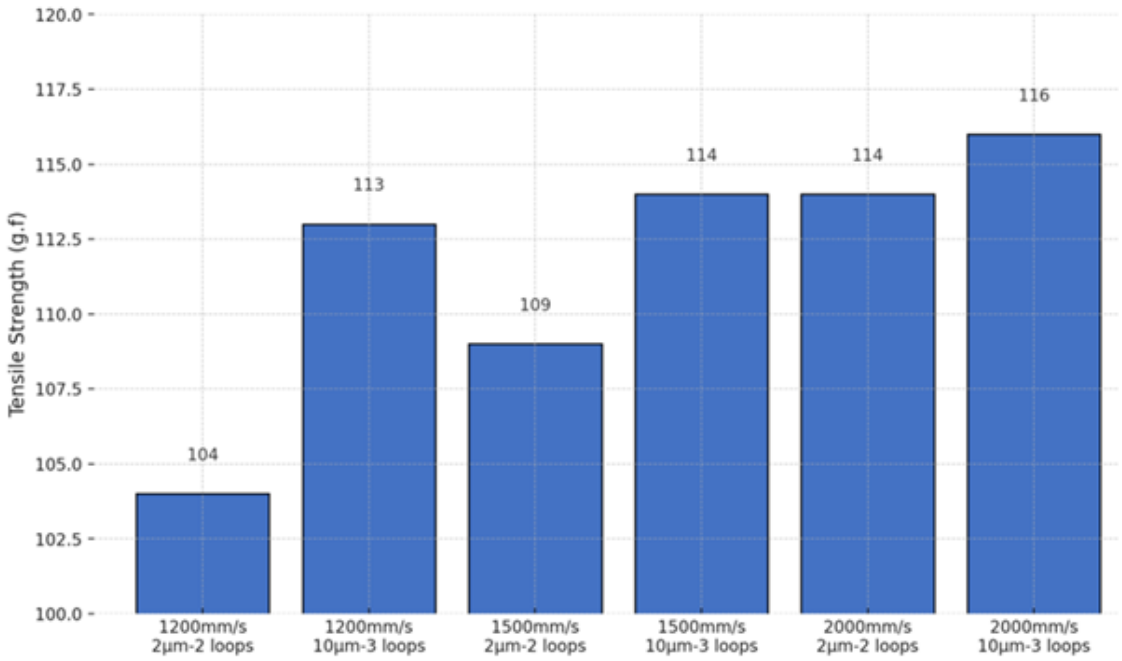

Figure 4.3 tensile strength results for confined adjustments

It is important to highlight that although all samples were evaluated using both the confocal microscope and the on-site microscope, only the samples processed at 1200 mm/s with a 2 µm line distance and at 1500 mm/s with a 2 µm line distance, both using 2 loops, exhibited surfaces completely free of debris. The remaining samples, despite showing partial coating removal, contained residual debris and were therefore not suitable for the next stage of the manufacturing process, which demands a high degree of cleanliness and precision due to the sensitivity of the application.

This outcome reflects a significant improvement attributed to the adjustment in focal length, which increased the laser spot diameter. This enhancement effectively compensated for the gaps in the y-axis, particularly at higher processing speeds such as 1500 mm/s with a 2 µm line distance in the x-axis direction. Notably, these results exceed the performance of previously recommended parameters from earlier studies, which were limited to lower speeds (1000 to 1200 mm/s) and a 1 µm line distance in the x-direction.

The choice of the experimental table design is also noteworthy. It was intended to enable a faster processing route while approximating the outcomes of conventional chemical methods. For example, the configuration using a 10 µm line distance in the x-axis, though substantially reducing the overlap, incorporated three consecutive ablation passes. This adjustment was found to effectively remove the coating without causing thermal damage or burning, though some sections still exhibited residual debris. Nonetheless, this setup provides a valuable framework for defining parameter boundaries in preparation for subsequent ANOVA analysis.

4.3.2 Roughness

The surface roughness values for each experimental adjustment were meticulously assessed using a confocal microscope, employing 3D scanning over a 645 × 645 µm area. To ensure accuracy, roughness measurements were conducted through line assessments at three distinct segments on three separate wire samples for each parameter configuration. As anticipated, a smaller line distance in the x-direction corresponding to a higher overlap yielded superior surface quality and lower roughness values. In contrast, processing speed exhibited an inverse correlation with surface roughness, as higher ablation speeds led to a decline in surface quality. Notably, increasing the number of ablation loops failed to compensate for the drawbacks of a larger line distance in the x-direction. This finding reinforces the critical role of a reduced line distance and greater overlap in achieving optimal surface smoothness. Figure 4.4 illustrates the results across all adjustments, further substantiating these observations and validating the underlying analysis.

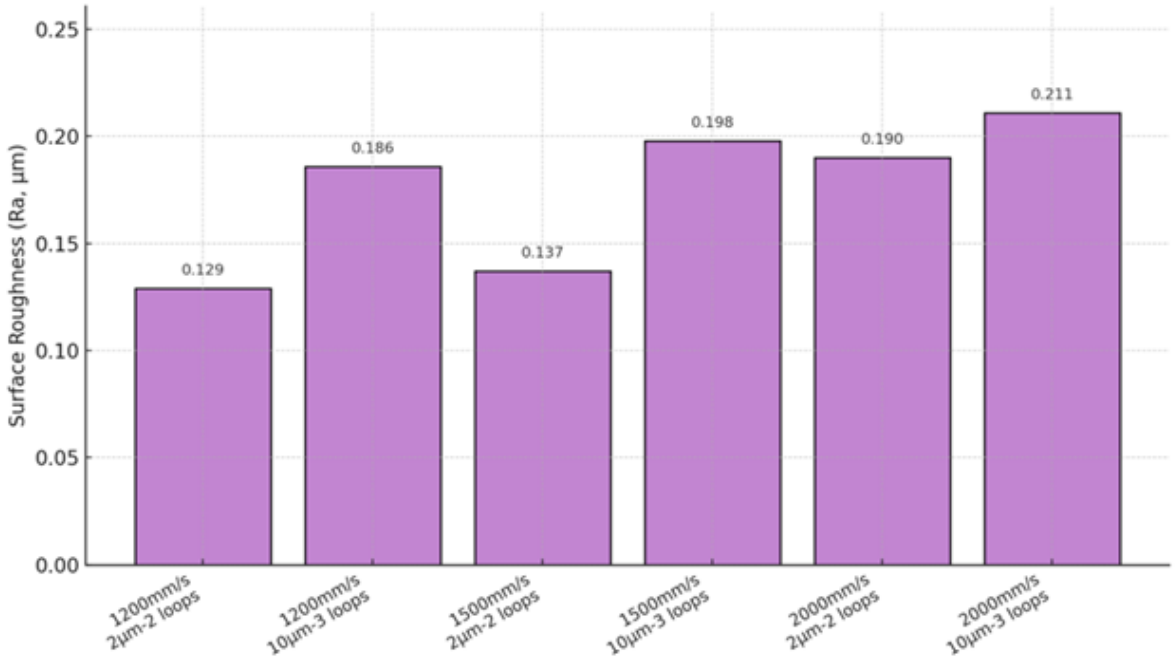

Figure 4.4 Roughness results for confined adjustments

After collecting all the data, the next step involves conducting an ANOVA evaluation to gain a comprehensive understanding of the effects of each parameter on the laser ablation process. This analysis serves as a valuable tool for future research involving fine and delicate wire samples, facilitating the identification of optimal process parameters efficiently, even when using different laser systems.

As shown in Figure 4.5, a speed of 1200 mm/s combined with a 2-µm line distance in the X direction and 2 loops produced effective results, yielding clean de-coating with no visible debris. Surface roughness measurements further confirm the effectiveness, with an Ra value of 0.110 recorded at the center of the ablated area. It is important to note that for each wire, roughness was measured at three different segments, and the average value was reported in Table 4.2. This approach ensured more reliable results for comparison and supported the validity of outcomes in the ANOVA analysis.

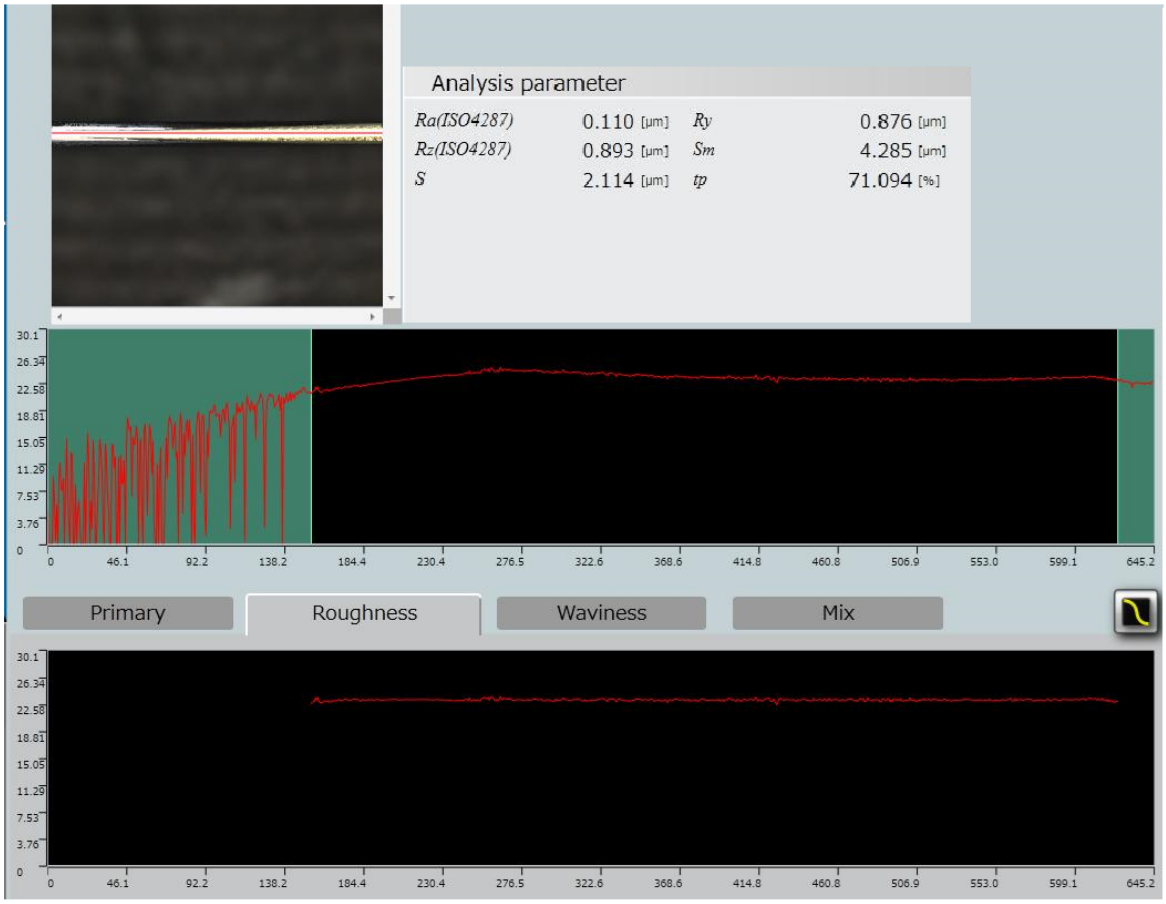

Figure 4.5 Sample ablated under 1200mm/s,2 µm line distance X combined with 2 loops, Under Lext 500 confocal Machine.

4.4 ANOVA Introduction

To evaluate the influence of key laser processing parameters on tensile strength and surface roughness, a multiple regression model incorporating interaction terms was employed. The primary factors considered in this study include scanning speed, which directly controls the line distance in the Y-direction, and line distance in the X-direction, which determines the overlap in X. Additionally, the number of loops was analyzed to assess its effectiveness in compensating for variations in other parameters. The analysis was conducted in two stages: first, the independent effects of speed, number of loops, and line distance in X were evaluated. Then, interactions between these factors were considered to better understand their combined influence on the response variables. The dataset consists of 18 samples with varying process

parameters: speed (mm/s), number of loops, and line distance in X (µm). The response variables measured are tensile strength (g/force) and surface roughness (µm).

Sample	Overlap X (%)	Line Distance X (µm)	Line Distance Y (µm)	Speed mm/s	Number of Loops	Tensile Strength (g/force)	Roughness (µm)
1	95.55	2	60	1200	2	105.5	0.126
2	95.55	2	60	1200	2	102	0.134
3	95.55	2	60	1200	2	104.8	0.123
4	77.77	10	60	1200	3	112.3	0.179
5	77.77	10	60	1200	3	114.6	0.192
6	77.77	1o	60	1200	3	110.8	0.186
7	95.55	2	75	1500	2	108.8	0.138
8	95.55	2	75	1500	2	106	0.145
9	95.55	2	75	1500	2	111.2	0.131
10	77.77	10	75	1500	3	112	0.201
11	77.77	10	75	1500	3	115.7	0.195
12	77.77	10	75	1500	3	113.5	0.194
13	95.55	2	100	2000	2	113.9	0.191
14	95.55	2	100	2000	2	112.8	0.197
15	95.55	2	100	2000	2	115.5	0.186
16	77.77	10	100	2000	3	118.7	0.218
17	77.77	10	100	2000	3	114.3	0.197
18	77.77	10	100	2000	3	115.7	0.214

Table 4.2 results of each adjustment for three samples.

Initially, a one-way ANOVA was conducted to evaluate the influence of each factor independently. The analysis revealed that as scanning speed increases, tensile strength generally improves; however, it tends to stabilize at higher speeds. In contrast, surface roughness exhibits a slight increase at 2000 mm/s, suggesting that elevated energy input influences material quality.

The number of loops also plays a crucial role in the process. Increasing the number of loops enhances tensile strength, likely due to improved material removal. However, roughness also increases with additional loops,

primarily because, at a higher line distance in X (10 µm), the overlap in X decreases, leading to inconsistent material removal. Furthermore, it was observed that using two loops at a lower line distance in X could result in excessive heat accumulation, causing burning and potential damage to the specimen. Therefore, this parameter configuration provided an optimal basis for analyzing the entire process.

Another key parameter assessed separately through ANOVA was the line distance in X, which directly determines the overlap in X. The results indicate that smaller line distances result in lower roughness values, implying a more uniform ablation process.

4.4.1 ANOVA for Main Effects (Tensile Strength)

The entire statistical analysis was performed using Python. As presented in Table 4.3, the sum of squares (SS) represents the proportion of variation in tensile strength attributable to each main factor: scanning speed, number of loops, and line distance along the X axis. Among these, scanning speed exhibited a statistically significant influence ($p = 0.00075$), with an increase from 1200 mm/s to 2000 mm/s correlating with enhanced wire strength. Similarly, line distance in the X axis showed a strong effect ($p = 0.00035$), where a tighter spacing of 2 µm contributed to improved structural integrity and minimized thermal damage. The number of loops demonstrated the most significant impact ($p = 0.00035$), indicating that increasing the loop count from 2 to 3 enhances the completeness of coating removal; however, it may also introduce additional thermal stress, which interacts with scanning speed to affect tensile strength.

Source	Sum of Squares	degree of freedom	F-value	p-value
Speed	140.57	2	12.57	0.00075
Line Distance X	123.25	1	22.04	0.00035
Number of Loops	123.25	1	22.04	0.00035
Residual (Error)	78.28	14	-	-

Table 4.3. ANOVA Values for main effects of Tensile strength

According to Table 4.3 as well of figure 4.2, the findings indicate that increasing speed enhances tensile strength up to a certain limit, beyond which the improvement levels off. At lower speeds, prolonged laser exposure leads to excessive heat buildup, which can result in over-ablation and structural weakening. In contrast, at very high speeds, the efficiency of the ablation process may diminish due to reduced energy deposition per unit area. This explains why tensile strength initially increases with speed but eventually stabilizes. Additionally, a smaller line distance X (corresponding to a higher overlap in X) facilitates more uniform and effective material removal, thereby improving structural integrity and tensile strength. However, when the line distance X is too large (resulting in lower overlap in X), the ablation process becomes inconsistent, leading to incomplete material removal in certain areas, which can introduce weak points in the wire structure.

4.4.2 ANOVA for Main Effects (Surface Roughness)

The main effects were also analyzed to determine which parameter has the most significant impact on surface quality. This assessment helps identify the primary contributors to variations in roughness. Table 4 presents the ANOVA results for surface roughness, highlighting the influence of each factor.

Source	Sum of Squares	degree of freedom	F-value	p-value
Speed	0.00627	2	20.08	0.000077
Line Distance X	0.00911	1	58.37	0.000002
Number of Loops	0.00911	1	58.37	0.000002
Residual (Error)	0.00219	14	-	-

Table 4.4 ANOVA Values for main effects of Tensile strength

According to the results presented in Table 4.4, scanning speed has a statistically significant effect on surface roughness ($p = 0.000077$). Higher scanning speeds are associated with increased roughness, likely due to insufficient interaction time between the laser and the surface, leading to incomplete or uneven material removal. Line distance in the X-axis also shows a strong influence ($p = 0.000002$); smaller line distances improve surface uniformity and reduce roughness by ensuring more overlap between laser paths.

Additionally, the number of loops significantly affects roughness ($p = 0.000002$). While increasing the number of loops enhances the completeness of ablation, it can also introduce excess heat, which contributes to increased surface irregularities and may interact with speed to further affect surface quality.

It is apparent that Surface roughness is highly sensitive to line distance X and the number of loops, with a strong interaction effect. A lower line distance X improves surface smoothness, while a larger line distance X combined with multiple loops significantly increases roughness due to inconsistent ablation.

4.5 Interactions Parameters

After analyzing the main effects, it was essential to examine key interaction effects that could significantly influence the process. The selection of these interactions was guided by their impact on ablation performance and the importance of optimizing them during processing. To account for the complex interdependencies between factors, the following interactions were analyzed:

Speed × Number of Loops

Speed influences the rate of energy delivery, while the number of loops determines the duration of exposure at each point on the wire. This interaction was chosen to assess how variations in speed, combined with repeated passes, affect both tensile strength and surface roughness. A higher number of loops at lower speeds may lead to excessive heat accumulation, potentially damaging the wire, whereas at higher speeds, multiple loops may ensure effective material removal without causing overheating. This interaction helps determine the optimal balance between speed and looping cycles for achieving the best mechanical properties.

Speed × Line Distance X

Line distance X controls the degree of overlap in the ablation process, affecting material removal consistency. The interaction between speed and line distance X is crucial because higher speeds with larger line distances may result in uneven energy distribution, leading to inconsistent ablation. At lower speeds, a smaller line distance X (higher overlap) can enhance uniformity, but at higher speeds, a large line distance X might cause insufficient overlap, leaving unprocessed regions. This interaction helps evaluate whether a higher processing speed can be compensated for by adjusting the line distance.

Number of Loops × Line Distance X

Increasing the number of loops while maintaining a smaller line distance X (higher overlap) may lead to excessive energy accumulation, potentially causing burning or material degradation. Conversely, a larger line distance X with more loops could result in incomplete ablation, leaving weak points in the wire structure. By analyzing this interaction, we can determine the optimal balance between the number of loops and line distance X to achieve consistent material removal without excessive damage.

4.5.1 ANOVA for Interaction Effects (Tensile Strength)

Before delving more to see which interaction has highest effect, it is noteworthy to mention that when analyzing the experimental results, we initially examined the main effects of Speed, Number of Loops, and Line Distance X separately to determine their individual influence on tensile strength and roughness. However, to better understand how these factors interact, we expanded the analysis to include interaction effects. When interactions are considered, the variance that was initially attributed solely to the main effects is redistributed among the interaction terms, leading to slight adjustments in the F-values and p-values. This difference arises because certain combinations of factors may influence the response more than the sum of their individual effects. If a significant shift in values is observed, it suggests that interactions play a crucial role in determining the final material properties. Conversely, if the differences are minor, it indicates that the primary factors are the dominant contributors. Understanding these interactions allows for a more precise interpretation of how process parameters collectively affect tensile strength and surface roughness.

Source of Variation	Sum of Squares	degree of freedom	F-value	p-value
Speed × Loops	29.83	2	3.69	0.0562
Speed × Line Distance X	29.83	2	3.69	0.0562
Loops × Line Distance X	107.53	1	26.63	0.0002
Residual	48.45	12	—	—

Table 4.5. ANOVA Values for interaction effects of Tensile strength

The interaction between scanning speed and number of loops yields a p-value of 0.0562, which is marginally above the conventional threshold for statistical significance ($\alpha = 0.05$). This suggests a potential interaction effect, implying that the impact of scanning speed on tensile strength may vary depending on

the number of loops. For instance, increased speed does not consistently enhance tensile strength across different loop counts. Similarly, the interaction between speed and line distance in the X-direction ($p = 0.0562$) is also near significance, indicating that the effect of speed on tensile strength may be influenced by the spacing between lines along the X-axis. In contrast, the interaction between number of loops and X-direction line distance is highly significant ($p = 0.0002$), demonstrating a strong dependency between these two factors. Specifically, a larger X-line distance appears to enhance tensile strength, particularly when a greater number of loops are applied. This suggests that wider spacing between lines allows better heat dissipation during multiple passes, reducing the risk of thermal damage and promoting improved wire integrity.

4.5.1.1 plots for Interaction Effects (Tensile Strength)

Speed × Number of Loops

The interaction plot demonstrates that tensile strength is influenced not only by scanning speed or loop count independently, but also by their combination. When the number of loops is set to 3, increasing the speed from 1200 mm/s to 2000 mm/s leads to a more pronounced improvement in tensile strength compared to when only 2 loops are used. This suggests that higher speeds are more effective at enhancing material strength when paired with a greater number of loops, likely due to more efficient ablation and better coating removal through multiple passes. However, this benefit is less evident at lower loop counts, indicating that speed alone cannot compensate for insufficient exposure.

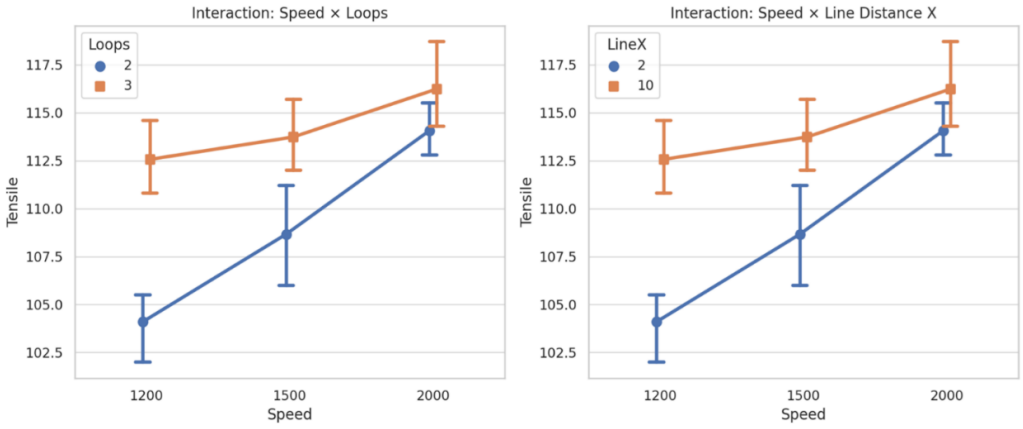

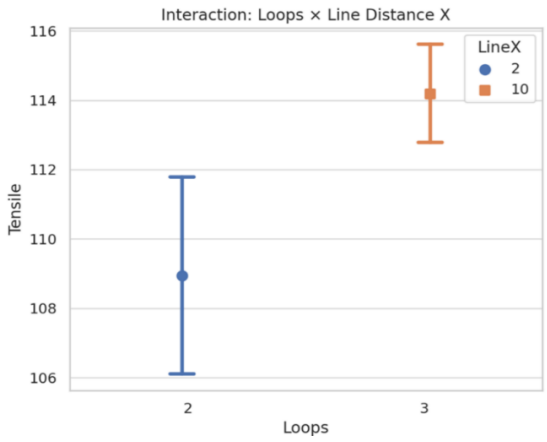

Figure 4.6 ANOVA plot for interaction effects of Tensile strength

Speed × Line Distance X

This interaction reveals how scanning speed and X-axis line distance jointly influence tensile strength. At lower speeds (1200 mm/s), a larger line distance (10 µm) results in higher tensile strength, likely due to minimized thermal overlap and reduced risk of overheating. However, this trend shifts at higher speeds. As speed increases, the benefit of the larger line distance becomes less significant or reverses, implying that at high speeds, tighter spacing (2 µm) may promote more complete coating removal. Importantly, although the 10 µm line distance yielded better tensile results, it was observed during experimentation that this setting often failed to achieve complete coating removal. This poses a significant limitation, as incomplete ablation undermines functional performance despite the apparent mechanical strength. Therefore, in real processing conditions, 10 µm cannot be recommended, and a tighter spacing—though potentially more thermally aggressive—may be necessary to ensure consistent and complete stripping.

Number of Loops × Line Distance X

The interaction between loop count and X-line distance highlights a shift in performance depending on the combination of settings. For 2 loops, a tighter line distance (2 µm) yields higher tensile strength, likely compensating for fewer passes by improving ablation density and surface interaction. In contrast, under 3-loop conditions, the 10 µm line distance surprisingly results in better tensile strength, possibly due to reduced cumulative heat input across multiple passes. However, as with the speed interaction, it's important to acknowledge that the 10 µm line distance failed to consistently remove the coating, making it unreliable for practical application. Despite its favorable mechanical readings, incomplete removal introduces

significant functional and reliability concerns, reinforcing that tighter spacing should be favored in real-world processing.

4.5.2 ANOVA for Interaction Effects (Surface Roughness)

According to Table 4.6, the interaction between Speed and Number of Loops is highly statistically significant, indicating that the influence of scanning speed on surface roughness varies depending on the number of applied loops. Specifically, at lower loop counts, increasing the scanning speed may contribute to lower surface roughness due to minimized thermal input. However, this benefit may diminish or reverse at higher loop counts, where cumulative heat from successive passes can lead to greater surface irregularities. The large F-value associated with this interaction further supports its strong effect. Similarly, the interaction between Speed and Line Distance X (horizontal line spacing) is also statistically significant, suggesting that surface finish is affected by how scanning speed interacts with the spacing between adjacent lines. At narrower line distances (2 μm), higher speeds may promote better heat dissipation and smoother surfaces. Conversely, with larger spacings (10 μm), insufficient overlap at high speeds can lead to uneven ablation and increased roughness. This reinforces the necessity of coordinating speed settings with scan density to achieve optimal surface quality.

The interaction between Number of Loops and Line Distance X demonstrates the most pronounced statistical significance, as reflected by the highest F-value and a near-zero p-value. This indicates a dominant role in influencing surface roughness. The effect of line spacing significantly changes with varying loop counts. At fewer loops, a denser scan pattern (smaller line distance) enhances surface uniformity through controlled ablation. However, under increased looping, the same tight spacing can result in thermal buildup, thereby deteriorating the surface finish. This interaction underscores a fundamental balance that must be maintained between spatial resolution and thermal effects to optimize the process.

Source of Variation	Sum of Squares	degree of freedom	F-value	p-value
Speed × Loops	0.00160	2	16.404	0.00037
Speed × Line Distance X	0.00160	2	16.404	0.00037
Loops × Line Distance X	0.00505	1	103.44875	0.0000
Residual	0.00059	12	—	—

Table 4.6 ANOVA Values for interaction effects of Surface Roughness

4.5.2.1 plots for Interaction Effects (Surface Roughness)

Speed × Number of Loops

Figure 4.7 presents the interaction between scanning speed and the number of loops, highlighting their combined influence on surface roughness. The results indicate that the effect of speed on roughness is contingent upon the number of loops applied. At two loops, surface roughness remains relatively low at reduced speeds but increases considerably with higher speeds, likely due to accumulated thermal effects. In contrast, when three loops are applied, surface roughness is consistently higher across all speeds, implying that additional scanning passes intensify heat accumulation, thereby diminishing any potential smoothing benefits associated with increased scanning velocity.

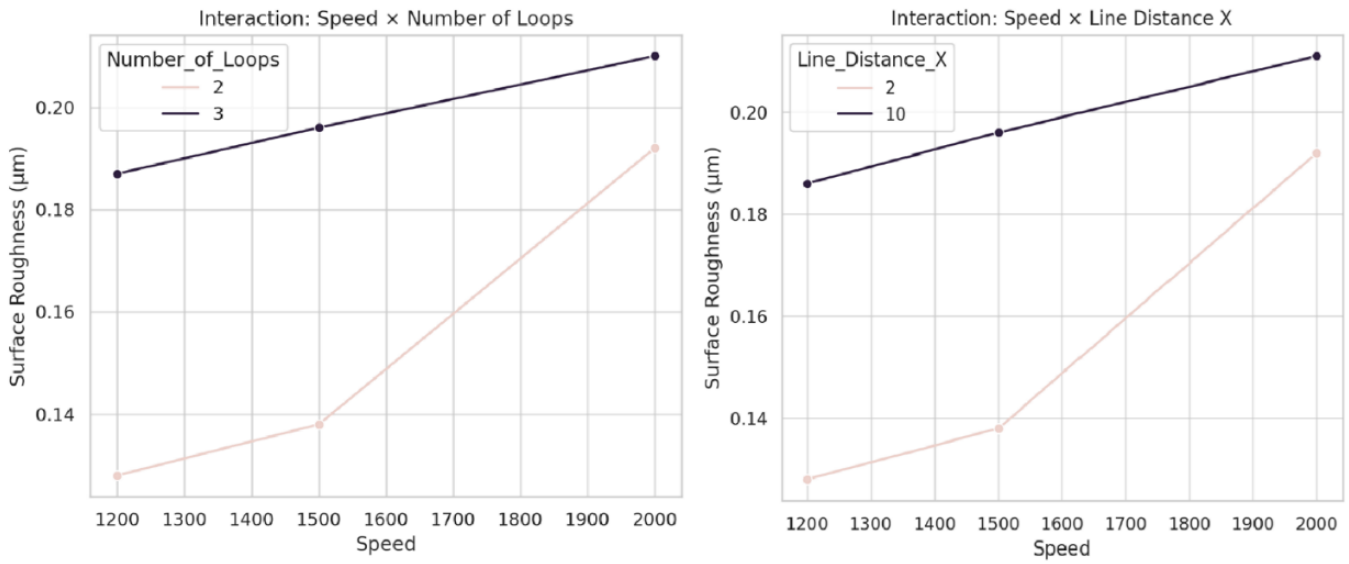

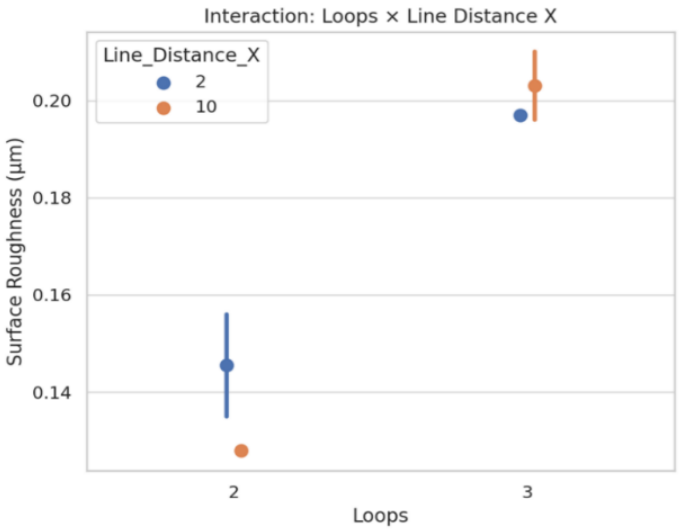

Figure 4.7. ANOVA plot for interaction effects of Average Roughness.

Speed × Line Distance X

As depicted in Figure 4.7, this interaction demonstrates that the impact of scanning speed on surface roughness is strongly influenced by the density of scan lines. When line spacing is narrow, higher scanning speeds can still yield satisfactory surface smoothness, likely due to uniform energy distribution and effective thermal management. However, at wider line spacing, increased scanning speed results in inadequate overlap between scan lines and reduced ablation consistency, thereby significantly elevating surface roughness.

Number of Loops × Line Distance X

This interaction is the most statistically significant, indicating that the influence of line spacing on surface roughness is strongly dependent on the number of loops. At lower loop counts, reduced line spacing enhances ablation control, contributing to improved surface smoothness. Conversely, at higher loop counts, the same tight spacing can lead to excessive thermal accumulation, which adversely affects the surface quality. This finding underscores a critical trade-off between spatial resolution and thermal regulation, necessitating careful optimization of processing parameters to achieve the desired surface characteristics.

Figure 8 illustrates the final result of the newly adjusted ablation settings. Notably, the insights gained through ANOVA analysis have provided a clearer understanding of the process, which can significantly enhance the efficiency and speed of future operations.

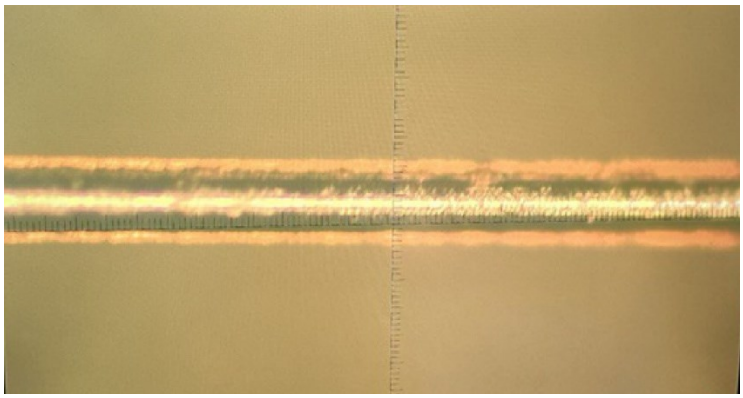

Figure 8.Ablated wire withspeed of 1200mm/s-2µm under on-site Microscope (Nikon Nomarski 20X).

4.6. Conclusion

This study provides a thorough statistical analysis of the factors affecting surface roughness in laser-based machining processes, with a particular focus on scanning speed, the number of loops, and X-direction line spacing. The results, derived from two-way Analysis of Variance (ANOVA), offer insightful conclusions about the individual and interactive effects of these parameters on the surface finish.

The main effects revealed that scanning speed and number of loops have a significant influence on surface roughness, with speed showing a more prominent impact at higher values and loop count influencing roughness, particularly at lower speeds. The line distance in the X-direction, while important, exhibited less significant effects in isolation, but its interaction with the other factors brought out key dependencies that were not evident from main effects alone.

The interaction effects demonstrated a deeper understanding of the relationship between the parameters. Specifically, the Speed × Loops interaction illustrated that the impact of loop count on roughness becomes more pronounced at lower speeds, likely due to longer exposure times and the accumulation of heat during the process. At higher speeds, the effect of increasing loops diminished, suggesting that the reduced interaction time at higher speeds may limit thermal buildup and, consequently, surface degradation.

Similarly, the Speed × Line Distance X interaction highlighted that while tighter spacing (2 µm) yielded smoother surfaces at lower speeds, this advantage was less evident at higher speeds, where thermal management becomes less dependent on the line spacing. The Loops × Line Distance X interaction revealed that, when the number of loops increased, the spacing between lines became less influential, as the thermal effects from multiple passes dominated the surface quality, regardless of the line distance.

These findings underscore the importance of considering both main effects and interactions when analyzing the outcomes of laser machining processes. The complex relationships between speed, loop count, and line distance suggest that optimal parameters for achieving low surface roughness cannot be determined by simply isolating each factor. Instead, a more nuanced approach is required, where the interplay between factors is carefully considered.

This study serves as a robust example of how statistical analysis—specifically, the use of ANOVA—can be leveraged to validate and expand upon experimental observations in a laser machining context. The identification of significant main effects and interactions provides valuable insights for refining process parameters, optimizing surface finish, and guiding future research in precision material processing.

CHAPTER 5: Conclusion and Future Work

5.1 Conclusion

In conclusion, the advancement of wire coating removal techniques is crucial for improving the precision, reliability, and sustainability of manufacturing processes, particularly in high-stakes industries such as aerospace, biomedical, automotive, and advanced electronics. This study comprehensively examined various de-coating methods, including ultrasonic stripping, chemical stripping, cryogenic treatment, and laser ablation, highlighting their respective effectiveness, limitations, and applicability to micro-scale wire systems.

Among the methods explored, laser ablation stands out as the most advantageous, offering exceptional precision, selective removal capabilities, and minimal thermal impact on the substrate. Ultraviolet nanosecond-pulsed lasers, especially when combined with a water-assisted environment, have proven highly effective in removing polyamide coatings from delicate platinum wires without compromising their integrity. In contrast, ultrasonic, cryogenic, and chemical stripping methods present significant challenges, particularly in fine wire applications, due to issues such as uneven energy distribution, potential damage to sensitive materials, and environmental and safety concerns. The findings of this study underscore the superiority of laser ablation in terms of both technical performance and alignment with sustainable manufacturing practices. This method eliminates the need for hazardous solvents, reduces waste, and supports eco-efficient production through localized, high-speed processing.

The study also emphasizes the importance of optimizing key laser parameters, including wavelength, pulse duration, scanning speed, and fluence, to achieve controlled energy deposition and minimize heat effects. By refining these parameters and leveraging statistical modeling and experimental validation, this research provides valuable insights for further enhancing the laser ablation process and advancing its application in various high-precision industries.

Given the polyamide coating and the microscale diameter of the platinum wires, it was essential to utilize a laser source with a lower wavelength to achieve precise and localized energy delivery. The use of a UV laser allowed us to operate at fluence levels that effectively interacted with the coating while minimizing thermal damage to the wire substrate. In contrast, using a fiber laser with a 1064 nm wavelength proved impractical for this application due to its deeper penetration and less controllable ablation at this scale.

This research is organized into three phases. The first phase involved an experimental investigation of the laser ablation process in an air ambient, which proved unsuccessful due to significant damage to the wires under all tested adjustments. The second phase involved changing the ambient to water in a controlled water-assisted setup, focusing on the removal of polyamide coatings from thin platinum wires. Among the various parameters tested, the most effective settings were found to be a scanning speed of 1200 mm/s, a 1 µm line distance in the X-direction, and one loop, which resulted in the cleanest and most uniform coating removal. Higher speeds caused incomplete de-coating, while lower speeds led to thermal degradation and compromised wire integrity.

In the final phase, a two-way ANOVA analysis was conducted to gain a deeper understanding of the main effects and interaction effects of key parameters—speed, line distance, and number of loops. To further explore parameter sensitivity, the line distance was increased (reducing overlap), and additional loops were added to compensate. Results showed that 1200 mm/s and 1500 mm/s, combined with a 2 µm line distance and 2 loops, produced favorable outcomes, though 1200 mm/s remained the most reliable across all trials. Interaction plots demonstrated the significant contributions of all parameters to the overall process outcome, indicating that the system is highly tunable.

Together, these three phases provide a comprehensive understanding of the laser-based wire stripping process, demonstrating that UV laser ablation is precise, controllable, and well-suited for delicate applications. The methodology balances experimental observations with analytical validation, offering a practical approach to high-precision, damage-free coating removal, making it ideal for industries such as aerospace, medical, and microelectronics

5.2 Future Work

The next phase of this project involves the development of a more stable and precisely engineered jig to securely hold the wires during the laser ablation process. Unlike the current method, which only allows access to one side of the wire, the upcoming setup will aim to enable complete circumferential, or 360°, ablation. This should ideally be achieved in a single or at most two ablation passes.

While the current technique of mounting the wires on solid cardboard sheets with pre-cut ablation windows has proven to be practical and capable of producing satisfactory results, it lacks the level of repeatability needed for microscale processing. One of the critical challenges is ensuring that the wires are consistently aligned and fully straightened across their length during ablation. Variability in the wire tension or slight

misalignments can lead to uneven coating removal or inconsistent exposure, especially considering the sensitive scale and properties of the wire.

To address this, a custom-designed fixture will be necessary. This fixture must be able to hold the wires with high mechanical stability, eliminating vibrations or unintentional movements. It should allow for full rotational access to the wire surface to achieve uniform coating removal around the entire circumference. Additionally, since water has shown to play a vital role in controlling heat accumulation and influencing the ablation outcome, the fixture must include a system for introducing and removing water in a controlled manner. This involves the design and calculation of both water inlet and outlet systems, ensuring that a stable, consistent water layer surrounds the wire during ablation. The water layer not only aids in thermal management but also contributes to bubble dynamics and particle removal, which directly affect the ablation quality.

Furthermore, the fixture must be compact and compatible with the spatial constraints of the existing laser system. An additional enhancement in the next phase will be the integration of a machine vision system, supported by a high-resolution camera setup currently under development by the partnering company. This system is intended to be universally adaptable to all laser workstations and will provide high-magnification visualization of the sample during processing. With the help of machine learning algorithms, the camera system can detect whether the wire is fully straightened and free from lamination or twisting. Once optimal alignment is verified, the system can notify the operator or trigger an automated mechanism to adjust the focal length and initiate the laser ablation process at the correct position.

This combination of improved mechanical design and intelligent vision-based feedback will significantly increase the reliability and efficiency of the process. It is expected that this advanced fixture will allow for the complete and uniform ablation of two wires simultaneously, with the entire setup cycle—including alignment and ablation—completed in approximately one minute. This development represents a crucial step toward scaling the process for more consistent and high-throughput applications in future studies and industrial implementations.

CHAPTER 6: References

[1] "Miller, R. A., Kazemba, C. D., Swanson, G. T., Williams, J. D., Hughes, S., & Cheatwood, N. (2023). Arcjet evaluation of thermocouple performance in flexible thermal protection system materials. Journal of Spacecraft and Rockets".

[2] "Reis, B., Della Cella, H., Ferreira, M., & Ferreira, F. F. V. M. (2024). A systematic review of automotive wiring harness innovations. SAE Technical Papers.".

[3] "Alotaibi, K. (2013). The fundamental component of telecommunications cabling. Proceedings of the 2013 American Society for Engineering Education Pacific Southwest Conference.".

[4] "Kim, S. H., & Lee, D. H. (2023). Polyetherimide for magnet wire applications. SAE International Journal of Advances and Current Practices in Mobility, 5(2), 517–520".

[5] "Ainul Hafiza, A. H., Khairunnisa-Atiqah, M. K., Nyak Mazlan, N. S., Mohd Salleh, K., & Zakaria, S. (2023). Biocompatible and biodegradable materials in medical applications. In Green Sustainable Process for Chemical and Environmental Engineering and Scien".

[6] "Long, Y., Dencker, F., Isaak, A., Hermsdorf, J., Wurz, M., & Twiefel, J. (2018). Self-cleaning mechanisms in ultrasonic bonding of Al wire. Journal of Materials Processing Technology, 258, 58-66.".

[7] "Maeno, T., Mori, K., Ogihara, T., & Fujita, T. (2019). Removal of thin oxide scale by ultrasonic cleaning with diluted hydrochloric acid in hot stamping of bare 22MnB5 sheet using resistance heating. Procedia Manufacturing, 29, 225-231.".

[8] "Weston, D. P., Shipway, P. H., & Harris, S. J. (2005). Coating removal from an industrial polypropylene blend by cryogenic blasting: The development of substrate damage. Wear, 258(1–4), 392–401".

[9] "Kapoor, J., Sehijpal, S., & Khamba, J. S. (2012). Effect of cryogenic treated brass wire electrode on material removal rate in wire electrical discharge machining. Proceedings of the Institution of Mechanical Engineers, Part C: Journal of Mechanical Engin".

[10] "Akıncıoğlu, S., Gökkaya, H., & Uygur, I. (2015). A review of cryogenic treatment on cutting tools. The International Journal of Advanced Manufacturing Technology, 78(9–12), 1463–1479.".

[11] "Arifvianto, B., Santoso, W., Rajagukguk, K., Hayyaulia, P. S., Salim, U. A., Mahardika, M., & Suyitno. (n.d.). Recycling of magnesium alloy scrap by remelting and chemical de-coating process. Metallurgical and Materials Engineering.".

[12] "Workmanship.NASA.gov," [Online].

[13] "Li, P., Zhou, B., Huang, H., Wang, P., Huang, G., Zhou, P., & Tian, C. (2022). Study on the optimal process parameters for stripping the X-ETFE insulation layer of aviation wires by a small semiconductor laser. Advances in Mechanical Engineering, 14(9), 1".

[14] "https://www.a-optowave.com/news/laser-induced-selective-micro-stripping/," [Online].

[15] "Ashfold, M. N. R., Claeyssens, F., Fuge, G. M., & Henley, S. J. (2004). Pulsed laser ablation and deposition of thin films. Chemical Society Reviews, 33(1), 23-31".

[16] "Gordon, P., Berenyi, R., & Balogh, B. (n.d.). Controlled laser ablation of polyimide substrates. Department of Electronics Technology, Budapest University of Technology and Economics".

[17] N. Neumann, Microwave Photonic Applications – From Chip Level to System Level. Clausthal University of Technology, ISBN: 978-3-95947-042-1.

[18] A. Martinez-Conde, T. Krenke, and U. Müller, “Comparative analysis of CO_2 laser and conventional sawing for cutting of wood-based materials..

[19] "A. A. Almutairi, A. A. Alharbi, and M. A. Alharbi, “Excimer laser for the treatment of psoriasis: safety, efficacy, and patient satisfaction,” Psoriasis: Targets and Therapy, vol. 5, pp. 1–9, 2015".

[20] "M. Abrouk, E. Levin, M. Brodsky, J. R. Gandy, M. Nakamura, T. H. Zhu, B. Farahnik, J. Koo, and T. Bhutani, “Excimer laser for the treatment of psoriasis: safety, efficacy, and patient acceptability,” Psoriasis: Targets and Therapy, vol. 6, pp. 1–6, 2016".

[21] "J. Cui, X. Fang, X. Dong, X. Mei, K. Xu, Z. Fan, Z. Sun, and W. Wang, “Fabrication of PCD Skiving Cutter by UV Nanosecond Laser,” Materials, vol. 14, no. 14, p. 4027, 2021.".

[22] "A. Hamja, R. Florentin, S. Chénais, and S. Forget, “Highly photo-stable, kHz-repetition-rate, diode-pumped circulation-free liquid dye laser with thermal lens management,” arXiv preprint arXiv:2203.16231, 2022".

[23] "M. S. Abid and K. J. Hussein, “The properties of Nd:YAG laser and its applications in medicine,” J. Appl. Phys., vol. 123, no. 4, pp. 1–6, 2018, doi: 10.1016/j.japphy.2018.02.012".

[24] "C. Magnus, Hybrid Metal to Polymer Joining Methods, M.Sc. thesis, Mechanical Engineering, University of Oulu, 2012.".

[25] "S. Ravi-Kumar, B. Lies, H. Lyu, and H. Qin, "Laser Ablation of Polymers: A Review," Science and Technology of Advanced Materials, vol. 22, no. 1, pp. 66-85, 2021".

[26] "M. Lu, M. Zhang, K. Zhang, Q. Meng, and X. Zhang, "Femtosecond UV Laser Ablation Characteristics of Polymers Used as the Matrix of Astronautic Composite Material," Materials, vol. 15, no. 19, p. 6771, 2022.".

[27] "W. Zhou, D. Bridges, R. Li, and A. Hu, "Recent progress of laser micro- and nano manufacturing," Sci. Lett., vol. 2015, no. 200638829, 2015.".

[28] ., "Á. Mechler, P. Heszler, Zs. Márton, M. Kovács, T. Szörényi, and Z. Bor, "Raman spectroscopic and atomic force microscopic study of graphite ablation at 193 and 248 nm," Journal of Applied Physics, vol. 87, no. 7, pp. 3514-3519, 2000".

[29] "www.edmundoptics.com," [Online].

[30] "https://www.mactrontech.net/product/mactron-jpt-mopa-split-fiber-laser-marking-machine/," [Online].

[31] "Garcia-Lechuga, M., & Grojo, D. (2021). Simple and robust method for determination of laser fluence thresholds for material modifications: an extension of Liu's approach to imperfect beams [Version 2]. Open Research Europe, 1, 7".

[32] "Brown, D. C. High-Peak-Power Nd:Glass Laser Systems. Springer, 1981.".

[33] "Simone D'Arcangelo, Leonardo Caprio, Davide Chesi, Methodological comparison of laser stripping solutions with contemporary pulsed lasers for e-drive copper hairpins, Production Engineering Volume 18, pages 557–572, (2024)".

[34] "Saunders, J., Elbestawi, M., & Fang, Q. (2023). Ultrafast laser additive manufacturing: A review. Journal of Manufacturing and Materials Processing, 7(3), 89".

[35] https://www.olympus-global.com. [Online].

[36] "Zeng, Y., Chen, G., Wu, C., Pan, X., Lin, F., Xu, L., Zhao, F., He, Y., He, G., Chen, Q., Sun, D., & Hai, Z. (2022). Thin-Film Platinum Resistance Temperature Detector with a SiCN/Yttria-Stabilized Zirconia Protective Layer by Direct Ink Writing for High-".

[37] "Basu, A. K., Tatiya, S., Bhatt, G., & Bhattacharya, S. (2019). Fabrication Processes for Sensors for Automotive Applications: A Review. In Sensors for Automotive and Aerospace Applications (pp. 3290). Springer Singapore.".

[38] "Zhang, Y., et al. (2015). Platinum-Based Nanostructures for Biomedical Applications. Journal of Biomedical Nanotechnology, 11(5), 885-897.".

[39] "Cao, Y., Zhang, Y., Ming, W., He, W., & Ma, J. (2023). Review: The Metal Additive-Manufacturing Technology of the Ultrasonic-Assisted Wire-and-Arc Additive-Manufacturing Process. Metals, 13(2), 398".

[40] "Cao, H., Shan, X., Liu, S., & Shi, Y. (2019). Ultra-fine high-carbon steel wire drawing with ultrasonic vibration. IOP Conference Series: Materials Science and Engineering, 531(1), 012027".

[41] "W. Charee, V. Tangwarodomnukun, and C. Dumkum, Ultrasonic-assisted underwater laser micromachining of silicon, Journal of Materials Processing Technology, vol. 234, pp. 231-237, 2016.".

[42] "Developments in Surface Contamination and Cleaning Particle Deposition, Rajiv Kohli, Control and Removal, Chapter 5 - Strippable Coatings for Removal of Surface Contaminants,2010, Pages 177-224.".

[43] "Hawkeye, M. M., & Brett, M. J. (2007). Glancing angle deposition: Fabrication, properties, and applications of micro- and nanostructured thin films. Journal of Vacuum Science & Technology A: Vacuum, Surfaces, and Films, 25(5), 1317-1335".

[44] "Wang, Y., Han, J., Gu, X., Dimitrijev, S., Hou, Y., & Zhang, S. (2017). Ultrathin Fe_2O_3 nanoflakes using smart chemical stripping for high performance lithium storage. Journal of Materials Chemistry A, 5(35), 18566-18575".

[45] "Borek, M., Qian, F., Nagabushnam, V., & Singh, R. K. (1993). Pulsed laser deposition of oriented VO2 thin films on R-cut sapphire substrates. Applied Physics Letters, 63(24), 3288–3290.".

[46] "Liao, Y., & Cheng, Y. (2014). Femtosecond Laser 3D Fabrication in Porous Glass for Micro- and Nanofluidic Applications. Micromachines, 5(4), 1106-1134".

[47] "Simone D'Arcangelo, Leonardo Caprio, Davide Chesi, Methodological comparison of laser stripping solutions with contemporary pulsed lasers for e-drive copper hairpins, Production Engineering Volume 18, pages 557–572, (2024)".

[48] "Saunders, J., Elbestawi, M., & Fang, Q. (2023). Ultrafast laser additive manufacturing: A review. Journal of Manufacturing and Materials Processing, 7(3), 89".

[49] "K. L. Choo, Y. Ogawa, G. Kanbargi, V. Otra, L. M. Raff, and R. Komanduri, "Micromachining of silicon by short-pulse laser ablation in air and under water," Mater. Sci. Eng. A, vol. 372, no. 1–2, pp. 145–162, 2004.".

[50] "A. Kruusing, "Underwater and water-assisted laser processing: Part 2 - Etching, cutting and rarely used methods," Opt. Lasers Eng., vol. 41, no. 2, pp. 329–352, 2004.".

[51] "Zhu, W., Liu, H., & Li, Z. (2017). The Effect of Overlapping on Laser Ablation of Metals: A Numerical Study. Applied Surface Science, 392, 453-461.".

[52] "N Takada, A Fujikawa, N Koshizaki (2013), Effect of ultrasonic wave on the syntheses of Au and ZnO nanoparticles by laser ablation in water, Vol 110, 835-839.".

[53] "Wang, X., & Zhang, L. (2020). Influence of Laser Parameters on Surface Quality in Laser Processing of Metals. Journal of Materials Processing Technology, 275, 116400.".

[54] "Danial Rahnama., Chila, G., & Narayanswamy, S. (n.d.). UV nanosecond pulsed laser parameter optimization for removal of polyamide coatings from fine platinum wires.Journal Of Manufacturing and Material Processing(under review)".

[55] "J. Bonse, J. Krüger, S. Höhm, and a. Rosenfeld, "Femtosecond laser-induced periodic surface structures," J. Laser Appl., vol. 24, no. 4, p. 042006, 2012.".

[56] "P. V. Kazakevich, a. V. Simakin, and G. a. Shafeev, “Formation of periodic structures by laser ablation of metals in liquids,” Appl. Surf. Sci., vol. 252, no. 13, pp. 4457–4461, 2006".

[57] "I. Sukhov, G. Shafeev, V. V. Voronov, M. Sygletou, E. Stratakis, and C. Fotakis, “Generation of nanoparticles of bronze and brass by laser ablation in liquid,” Appl. Surf. Sci., vol. 302, pp. 79–82, 2014.".

[58] "K. L. Choo, Y. Ogawa, G. Kanbargi, V. Otra, L. M. Raff, and R. Komanduri, “Micromachining of silicon by short-pulse laser ablation in air and under water,” Mater. Sci. Eng. A, vol. 372, no. 1–2, pp. 145–162, 2004.".

[59] "A. Kruusing, “Underwater and water-assisted laser processing: Part 1 - General features, steam cleaning and shock processing,” Opt. Lasers Eng., vol. 41, no. 2, pp. 307–327, 2004. 88".

[60] "Kekana, N.; Shongwe, M. B.; Mpofu, K.; Muvunzi, R. Investigation into Process Parameter Optimization of Selective Laser Melting for Producing AlSi12 Parts Using ANOVA. Appl. Sci. 2024, 14(15), 6519.".

[61] "Özbey, S.; Tıkız, İ. ANOVA-Based Analysis of Laser Cutting Parameter Effects on ST52 Steel. 4th International Conference on Frontiers in Academic Research, Konya, Turkey, 13-14 December 2024; pp. 382-386.".

[62] X. Zhang, Z. Zhan, H. Liu, H. Zhao, S. Xie and Q. I. o. W. L. T. o. H. T. A. w. P. C. L. J. o. B. O. 2. 1. 0. Ye.

[63] "Aghayan, M. (2015). Laser Surface Texturing of Mult crystalline Silicon to Reduce Solar Weighted Reflectance. Engineering, Materials Science, Physics, Environmental Science".

[64] "Liao, Y., & Cheng, Y. (2014). Femtosecond Laser 3D Fabrication in Porous Glass for Micro- and Nanofluidic Applications. Micromachines, 5(4), 1106-1134".

[65] "Varlamov, P., Marx, J., Urbina Elgueta, Y., Ostendorf, A., Kim, J.-W., Vavassori, P., & Temnov, V. (2024). Femtosecond laser ablation and delamination of functional magnetic multilayers at the nanoscale, Nanomaterials, 14(18), 1488.".

[66] "Y. Yang, J. Yang, and J. Vučković, “Titanium:sapphire-on-insulator integrated lasers and amplifiers,” Nature, vol. 618, pp. 123–127, 2024. doi: 10.1038/s41586-024-07457-2".

[67] "Performance Analysis of NR-DCSK Based Copper Cable Model for G.fast Communication March 2024, Fractal and Fractional, Vol. 6(1), Article No. 5Md I. Uddin, P. K. Raj, Md R.Rahman, Md A. Islam".

[68] "Joy Rempe, S. C. Wilkins ,High Temperature Thermocouples for In-Pile Applications, Proceedings of the 11th International Topical Meeting on Nuclear Reactor Thermal, Hydraulics (NURETH-11), Avignon, France, January 2005".

[69] "B. Reis, H. Della Cella, M. Ferreira, S. Vaz, G. Cossolino, R. Montes, and F. F. V. M. Ferreira, "A Systematic Review of Automotive Wiring Harness Innovations," in SAE Brasil 2023 Congress, IEL Bahia & Ford Motor Company Brasil, 2023, pp. 1–11.".

[70] "J. L. Gbur and J. J. Lewandowski, "Fatigue and fracture of wires and cables for biomedical applications," Int. Mater. Rev., vol. 61, no. 4, pp. 231–314, May 2016.".

[71] " S. Ota, M. Yamauchi, A. Mizoguchi, Y. Tamura, and others, “Magnet wire with enhanced tolerance for high frequency voltage,” SEI Technical Review, Apr. 2017.".